Wilson Fermions In Lattice Quantum Chromodynamics

Rahim Setoodeh

Thesis

Presented for the degree of Doctor of Philosophy

Department of Physics and Astronomy

University of Glasgow

August 1990

ProQuest LLC.
789 East Eisenhower Parkway
P.O. Box 1346
Ann Arbor, MI 48106 – 1346

In the Name of God

To the memory of my mother
whose love, support, and encouragement
over the years made to a large extent
the accomplishment of this work possible.

Declaration

Except where specific reference is made to the work of others, this thesis has been composed by the author. It has not been accepted in any previous application for a degree. I further state that no part of this thesis has already been or is being concurrently submitted for any such degree or qualification at any other university.

Rahim Setoodeh

Acknowledgements

I would like to thank Professor I.S. Hughes the ex-head of the Department of Physics and Astronomy especially for sending me to the "32nd Scottish Universities Summer School in Physics" in St. Andrews, Scotland in August 1987 and "18th British Universities Summer School in Theoretical Elementary Particle Physics" in Lancaster, England in September 1988. I am very grateful to my supervisors, Professor R.G. Moorhouse, Dr. I.M. Barbour and in particular Dr. C.T.H. Davies for their constant enthusiasm for this work and for their many helpful and constructive suggestions. I am also indebted to Dr. D. Sutherland and the other members of the Theoretical Physics Division whom I benefited from their encouragement as well as their lectures. Special thanks must be given to M. Mimi whose friendship is worth to treasure and also to Z.A. Sabeur, K. Ayat and my other fellow research students at the Department of Physics and Astronomy.

The numerical work described was done using Glasgow University's IBM 3090-150E/VF supported by IBM under the Kelvin Project and also IBM 3090-600E/VF and Atlas Cray X-MP/48 computers at the Rutherford Appleton Laboratory.

Finally I acknowledge the financial support I received from the Islamic Republic of Iran whilst the work for this thesis was carried out.

Abstract

We have studied the Wilson fermion matrix in the lattice QCD in the quenched approximation. Having implemented the Lanczos algorithm to study Wilson fermion spectrum on finite volumes we have presented results to confirm the existence of a phase transition accompanied by a massless mode from a phase where parity is restored to a phase where this discrete symmetry is violated in accordance with Aoki's lattice QCD phase diagram.

In an effort to set up the most suitable algorithm to investigate hadron spectrum for Wilson fermions, we have also studied different versions of the Lanczos and conjugate gradient algorithms and have found that the block Lanczos algorithm is really superior for inverting large sparse matrices. In particular we have shown that the rate of convergence of the block Lanczos algorithm becomes effectively independent of the details of the fermion matrix such as gauge coupling constant and hopping parameter.

The application of the block Lanczos algorithm to investigate scalar and pseudoscalar meson propagators shows that the massless mode associated with the transition from parity-restoring to parity-violating phase in the above phase structure is indeed where the pion becomes massless.

Contents

Chapter 1

Lattice Gauge Theory

1.1 Introduction

Gauge theories are inevitable for our understanding of particle systems. Most of the present models developed to describe such systems at a fundamental level make use of the notion of a gauge field. To have a well defined mathematical meaning the corresponding quantum systems must be regularized so that all divergent integrals are made finite. However, almost all techniques currently employed for this purpose are based on the weak coupling parameters in which the theory can be expanded perturbatively. Needless to say they are impotent for the analysis of phenomena governed by large coupling constants. They become even more useless where the behaviour of the theory at the origin, in coupling parameter space, is not analytic. To overcome these difficulties one requires a non-perturbative regularization scheme i.e. one which can be directly applied to fields, not to Feynman diagrams. Based on this notion an alternative method of regularization has been suggested by Wilson [1]. His method consists of putting the theory onto a discrete hypercubic lattice of space-time points, and to attempt to define the continuum limit theory as the limit of this lattice field theory as the lattice spacing goes to zero. The cost of doing this is to break the manifest Poincare' invariance of the original theory, in the hope that it will return in the continuum limit. This method provides a natural cut-off scheme as wavelengths shorter than twice the lattice spacing, a, have no meaning and this restricts the domain of momenta to a region bounded by $\frac{\pi}{a}$. As a result the ultraviolet divergences are thus removed.

For technical convenience we formulate the lattice theory in a four dimensional Euclidean space-time defined by the Wick rotation ($t \rightarrow -it$) of the Minkowski space theory. This completes the analogy of the field theory as formulated above with a statistical mechanics system. So we can call upon all our experience of statistical mechanics to solve problems in quantum field theory. In fact with a cut-off on high momenta the action is bounded and therefore we can treat it as a perturbation in the strong coupling limit to open a new domain of analytical investigations inaccessible to perturbation theory in terms of Feynman diagrams. This corresponds to the method of high-temperature expansion in statistical mechanics.

On the other hand if the space-time volume of the whole system is made finite there are only a finite number of variables and it is then possible to study various physically interesting quantities such as energy spectrum, correlation functions etc. in the path-integral formulation by the technique of numerical importance sampling i.e. by simulation based on the Monte Carlo method. Now all quantum averages are given by mathematically well-defined expressions irrespective of the value of the coupling constant. This numerical analysis thus bridges the gap between the strong coupling domain and the region of weak coupling which can be studied by perturbation theory.

Though lattice gauge theory seems promising in dealing with pure gluonic theories it creates its own problems for fermionic systems. An obstacle to handling the gauge theories with quarks is the uncertainty about the formulation of lattice fermions. The most straightforward fermion formulation, the so called naive theory, produces too many fermions. The two most popular ways of avoiding this multiplicity of fermions have no explicit continuous chiral invariance on the lattice. Chiral symmetry, realized in the Nambu-Goldstone mode, is supposed to be an important approximate (exact for massless fermions) symmetry of the strong interactions, one of the consequences of which is the smallness of the pion mass.

Lack of chiral invariance in the continuum limit of lattice quantum chromodynamics (QCD) will reflect directly on the value of the pion mass.

In practice the finite-size effects might alter the results. For instance, strong coupling calculations with one of the above methods, known as staggered fermions, give much too high an $\frac{m_\pi}{m_N}$ [2] despite the presence of a remnant of chiral symmetry. Finite-size effects seem less severe in calculations with the second method which is referred to as Wilson fermions. In this method, despite its explicit break down of the chiral symmetry, low pion mass is indicated to be no problem [3].

In the following sections we review the generalities of lattice field theories for pure gauge theories as well as theories with fermions. Special attention is paid to the Wilson fermions which form the central subject of the subsequent chapters.

1.2 Quantum Chromodynamics On The Lattice

Quantum chromodynamics which is the candidate field theory for the strong interactions is described by the Lagrangian density $\mathcal{L}$ which is written in terms of quark fields ψ and gluon fields A^a_μ in brief notations as:

$$\mathcal{L} = -\frac{1}{4} F_{\mu\nu} F^{\mu\nu} + \bar{\psi} (i \not{D} - m)\psi \tag{1.1}$$

where $F_{\mu\nu}$ is the field-strength tensor built out of Lie algebra valued gauge fields as:

$$F_{\mu\nu} = \partial_\mu A_\nu - \partial_\nu A_\mu - ig[A_\mu , A_\nu] \tag{1.2}$$

D_μ, being multiplied by Dirac matrices γ_μ in $\not{D}$ is the covariant derivative defined by,

$$D_\mu = \partial_\mu - igA_\mu \tag{1.3}$$

In the above g is the coupling constant and $A_\mu = A^a_\mu T_a$ is the vector potential. T_a are the generators of G the corresponding group transformations satisfying the Lie algebra:

$$[T_a , T_b] = i f_{ab}{}^c T_c \tag{1.4}$$

where $f_{ab}{}^{c}$ are the totally antisymmetric structure constants.

In QCD where the gauge group is $SU(3)$, T_a are related to Gell-Mann matrices[1] t_a by $T_a = \frac{1}{2} t_a$ where $a = 1, 2, 3, ..., 8$.

The Lagrangian density (1.1) or the corresponding action does not completely specify the theory. We also require to specify the functional integral measure or equivalently the partition function,

$$Z = \int \mathfrak{D}A \, \mathfrak{D}\psi \, \mathfrak{D}\bar{\psi} \, e^{i\int dt \, d^3x \, \mathcal{L}} \tag{1.5}$$

to obtain the vacuum expectation values of time ordered product of fields (Green's functions).

Eq. (1.5) does not have too much meaning until its strange mathematical content i.e. the infinite-dimensional functional integration, is defined in a sensible way. To do this we put the theory onto an Euclidean space-time lattice with a spacing a. The lattice sites will be labelled by a four-vector n i.e.

$$x = (x_1, x_2, x_3, x_4) \rightarrow n = (n_1, n_2, n_3, n_4)a \tag{1.6}$$

and the four-dimensional integrations will be replaced by a sum,

$$\int d^4x \rightarrow a^4 \sum_n \tag{1.7}$$

Naturally the scalar fields $\phi(n)$ are defined on the sites n and the vector fields $A(n,\mu)$ (characterized by a position and a direction) on the links joining the neighbouring sites of the lattice. As a result each field has a finite number of degrees of freedom and consequently the infinite-dimensional functional integrations over the field configurations will be represented by ordinary multiple integrals i.e.

$$\int \mathfrak{D}\phi \rightarrow \prod_n \int d\phi(n) \tag{1.8}$$

$$\int \mathfrak{D}A \rightarrow \prod_{n,\mu} \int dA\,(n,\mu) \tag{1.9}$$

[1] General properties of Dirac and Gell-Mann matrices are given in Appendix.

And finally the natural modification of derivatives on the lattice is to replace them with finite differences,

$$\partial_\mu \phi(x) \rightarrow \frac{\phi(n + a\hat{\mu}) - \phi(n - a\hat{\mu})}{2a} \tag{1.10}$$

where $\hat{\mu}$ is the unit vector in μ direction.

The lattice field theory introduced by the above procedure not only makes the path integrals well defined but regularizes the theory as well. This comes about through the transformation of the field $\phi(n)$ to momentum space,

$$\tilde{\phi}(p) = a^4 \sum_n e^{ip.n} \phi(n) \tag{1.11}$$

The result is that $\tilde{\phi}(p)$ is periodic in p with period $p_\mu = \frac{2\pi}{a}$. The momenta may therefore be restricted to lie in the first Brillouin zone i.e. $\frac{-\pi}{a} \leq p_\mu \leq \frac{\pi}{a}$. Then on an infinite lattice the inverse transform reads,

$$\phi(n) = \frac{1}{(2\pi)^4} \int_{\frac{-\pi}{a}}^{\frac{\pi}{a}} d^4p \, e^{-ip.n} \tilde{\phi}(p) \tag{1.12}$$

So the latticization provides a cut-off in momentum space as the largest component of momentum in any direction is $\pm\frac{\pi}{a}$.

What happens to the symmetries of the theory under such a latticization process? Obviously as the global internal symmetries are not affected by discretizing the space-time the lattice action would preserve such symmetries. We are most concerned about the local gauge symmetries. The Lagrangian (1.1) is invariant under the local gauge transformation described by the G-valued function V as follows:

$$\psi \rightarrow V\psi \tag{1.13}$$

$$\bar{\psi} \rightarrow \bar{\psi} V^{-1} \tag{1.14}$$

$$A_\mu \rightarrow V A_\mu V^{-1} - \frac{i}{g} (\partial_\mu V) V^{-1} \tag{1.15}$$

Unfortunately this gauge symmetry is lost if we latticize the lagrangian density by the above method. It is straightforward to see that the gauge invariant terms in the

action, e.g. $\bar{\psi}D\psi$, will remain invariant under the corresponding lattice gauge transformation only as $a \rightarrow 0$. We are interested to preserve gauge invariance for any finite value of lattice spacing a. However the freedom in lattice formulation provides a solution to this problem as one is free to add to the Lagrangian terms which will not contribute in the continuum limit. Using this freedom, the so called *universality*, Wilson has presented a particularly elegant lattice formulation for gauge theories. In his prescription which keeps local gauge invariance as an exact symmetry we require to redefine the gauge fields on the lattice. To see how it comes about let us consider the non-local operator $U(x,y)$,

$$U(x,y) = p\, e^{-ig\int_x^y A_\mu(Z)\, dZ^\mu} \tag{1.16}$$

where the integral is taken along some path Γ connecting the points x and y and p denotes the path ordering required to define U by expanding the exponential i.e. $A_\mu(z_1)$ is to the left of $A_\mu(z_2)$ if, along the path, z_1 is closer to x than z_2. The fact that A_μ are traceless shows that $det\ U(x,y) = 1$. Moreover $U(x,y)$ are manifestly unitary. Therefore $U(x,y)$ are elements of the gauge group rather than the Lie algebra. Let us check the properties of $U(x,y)$ under a gauge transformation $V(x)$. For an infinitesimal path where $y = x+dx$, $U(x,y)$ is easily shown to transform like:

$$U(x,x+dx) \rightarrow V(x)\, U(x,x+dx)\, V^{-1}(x+dx) \tag{1.17}$$

By performing similar transformation successively along the path elements one establishes the same result for finite separations i.e.

$$U(x,y) \rightarrow V(x)\, U(x,y)\, V^{\dagger}(y) \tag{1.18}$$

and similarly

$$U^{\dagger}(x,y) \rightarrow V(y)\, U^{\dagger}(x,y)\, V^{\dagger}(x) \tag{1.19}$$

where $V^{\dagger} = V^{-1}$. These gauge transformation properties of U ensure the gauge invariance of $\bar{\psi}(x)\, U(x,y)\, \psi(y)$ and its hermitian conjugate $\bar{\psi}(y)\, U^{\dagger}(x,y)\, \psi(x)$. On

the other hand if we let $y = x+\varepsilon_\mu$ we see that,

$$\lim_{\varepsilon_\mu \to 0} \frac{1}{\varepsilon_\mu}\left[\bar{\psi}\ (x)U(x,x+\varepsilon_\mu)\psi(x+\varepsilon_\mu) - \bar{\psi}(x)\psi(x)\right] \to \bar{\psi}(x)D_\mu\psi(x) \quad (1.20)$$

i.e. we can recover the continuum version of fermionic part of the Lagrangian (1.1) by using this interesting property of gauge invariant expression in the l.h.s. of Eq. (1.20).

These considerations suggest that the fundamental variable on the lattice is $U(n,n+a\hat{\mu})$ rather than $A(n,\mu)$. $U(n,n+a\hat{\mu})$ which we denote by $U_\mu(n)$ is the lattice version of the gauge field and sits on the link joining sites n and $n+a\hat{\mu}$. $U^\dagger_\mu(n)$ is then associated with the link in opposite direction i.e. from site $n+a\hat{\mu}$ to site n therefore:

$$U^\dagger_\mu(n) = U_{-\mu}(n+a\hat{\mu}) \quad (1.21)$$

To make the theory (discrete) translational invariant one imposes periodic boundary conditions on the gauge fields $U_\mu(n)$.

1.3 Lattice Action

Beginning with the Lagrangian (1.1) the continuum action in Euclidean space[2] is given by

$$S = \int d^4x\left\{\left[\bar{\psi}\ (x)\gamma_\mu(\partial_\mu - igA_\mu)\psi(x) + m\bar{\psi}(x)\psi(x)\right]\right.$$

$$\left. + \frac{1}{4}F_{\mu\nu}F^{\mu\nu}\right\} \quad (1.22)$$

we want to construct the lattice version of both fermionic and gluonic parts of the action S in terms of lattice variables $U_\mu(n)$.

1.3.1 Fermionic Action

The hermicity of the action (1.22)[3] and the property (1.20), which holds in

[2] See Appendix for the relations between Minkowski and Euclidean spaces.

Euclidean space as well, guide us to write the gauge invariant hermitian fermion action for any value of a by taking the hermitian part of (1.20) after $\bar{\psi}(x)$ is replaced with $\bar{\psi}(x)\gamma_\mu$. In lattice notation this leads to:

$$S_f = a^4 \sum_n \left\{ \frac{1}{2a} \left[\bar{\psi}(n)\gamma_\mu U_\mu(n)\psi(n+\hat{\mu}) - \bar{\psi}(n+\hat{\mu})\gamma_\mu U_\mu^\dagger(n)\psi(n) \right] + m\,\bar{\psi}(n)\psi(n) \right\} \tag{1.23}$$

where

$$U_\mu(n) = e^{-igaA_\mu(n)} \tag{1.24}$$

Needless to say that S_f reduces to fermion part of continuum action as $a \to 0$. In Eq. (1.23) the Einstein summation convention as well as the summation over colour and spin indices which are suppressed are understood. Usually ψ is replaced by $4(\sqrt{2a})^{-3}\psi$ and $a\hat{\mu}$ by $\hat{\mu}$ to obtain the standard form of S_f as:

$$S_f = \sum_n \left\{ \bar{\psi}(n)\gamma_\mu U_\mu(n)\psi(n+\hat{\mu}) - \bar{\psi}(n+\hat{\mu})\gamma_\mu U_\mu^\dagger(n)\psi(n) + 2ma\,\bar{\psi}(n)\psi(n) \right\} \tag{1.25}$$

It is interesting that contrary to the case of the continuum theory, the gauge coupling does not appear in S_f, because it has been in a sense reabsorbed in the definition of the lattice gauge variables $U_\mu(n)$.

As mentioned earlier $U_\mu(n)$ are the elements of gauge group. For $SU(N_c)$ which is a compact group the coefficients of the group generators T_a in the exponent i.e. $gaA^a_\mu(x)$ range between π and $-\pi$. This restricts the values of A^a_μ to the range $(-\frac{\pi}{ga}, \frac{\pi}{ga})$. In the continuum limit when $a \to 0$ this restriction is lifted and A^a_μ will regain its infinite domain $(-\infty, \infty)$. However the U variables, contrary to A_μ, have finite domain of variation for any value of a. This is important because in the continuum theory one must remove the redundant degrees of freedom, resulting from gauge invariance, of the theory by some gauge-fixing

[3] The hermicity of $\int d^4x\ \bar{\psi}\partial\psi$ is established by integration by parts and anticommutativity of γ-matrices.

conditions. In the language of path integral quantization formalism, one must restrict the functional integration to reflect these gauge-fixing conditions. So the lattice regularization automatically provides such a restriction via the finite range of U. So no gauge fixing is necessary on the lattice.

1.3.2 Gluonic Action

In constructing the lattice action we wish to keep most of the properties of continuum formalism at least to the extent the lattice structure allows to keep them. In case of gluonic action this means that we require it to be gauge invariant, local and have the global symmetries of the continuum Yang-Mills action and must reduce to it i.e. to $-\frac{1}{4}\int d^4x\, F_{\mu\nu}F^{\mu\nu}$ as $a \to 0$. However these requirements do not uniquely specify the lattice action as there are a whole class of actions which give the same physics in the continuum limit (*universality*). Clearly the gluonic action which is expressed in terms of gauge fields A^a_μ in the continuum theory must be composed of link variables $U_\mu(n)$ on the lattice. The gauge transformation property of U i.e. Eq. (1.18) implies that the trace of the product of U matrices along a closed loop, called a *Wilson loop* is gauge invariant. The simplest gauge invariant local interaction can be defined as,

$$S_g = \beta \sum_p \left[1 - \frac{1}{2N_c} \mathrm{Tr}\,(U_p + U_p^\dagger) \right] \tag{1.26}$$

where p refers to the simplest closed loop i.e. 1×1 loop called the *plaquette* and U_p is defined as:

$$U_p = U_p(n,\hat{\mu},\hat{\nu}) = U_\mu(n)U_\nu(n+\hat{\mu})\,U_\mu^\dagger(n+\hat{\nu})U_\nu^\dagger(n), \tag{1.27}$$

the sum $\sum_p = \sum_{n,\hat{\mu},\hat{\nu}}$ is over all plaquettes of the lattice and trace (Tr) is taken in colour space. As $a \to 0$ the terms like $A_\nu(n+\hat{\mu})$ and $A_\mu(n+\hat{\nu})$ which appear in U_p and $U_p^\dagger$ through Eq. (1.24) can be expanded in powers of a. Using such expansions along with the Baker-Hausdorff identity for any two arbitrary operators f and g

i.e.

$$e^f e^g = e^{f+g+\frac{1}{2}[f,g]+\ldots} \tag{1.28}$$

and the properties of *SU(3)* group generators[4] one can show that the Euclidean naive continuum limit can be recovered as,

$$\lim_{a\to 0} S_g \to \int \frac{1}{4} d^4x \, F_{\mu\nu} F^{\mu\nu} \tag{1.29}$$

if β is set equal to $\frac{2N_c}{g^2}$ for $SU(N_c)$ gauge theories.[5]

Together with the fermion action (1.25), the gauge action (1.26), which is known as the *Wilson action*, forms an explicit gauge invariant lattice regularized version of classical QCD. In the following section we will see how to quantize this lattice system.

1.4 Field Quantization

To quantize lattice QCD we adopt the Feynman path-integral approach [4, 5]. Here the transition amplitudes are expressed as some functional integrals over all possible paths between the initial and final states, weighted by the factor e^{-S} (in Euclidean space) where S is the action for the particular path. In the lattice QCD where we choose to work with the link variables as the basic dynamic degrees of freedom for the action,

$$S = S_f + S_g = S(\psi,\overline{\psi},U) \tag{1.30}$$

the vacuum to vacuum amplitude (partition function) reads,

$$Z = \int \mathfrak{D}\overline{\psi}\, \mathfrak{D}\psi\, \mathfrak{D}U\, e^{-S(\psi,\overline{\psi},U)} \tag{1.31}$$

where

$$\mathfrak{D}\overline{\psi} = \prod_n d\overline{\psi}(n) \tag{1.32}$$

$$\mathfrak{D}\psi = \prod_n d\psi(n) \tag{1.33}$$

---

[4] See Appendix.

[5] β turns out to be $\frac{1}{g^2}$ for *U(1)* gauge theories.

$$\mathbb{D}U = \prod_{n,\mu} dU_\mu(n) \tag{1.34}$$

Since the fermion fields are anticommuting C-number functions i.e.

$$\left\{\psi(n), \psi(n')\right\} = \left\{\bar{\psi}(n), \bar{\psi}(n')\right\} = \left\{\psi(n), \bar{\psi}(n')\right\} = 0 \tag{1.35}$$

they are the elements of Grassmann algebra [6] and the fermionic integration in Eq. (1.31) must be taken over such elements. Integration over Grassmann variables are defined so that they are invariant under a translation of the integration variable by a fixed element ϕ in the Grassmann algebra which is independent of ψ and anticommutes with $\int d\psi\, f(\psi) = \int d\psi\, f(\psi+\phi)$

$$\int d\psi\, f(\psi) = \int d\psi\, f(\psi+\phi) \tag{1.36}$$

and similar expression for $\bar{\psi}$. Eq. (1.36) implies that

$$\int d\psi = \int d\bar{\psi} = 0 \tag{1.37}$$

and the anticommutativity (1.35) results in

$$\left[\psi(n)\right]^2 = \left[\bar{\psi}(n)\right]^2 = 0 \tag{1.38}$$

The properties (1.37) and (1.38) make the integral over the Grassmann variables in Eq. (1.31) vanish except when the integrand is a product of all the Grassmann variables, each variable occurring once and only once. These properties of Grassmann variables for $\psi(n)$ and $\bar{\psi}(n)$ are then summarized as follows:

$$\int d\bar{\psi}\, \psi = \int d\bar{\psi}\, d\psi\, \psi = \int d\bar{\psi}\, d\psi\, \bar{\psi} = 0 \tag{1.39}$$

$$\int d\bar{\psi}\, d\psi\, \bar{\psi}\, \psi = -\int d\bar{\psi}\, d\psi\, \psi\, \bar{\psi} = 1 \tag{1.40}$$[6]

Since the fermion fields always enter the action quadratically as $\bar{\psi}M\psi$, where $M = \not{D}+m$ is the fermion matrix, the fermionic part of the functional integral (1.31) will be a generalized Gaussian integral. One can then show that:

$$\int \mathbb{D}\bar{\psi}\, \mathbb{D}\psi\, e^{-\bar{\psi}M\psi} = \det M \tag{1.41}$$

[6] The normalization is arbitrary.

We now consider the gauge integration part of (1.31). Here one should note that no gauge-fixing term has been added to the action because, as we mentioned in previous section, the link variables (i.e. lattice gauge fields) are group elements and have only finite range. $dU_\mu(n)$ is the Haar measure with arbitrary normalization:

$$\int dU = 1 \tag{1.42}$$

As a consequence of the invariance of Haar measure [7] under a fixed shift U' in integration variable we have:

$$\int dU\, f(U) = \int dU\, f(UU') \tag{1.43}$$

If the gauge group manifold is $SU(N_c)$ we also have the orthogonality properties:

$$\int dU\, U_{ij} = \int dU\, U^{\dagger}_{ij} = 0 \tag{1.44}$$

$$\int dU\, U_{ij} U^{\dagger}_{kl} = \frac{1}{N_c}\, \delta_{il}\delta_{jk} \tag{1.45}$$

$$\int dU\, U_{ij} U_{kl} = \int dU\, U^{\dagger}_{ij} U^{\dagger}_{kl} = 0 \tag{1.46}$$

These relations make the group integration practically feasible especially in the strong coupling region where the exponent e^{-S_g} can be expanded in powers of small parameter β.[7]

1.5 Continuum Limit

In the previous section we formulated the quantized lattice QCD. However one should remember that such a theory or any other regularized theory is only an intermediate step in solving a highly involved system of an infinite number of degrees of freedom. We are eventually interested to remove the cut-off i.e. the lattice spacing a introduced by the regularization scheme to recover the continuum limit where $a \to 0$. This renormalization procedure must be carried out in such a way that the physical predictions become independent of the lattice spacing and remain finite and fixed when a is small. As a is the only dimensionful parameter on the lattice the result of any calculation of a physical quantity q takes the form:

[7] See §1.6.

$$q = (\frac{1}{a})^d f(g) \tag{1.47}$$

where $\frac{1}{a}$ has dimension of mass (in natural units) and the content of the theory is expressed by the function f of dimensionless coupling g. Clearly the continuum limit can not be obtained for the observable q by merely letting $a \rightarrow 0$ unless g changes simultaneously so that q approaches a well defined finite limit in Eq. (1.47). So as $a \rightarrow 0$, there must be a critical value g^* of g such that $f(g)$ tends either to infinity (if $d < 0$) or to zero (if $d > 0$) as $g \rightarrow g^*$. g^* is the bare coupling constant of the resulting continuum QCD. On the other hand, this theory is asymptotically free[8], therefore the bare coupling, which describes the interactions at the scale of the cut-off, must be zero when the cut-off ($\sim \frac{1}{a}$) goes to infinity i.e. $g^* = 0$.

The above argument indicates that the transition to continuum limit requires a definite relationship between a and g. This could be achieved by demanding that the physical quantity q remains unchanged throughout the process of renormalization. This cut-off independence of q implies:

$$\frac{d}{da} q = 0 \tag{1.48}$$

As $q = q(a,g)$ the renormalizability requirement (1.48) implies:

$$a \frac{\partial q}{\partial a} - \beta(g) \frac{\partial q}{\partial g} = 0 \tag{1.49}$$

where

$$\beta(g) = -a \frac{dg(a)}{da} \tag{1.50}$$

β, the so called *β-function* specifies the lattice spacings at different coupling

[8] Theories having the property that the slope of the renormalization group β-function (discussed in this section) at the origin is negative are referred to as being *asymptotically free* [8]. Moreover only non-Abelian gauge theories are asymptotically free [9]. For such theories in 4 dimensions the origin is called an *ultraviolet stable fixed point* and the coupling constant region where physical predictions are cut-off independent is known as the *scaling region.*

constants (or vice versa). If Eq. (1.47) is used in Eq. (1.49) then one ends up with:

$$q = C[\Lambda_L]^d \tag{1.51}$$

where C is an integration constant and should be found by non-perturbative methods for different physical quantities, and

$$\Lambda_L = \frac{1}{a} e^{-\int \frac{1}{\beta(g)} dg} \tag{1.52}$$

Λ_L has the dimension of mass and sets the scale for QCD. As well as q, Λ_L is cut-off independent and as a free parameter must be measured by experiment. For small values of g where perturbative arguments determine the β-function [10] as,

$$\beta(g) = -\beta_0 g^3 - \beta_1 g^5 + \ldots \tag{1.53}$$

where

$$\beta_0 = \frac{11}{3} \frac{N_c}{16\pi^2}, \quad \beta_1 = \frac{34}{3} \left(\frac{N_c}{16\pi^2}\right)^2 \tag{1.54}$$

Λ_L reads as:

$$\Lambda_L = \frac{1}{a} e^{-\frac{1}{2\beta_0 g^2}} (\beta_0 g^2)^{-\frac{\beta_1}{2\beta_0^2}} \left[1+O(g^2)\right] \tag{1.55}$$

One must take $g \rightarrow 0$ to get to continuum limit in lattice QCD. Eq. (1.55) shows that, in this limit the only way Λ_L and accordingly the renormalized quantity q remains finite is by $a \rightarrow 0$ [9] and vice versa. This implies asymptotic freedom and also justifies our previous calculation that $g^* = 0$. It is also interesting to note that the singularity of $\frac{1}{2\beta_0 g^2}$ at $g = 0$ means that Λ_L and similarly q do not have perturbative expansions. That is to say the evaluation of a physical quantity like q requires a non-perturbative regularization scheme such as lattice regularization.

1.6 Wilson Loop And Confinement

Confinement of quarks is an outstanding problem in QCD. The possibility of performing strong coupling expansions provided by lattice regularization paves the

[9] Since $exp(-\frac{1}{2\beta_0 g^2}) \rightarrow 0$.

way to study this problem [1]. In the following we obtain the quark confinement for the special case of heavy quarks. In such a case quarks enter only as external static sources in a pure gauge theory. Consider a system composed of a pair of quark $\psi(\underline{Q},t)$ and antiquark $\bar{\psi}(\underline{R},t)$ separated by a distance $\underline{R}$. We can represent this system at time t by the gauge invariant operator $\Omega(t)$ as:

$$\Omega(t) = \bar{\psi}(\underline{R},t)\, U[(\underline{R},t),(\underline{Q},t)]\psi(\underline{Q},t) \tag{1.56}$$

where $U[(\underline{R},t),(\underline{Q},t)]$ is the product of gauge links joining the points $(\underline{R},t)$ and $(\underline{Q},t)$. We can evaluate the correlation between $\Omega(T)$ and $\Omega(0)$ [10] as:

$$\lim_{T\to\infty} <\Omega^{\dagger}(T)\,\Omega(0)> \sim e^{-E_0 T} \tag{1.57}$$

where E_0 is the ground state energy of the $q\bar{q}$ system. In case of heavy quarks where there is no dynamics E_0 is just the inter quark potential $V(R)$ i.e.

$$\lim_{\substack{T\to\infty \\ m_q\to\infty}} <\Omega^{\dagger}(T)\,\Omega(0)> \sim e^{-V(R)\,T} \tag{1.58}$$

In terms of fermion fields the l.h.s. of Eq. (1.58) may be written as:

$$\begin{aligned} <\Omega^{\dagger}(T)\,\Omega(0)> &= <\bar{\psi}(\underline{Q},T)\, U[(\underline{Q},T),(\underline{R},T)]\psi(\underline{R},T) \\ &\qquad \bar{\psi}(\underline{R},0)U[(\underline{R},0),(\underline{Q},0)]\psi(\underline{Q},0)> \\ &= \frac{1}{Z}\int \mathcal{D}\bar{\psi}\,\mathcal{D}\psi\,\mathcal{D}U\,\bar{\psi}(\underline{Q},T)U[(\underline{Q},T),(\underline{R},T)]\psi(\underline{R},T) \\ &\qquad \bar{\psi}(\underline{R},0)\,U[(\underline{R},0),(\underline{Q},0)]\,\psi(\underline{Q},0)\,e^{S_f+S_g} \end{aligned} \tag{1.59}$$

where S_f, S_g, and Z are given by Eqs. (1.25), (1.26) and (1.31) respectively. In case of heavy quarks we can integrate out the fermion fields by expanding e^{S_f} in powers of $\frac{1}{2ma}$. Using the properties of Grassmann variables i.e. Eqs. (1.37), (1.39) and (1.40), the leading non-vanishing term in (1.59) is obtained to be proportional to $(\frac{1}{2ma})^{T}$ and results in:

[10] See §4.1.

$$<\Omega^{\dagger}(T)\,\Omega(0)> \sim \int \mathcal{D}U W_C(\underline{R},T)\, e^{S_g} = <W_C(\underline{R},T)>_G \qquad (1.60)$$

where G means averaging over gauge field configurations and

$$W_C(\underline{R},T) = U[(\underline{0},T),(\underline{R},T)]\; U[(\underline{R},T),(\underline{R},0)]\; U[(\underline{R},0),(\underline{0},0)]$$

$$\times U[(\underline{0},0),(\underline{0},T)] \qquad (1.61)$$

that is to say $W_C(\underline{R},T)$ is just trace of the product of gauge links around the closed $T\times R$ rectangular loop C i.e. the Wilson loop operator. Combining Eqs. (1.58) and (1.60) we obtain:

$$< W_C(\underline{R},T) >_G \sim e^{-V(R)T} \qquad (1.62)$$

We next want to calculate the expectation value of Wilson loop. In the strong coupling limit e^{S_g} can be expanded in powers of β. Therefore:

$$<W_C(\underline{R},T)>_G \sim \int \mathcal{D}U\, W_C(\underline{R},T)\Big[1 - \frac{\beta}{2N_C}\sum_P \mathrm{Tr}\,(U_P + U_P^{\dagger}) + \frac{1}{2!}\Big(\frac{\beta}{2N_c}\Big)^2$$

$$\times \sum_P \sum_{P'} \mathrm{Tr}\,(U_P + U_P^{\dagger})\,\mathrm{Tr}\,(U_{P'} + U_{P'}^{\dagger}) + \cdots\Big] \qquad (1.63)$$

Due to the orthogonality properties of link variables, Eqs. (1.44), (1.45) and (1.46), each link on the Wilson loop must be matched with its hermitian conjugate in order to not yield vanishing result in Eq.(1.63). This requires the appropriate plaquette from the action which in turn introduces more links. The new links must be matched too. This procedure will eventually cover the surface of Wilson loop by the plaquettes so that no loose links are left unmatched. As a result the lowest-order non-vanishing contribution to $<W_C(\underline{R},T)>_G$ is $(\frac{\beta}{2N_c})^{N_P}$ term where Np is the minimal number of plaquettes required to cover area of Wilson loop,

$$< W_C(\underline{R},T) >_G \sim \Big(\frac{\beta}{2N_c}\Big)^{N_p} \qquad (1.64)$$

Noticing that $N_p = \frac{RT}{a^2}$ and $\beta = \frac{2N_c}{g^2}$ we compare (1.62) with (1.64) to obtain:

$$V(R) = \sigma R \qquad (1.65)$$

where $\sigma = \frac{\ln g^2}{a^2}$ is called the *string tension*. The linearly arising potential (1.65) implies the confinement of quarks. As this result is the consequence of *area law* (1.64) for Wilson loop, the vacuum expectation value of the large Wilson loops can be used as an order parameter for confinement.

We derived the above strong coupling result without resorting to the non-Abelian nature of *SU(3)* gauge group. In other words electric charge confinement result also holds in quantum electrodynamics (QED). However it has been proven [11] that in four dimensions Abelian gauge theories undergo a discontinuous phase transition from the confining phase (characterized by an area law) at strong coupling region to the real world of deconfining phase (characterized by a *perimeter law*) at weak coupling region, but similar analytic proof that QCD does possess such a phase structure is not obtained. Whether the quarks are really confined at finite β requires numerical investigations based on Monte Carlo simulations with which we deal in the next section.

1.7 Monte Carlo Simulation

Our lattice gauge theory based on path integral formulation enables us to extract physical quantities from appropriate gauge invariant expectation values. Using the partition function (1.31) this reads as:

$$< O > = \frac{1}{Z} \int \mathcal{D}\bar{\psi}\, \mathcal{D}\psi\, \mathcal{D}U\, O\,(\psi,\bar{\psi},U)\, e^{-S(\psi,\bar{\psi},U)} \qquad (1.66)$$

On a finite lattice Eq. (1.66) is a well defined multidimensional integral. If the integrals are approximated by sums over a sufficiently dense set of points Eq. (1.66) reduces to sums over a finite number of terms. Each term is represented by a set of gauge variables on the links $\{U_l\}$ called a gauge field configuration $\mathcal{C}$. For continuous gauge groups the number of gauge configurations is infinite. Let us first ignore the quark fields.[11] In this case for a *SU(3)* gauge theory on an L^3T lattice

[11] Fermionic systems are discussed in §1.10.

one has to evaluate a $32\ L^3T$ dimensional integral! Even for a relatively small lattice this multidimensional integral is beyond the possibilities of the most powerful computers.[12] Although this direct summation is quite hopeless, however we might think of an alternative approach by using the fact that most of the configurations have very small Boltzmann factor e^{-S} therefore their contribution to the total sum is negligible. In other words only a relatively small subset of configurations which have a small action (and large frequency of occurrence) effectively contribute the most to the quantum averages. If by means of a suitable random process a large sample of configurations is selected among the important ones (*importance sampling*), such that the frequency of occurrence of a given configuration is proportional to the measure factor e^{-S}, then $< O >$ may be approximated by averages taken over this large sample of configurations [12] i.e.

$$<O> = \frac{1}{N} \sum_{n=1}^{N} O_n + O\left(\frac{1}{\sqrt{N}}\right) \tag{1.67}$$

The above described procedure is known as Monte Carlo simulation. This procedure comes about by starting from an initial configuration $\mathcal{C}_1$. Then according to an algorithm which involves the extraction of random numbers we generate a new configuration $\mathcal{C}_2$. In the next step we start from $\mathcal{C}_2$ and following the same procedure we generate a new configuration $\mathcal{C}_3$ and so on so that eventually a large number of configurations are generated. The transition between one configuration $\mathcal{C}$ and the next $\mathcal{C}'$ is defined by a transition probability $W\ (\mathcal{C} \rightarrow \mathcal{C}')$. The procedure is designed in such a way that the probability of encountering any definite configuration $\mathcal{C}$ at the n^{th} step is proportional to $e^{-S[\mathcal{C}]}$ (for large n). The transition probability W is required to satisfy the following general properties:

I The algorithm must be capable of generating all configurations i.e.

$$W(\mathcal{C} \rightarrow \mathcal{C}') > 0 \tag{1.68}$$

[12] E.g. if we approximate the integrals by sums over 10 points per variable it amounts to 10^{320000} points at which to evaluate for a 10^4 lattice!

II Normalization condition requires:

$$\sum_{C'} W(C \to C') = 1 \tag{1.69}$$

III Let $P_n(C)$ be the probability distribution for configurations generated at step n by the algorithm. Then we have:

$$P_{n+1}(C) = \sum_{C'} P_n(C')\, W(C' \to C) \tag{1.70}$$

At equilibrium we must have:

$$P_{n+1}(C) = P_n(C) = e^{-S[C]} \tag{1.71}$$

Using Eqs. (1.69) and (1.70) the equilibrium condition reads as:

$$\sum_{C'} P_n(C)\, W(C \to C') = \sum_{C'} P_n(C')\, W(C' \to C) \tag{1.72}$$

A sufficient (though not necessary) condition to satisfy Eq. (1.72) is:

$$\frac{W(C \to C')}{W(C' \to C)} = \frac{P_n(C')}{P_n(C)} = \frac{e^{-S(C')}}{e^{-S(C)}} \tag{1.73}$$

which is called the *principal of detailed balance.*

The properties I, II and III do not fix the algorithm completely. The algorithm which is often used when fermions are ignored is the one due to Metropolis *et al.*

1.8 Metropolis Algorithm

The *Metropolis algorithm* [13] is set up by transition probability $W(C \to C')$ defined as:

$$W(C \to C') \propto \begin{cases} 1 & \text{if } \Delta S < 0 \\ e^{-\Delta S} & \text{if } \Delta S > 0 \end{cases} \tag{1.74}$$

where $\Delta S = S[C'] - S[C]$. It is straightforward to verify that $W(C \to C')$ defined by Eq. (1.74) satisfies the condition of detailed balance, Eq. (1.73). Transition probability (1.74) implies that if the passage from C to C' lowers the action the change is always accepted. On the other hand if the proposed change of configuration increases the action, the new action is accepted only with conditional

probability $e^{-\Delta S}$. It is this occasional acceptance of the changes which increase the action that simulates the effects of quantum fluctuations. In practice this conditional probability is implemented by comparing $e^{-\Delta S}$ with a selected random number r with uniform probability distribution between 0 and 1. If $e^{-\Delta S} > r$ the change is accepted and the new configuration in the sequence is $\mathcal{C}'$ and otherwise the change is rejected and the new configuration is again $\mathcal{C}$.

In lattice gauge theory applications the configuration is changed locally that is to say the configuration $\mathcal{C}'$ is the same as $\mathcal{C}$ except on a given link l where $U_l \rightarrow U'_l = VU_l$. V is chosen randomly from the set of the elements of gauge group close to $\mathbb{1}$.[13] Accordingly the change ΔS is local to the link that we change. Then:

$$\Delta S = -\frac{\beta}{2N_c} \mathrm{Re\ Tr}\left[\left(\sum_{\text{staple}} \sqcap\!\!\sqcup\right)(U' - U)\right] \tag{1.75}$$

where $\sum_{staple} \sqcap\!\!\sqcup$ is the sum of the staples attached to that link. Eq. (1.75) suggests that it is actually more efficient to update a given link several times before moving to the next link. The reason is that in updating (hitting) the same link subsequently several times the calculation of $\sum_{staple} \sqcap\!\!\sqcup$ which is quite time consuming need not be repeated. This multiple updating of the same link which may achieve a faster rate of convergence to statistical equilibrium is particularly convenient when the rate of rejection is high. This improved multihit Metropolis algorithm is referred to as a *heat bath algorithm* because it is like attaching a local heat bath to the link which is updated.

To be able to use Eq. (1.67) to approximate quantum averages $< O >$, the configurations over which O is evaluated must have come into equilibrium and should be statistically independent. Since the update changes one link only at a time, it requires updating the whole lattice (sweep) many times before statistical

[13] In practice we first construct the matrix $\mathbb{1}+\varepsilon A$ where ε is an arbitrary small number and A is a 3×3 matrix with random elements. V is then obtained by renormalizing $\mathbb{1}+\varepsilon A$ to a $SU(3)$ matrix.

equilibrium is achieved. The number of sweeps required for the probability distribution to reach equilibrium is called *equilibration time*. The measurements during this time must be discarded. Then many more sweeps are required before each statistically independent configuration is generated. The number of sweeps over which the data are correlated is called *correlation time*. Any error analysis should also take these correlations into account.

Based on these considerations we set up some criteria to see how suitable the generated configurations are.

1.9 Configuration Criteria

1.9.1 Average Trace Link

Average Trace Link (*Av.Tr.Link*) is defined on a single configuration as:

$$\text{Av.Tr.Link} = \frac{1}{N_c} \frac{1}{N_{site} N_{direction}} \sum_{n,\mu} \text{Tr}\, U_\mu(n) \qquad (1.76)$$

As *Av.Tr.Link* is not gauge invariant it must be zero (unless the gauge links are fixed). The equilibration time is then the number of sweeps (iterations) required before *Av.Tr.Link* falls to around zero as shown in Fig. 1.1 for a 4^4 lattice at β = *5.0* starting from a *hot start* [i.e. random $U_\mu(n)$'s] while each link is updated by 10 hits in every sweep. To estimate the correlation time we form block *Av.Tr.Link*'s which represent average of 2 adjacent measurements of *Av.Tr.Link*'s. This step averages over the short range fluctuations below 2 iterations while the long-range correlations between the block *Av.Tr.Link*'s are expected to be the same as those between the original *Av.Tr.Link*'s. Therefore, when measured in terms of the block lengths b_l, the correlation length reduces by $\frac{1}{2}$. By repeating this elementary step n times the dimensionless correlation length is reduced by $(\frac{1}{2})^n$ and if n is large enough the final block *Av.Tr.Link*'s are coupled over a few blocks only. In each step the correlation is estimated by calculating the corresponding mean square deviation $S_b = \sigma_b / \sqrt{b-1}$, where σ_b is

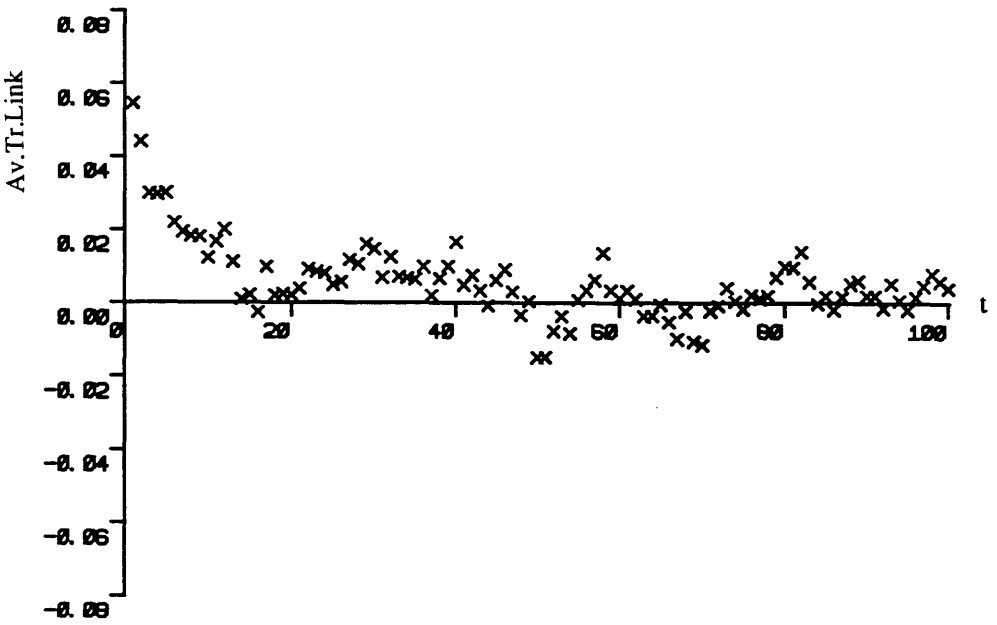

Fig. 1.1 Average Trace Link vs. time (sweep) for a 4^4 lattice at $\beta = 5.0$.

the standard deviation and b is the number of blocks, the larger S_b implies the less correlated blocks. If after N steps S_b approaches its maximum value then the corresponding blocks are well decorrelated and in terms of original *Av.Tr.Link*'s the correlation time is about 2^N sweeps as shown in Table 1.1 for the same measurements of Fig. 1.1. These measurements are obtained from 2048 sweeps after the first 952 sweeps are discarded.

1.9.2 Average Plaquette

Average Plaquette (*Av.Plaq*) is defined on a single configuration as:

$$\text{Av.Plaq.} = \frac{1}{N_c} \frac{1}{N_{site} N_{direction} (N_{direction} - 1)} \sum_p \text{Tr } U_p \qquad (1.77)$$

As U_p is gauge invariant *Av.Plaq.* does not necessarily vanish, however the reality of the action (1.26) results in a real value for *Av.Plaq.* once averaged over all gauge fields. One might use *Av.Plaq.* results to estimate equilibration and correlation times exactly in the same way as was discussed for *Av.Tr.Link.* Table 1.2 and Fig. 1.2 show the corresponding results.

Table 1.1

Adjusted root mean square deviation S_b for blocks of b_l Average Trace Links for a 4^4 lattice at $\beta = 5.0$. The correlation time is about 2^7 sweeps where S_b maximizes. The mean of average Trace link over 2048 sweeps is evaluated to be -0.00081.

n	b_1	b	s_b
0	1	2048	0.00016
1	2^1	1024	0.00021
2	2^2	512	0.00028
3	2^3	256	0.00035
4	2^4	128	0.00041
5	2^5	64	0.00046
6	2^6	32	0.00055
7	2^7	16	0.00069
8	2^8	8	0.00066
9	2^9	4	0.00055
10	2^{10}	2	0.00023

Table 1.2

Adjusted root mean square deviation S_b for blocks of b_l Average Plaquettes for a 4^4 lattice at $\beta = 5.0$. The correlation time is about 2^8 sweeps where S_b maximizes. The mean of Average Plaquette over 2048 sweeps is evaluated to be 0.39869

n	b_1	b	s_b
0	1	2048	0.00019
1	2^1	1024	0.00026
2	2^2	512	0.00034
3	2^3	256	0.00043
4	2^4	128	0.00052
5	2^5	64	0.00060
6	2^6	32	0.00063
7	2^7	16	0.00070
8	2^8	8	0.00085
9	2^9	4	0.00057
10	2^{10}	2	0.00072

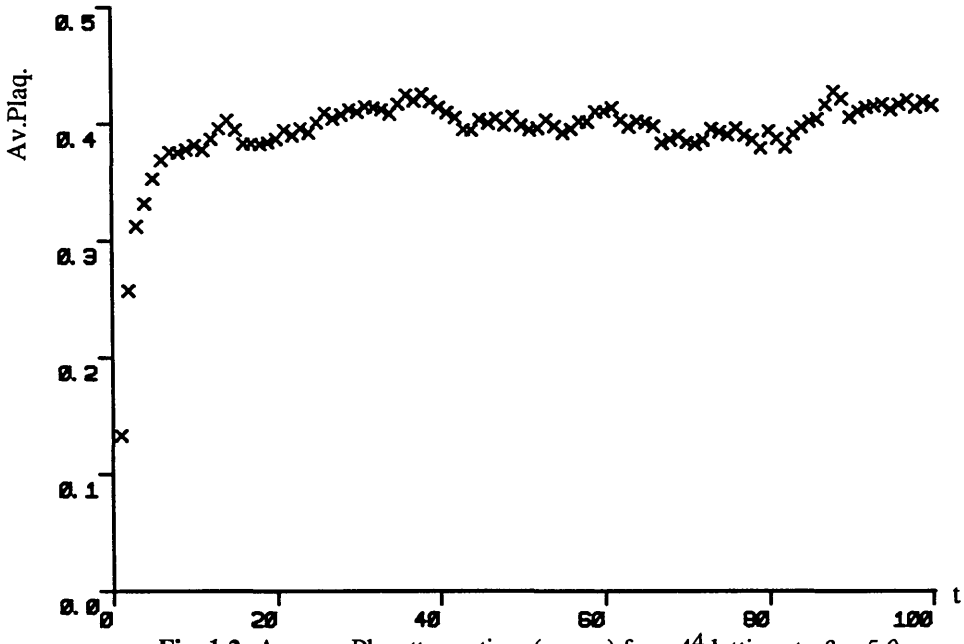

Fig. 1.2 Average Plaqette vs. time (sweep) for a 4^4 lattice at $\beta = 5.0$.

Using strong coupling expansion technique, the *Av.Plaq.* in strong coupling region is calculated to leading order as:

$$\text{Av.Plaq.} = \frac{\beta}{2N_c^2} \tag{1.78}$$

The Monte Carlo results for *Av.Plaq.* can be checked against this analytic value at small β to test the configuration generator programme.

1.9.3 Average Wilson Line

Since QCD is a confining theory we are interested to generate configurations in the confining phase. We then require an order parameter to distinguish if the gauge field configuration is not generated in the confining phase.

Consider an isolated heavy quark $\psi(\underline{0},0)$. Following the same procedure that we derived Wilson loop in §1.6 we obtain:

$$\langle \psi^\dagger(\underline{0},T)\, \psi(\underline{0},0)\rangle \sim e^{-F_q T} \sim \langle W \rangle_G \tag{1.79}$$

where F_q is the free energy of an isolated heavy quark in a background gauge field

and

$$W = U[(0,0),(0,T)] \tag{1.80}$$

If periodic boundary condition is imposed on the gauge fields along the time direction then W is just the trace of the product of gauge fields along a line that wraps around the lattice in time direction. Usually W is averaged over all the sites in the original spatial plane and is called *Average Wilson Line* or *Polyakov Loop*,

$$\text{Av. Wilson Line} = \frac{1}{N_c}\frac{1}{L_x L_y L_z}\sum_{\underline{x}} \mathrm{Tr}\prod_{t=0}^{T} U_0(\underline{x},t) \tag{1.81}$$

In the confined phase $F_q \rightarrow \infty$ as a result of which the vacuum expectation value (*VEV*) of *Av. Wilson Line* vanishes according to Eq. (1.79). In the deconfining phase F_q is finite and expectation value of the *Av. Wilson Line* picks up a non-vanishing *VEV*. Therefore the vacuum expectation value of *Av. Wilson Line* provides us with the order parameter for the above phase transition. This phase transition could also be explained by a spontaneous symmetry breaking mechanism. Clearly the *SU(3)* Wilson action is invariant if all the links, or just links on temporal directions, are multiplied by an element of its center Z_3 while *Av. Wilson Line* is not invariant under the same transformation (unless L_T is a multiple of 3). As a result while this symmetry is not broken < *Av. Wilson Line* > = 0 and therefore we are in the confined phase. If this Z_3 symmetry is spontaneously broken < *Av. Wilson Line* > picks up a Z_3 *VEV* and indicates that the phase is deconfining. Fig. 1.3 shows scatter plots of *Av. Wilson Line* in the complex plane obtained from 100 configurations for a 4^4 lattice at β = *5.2, 5.5* and *5.8*. Beginning from a hot start, every configuration is generated from the previous one by 10 sweeps. *Av. Wilson Line* is symmetric at β = *5.2* while the Z_3 symmetry is totally broken at β = *5.8*. The transition from symmetric to asymmetric phase is just about to take place at β = *5.5*. Note however, that on a finite lattice due to the tunnelling between equivalent vacua the symmetry can not be broken spontaneously, and if one waits long enough the true distribution becomes

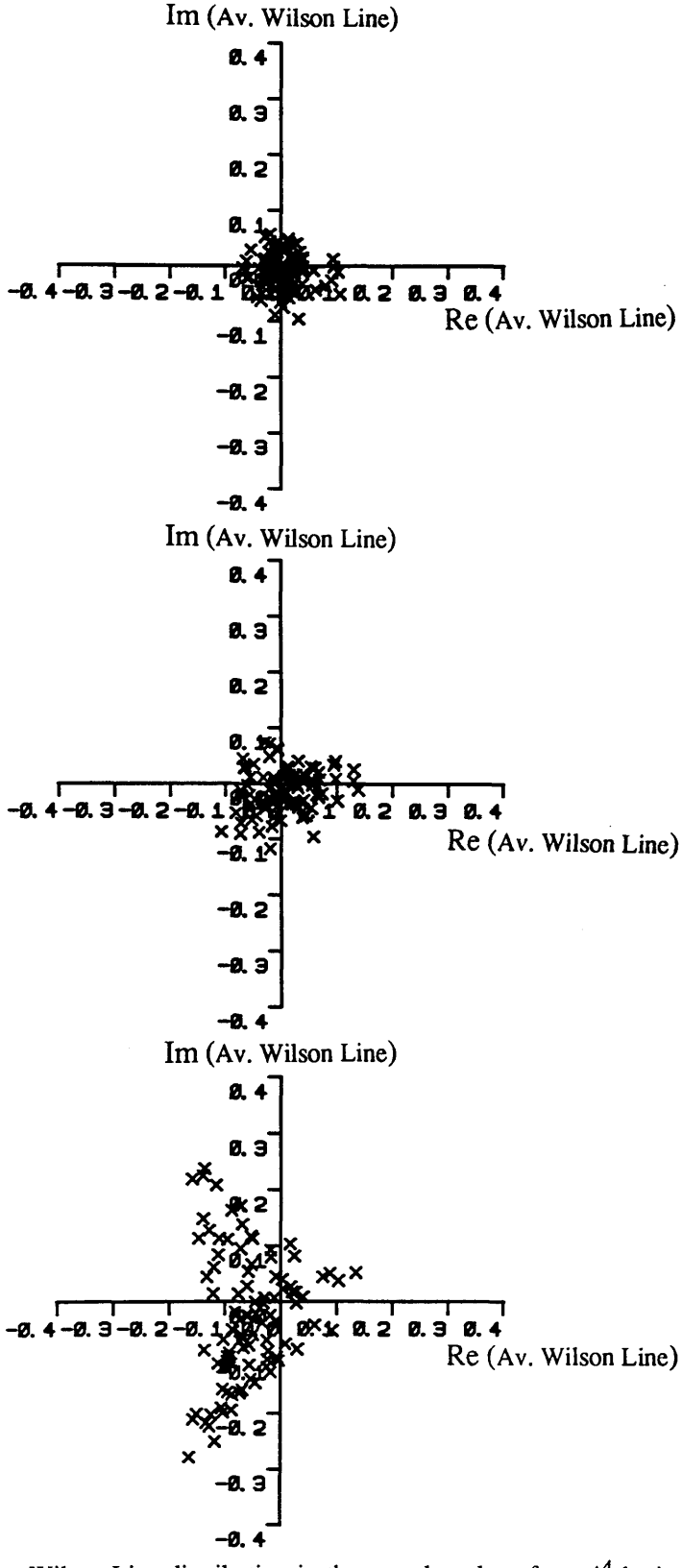

Fig. 1.3 Average Wilson Line distribution in the complex plane for a 4^4 lattice. Z_3 symmetry is nearly maintained at $\beta = 5.2$ (top) and just about to break as β comes across the phase transition point at $\beta = 5.5$ (middle). At $\beta = 5.8$ (above) Z_3 symmetry is clearly broken and that is why the Average Wilson Line becomes nonzero.

symmetric independently of β as in Fig. 1.4 where *Av. Wilson Line* is shown for 500 configurations i.e. over 5000 sweeps.

1.10 Numerical Methods For Fermionic Systems

Contrary to the pure gauge action, the fermion action is not positive definite. As a result the large fluctuations in ΔS_f during the updating process of the fermion fields would cause a large cancellation and accordingly a large variance. Moreover as the fermion fields are represented by anti-commuting Grassmann variables they can not be dealt with on the computers. However one can escape from these difficulties by integrating out the fermionic fields explicitly. Using the properties of Grassmann variables discussed in §1.4 in particular Eqs. (1.36) and (1.41), the expectation value of operator $O(U,\psi,\bar{\psi})$ i.e.

$$<O> = \frac{1}{Z}\int \mathcal{D}\bar{\psi}\,\mathcal{D}\psi\,\mathcal{D}U\, O(\psi,\bar{\psi},U)\, e^{-\bar{\psi}M\psi - S_g(U)} \tag{1.82}$$

where

$$Z = \int \mathcal{D}\bar{\psi}\,\mathcal{D}\psi\,\mathcal{D}U\, e^{-\bar{\psi}M\psi - S_g(U)} \tag{1.83}$$

can be given only in terms of bosonic gauge variables as:

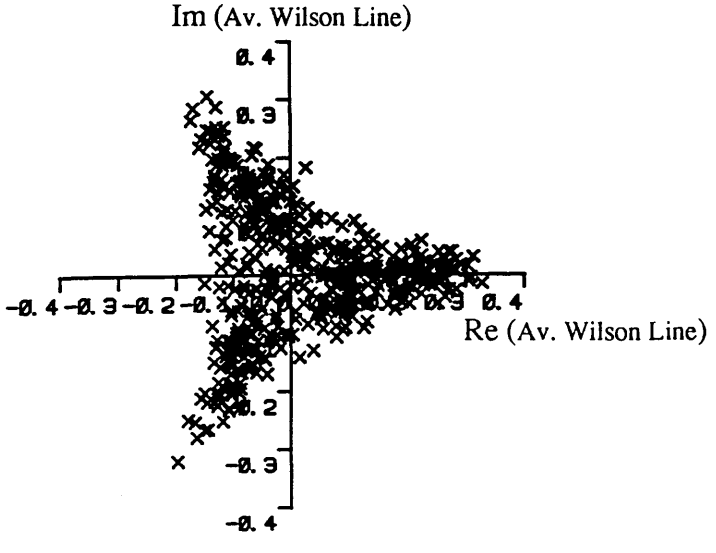

Fig. 1.4 Average Wilson Line distribution in the complex plane for a 4^4 lattice at $\beta = 5.8$. The asymmetric distribution obtained by 1000 sweeps (Fig. 1.3) becomes symmetric again over 5000 sweeps.

$$<O> = \frac{1}{Z'}\int \mathcal{D}U O'(U) \det M(U) e^{-S_g(U)} \tag{1.84}$$

where

$$Z' = \int \mathcal{D}U \det M(U) e^{-S_g(U)} \tag{1.85}$$

and

$$O'(U) = O\left(\frac{\delta}{\delta\bar{\eta}}, \frac{\delta}{\delta\eta}, U\right) e^{\bar{\eta} M^{-1}(U)\eta}\Big|_{\eta=\bar{\eta}=0} \tag{1.86}$$

and η and $\bar{\eta}$ are sources for the quarks. Eq. (1.84) indicates that Monte Carlo techniques can be applied to calculate $<O>$ provided that the probability distribution e^{-S_g} is represented by $e^{-S_{eff}}$ where

$$e^{-S_{eff}} = \det M\, e^{-S_g} = e^{-(S_g - \mathrm{Tr\,Ln}\, M)} \tag{1.87}$$

The term $e^{-Tr\,Ln\,M}$ represents the effect of virtual quark loops and contrary to S_g it is extremely non-local. Monte Carlo method requires the calculation of $e^{-\Delta S_{eff}}$ in each step of the algorithm. If M changes by δM then $e^{-\Delta S_{eff}}$ reduces to

$$e^{-\Delta S_{eff}} = e^{-\Delta S_g} \det (1 + M^{-1}\, \delta M) \tag{1.88}$$

The computation of the above determinant which must be done an enormous number of times is considerably time consuming. However, as the fermionic determinant enters both the numerator and the denominator in Eq. (1.84) one might replace it by its expectation value. This approximation which neglects the effect of dynamical quarks by suppressing the fluctuations of *det M*, drops out the *det M* from the expression (1.84). As a result it does not really allow the feedback of the quarks into gluon sector. In this approximation which is called *quenched approximation* one measures the fermionic variables in a background field generated with gauge action only. All our calculations in the present work are performed in the quenched approximation

The difficulties one encounters in dealing with fermionic systems are not

restricted to the numerical ones which were just discussed. There are more theoretical problems arising from the effect of space-time structure of the lattice on the chiral properties of the theory. We will explain the chiral properties in §3.1 where the strong interaction symmetries are discussed. Here we just recall that chiral invariance is the symmetry of the action under global axial phase transformations in flavour space. The presence of both axial and vector symmetries implies the symmetry of the action under independent rotations in flavour space of the left-handed and right-handed fermions.

The above effects which eventually cause the notorious species doubling problem are discussed in the following section.

1.11 Species Doubling

In §1.3.1 we derived the fermionic action S_f as Eq. (1.25). Unfortunately the said S_f, the so called *naive action* is not appropriate to describe QCD. The latticization process which led to Eq. (1.25) introduces unwanted fermionic degrees of freedom. To illustrate this problem consider the simple case of the free fermion action. In this case Eq. (1.25) gives the free fermion matrix M as:

$$M_{nn'} = \sum_{\mu} \gamma_\mu (\delta_{n+\mu,n'} - \delta_{n-\mu,n'}) + 2ma\, \delta_{n,n'} \tag{1.89}$$

Transforming M in Fourier space we get:

$$\begin{aligned} M_{pp'} &= \sum_{n,n'} e^{-iP.na} M_{nn'} e^{iP'.n'a} \\ &= 2\, \delta(pa - p'a) \left[i \sum_{\mu} \gamma_\mu \sin p_\mu a + ma \right] \end{aligned} \tag{1.90}$$

which gives for the fermion propagator $S(p)$,

$$S(p) = \left[i \sum_{\mu} \gamma_\mu \sin p_\mu a + ma \right]^{-1} \tag{1.91}$$

For massless theory Eq. (1.91) reproduces the correct continuum propagator $\frac{1}{\not{p}}$ for small $p_\mu a$ and has a pole at $p_\mu a = (0,0,0,0)$, However $S(p)$ has 15 more poles at

the corners of the first Brillouin zone i.e. at the points,

$$p_\mu = (\frac{\pi}{a}, 0, 0, 0), (0, \frac{\pi}{a}, 0, 0), \ldots, (\frac{\pi}{a}, \frac{\pi}{a}, \frac{\pi}{a}, \frac{\pi}{a}) \qquad (1.92)$$

This means that the original naive lattice action (1.25) describes one fermion plus 15 replicas.

As this so called *species doubling* problem originated from the discretization of the space-time, one might think of different ways to discretize the continuum action (1.1). This idea is of course justified because due to the universality the fermionic lattice action (1.25) is not unique. However it turns out that in any lattice formulation with no species doubling one has to give up either chiral invariance or the locality of the action. Otherwise we should compromise between these formal properties of the continuum action and the number of replica fermions!

Suppose, for example, we insist on maintaining the chiral invariance which is manifest in the continuum action (1.1) when $m = 0$. Having adopted any scheme to discretize the action (1.1) the general form of propagator for lattice fermions compatible with chiral invariance turns out to be,

$$S(p) = \left[\sum_\mu \gamma_\mu \sin F_\mu(p) \right]^{-1} \qquad (1.93)$$

In §1.2 we noticed that the latticization of configuration space with lattice spacing a resulted in a periodicity in momentum space with the period $\frac{2\pi}{a}$. The discrete translational invariance of the action in momentum space will ensure the translational invariance of the fermion matrix or fermion propagator $S(p)$. This means that $S(p)$ and as a result $F_\mu(p)$ must be periodic with period $\frac{2\pi}{a}$. To describe one fermion in the continuum limit (i.e. $a \to 0$), $F_\mu(p)$ as a function of p_μ should vanish (i.e. cross p_μ axis) once, e.g. at $p_\mu = 0$ [and behave like $F_\mu(p) \approx p_\mu$ around $p_\mu = 0$]. Periodicity of $F_\mu(p)$ implies that F_μ crosses p_μ axis once again at $p_\mu = \frac{2\pi}{a}$ with the same derivative. Somewhere between 0 and $\frac{2\pi}{a}$ there

must be another crossing across the axis for continuous $F_\mu(p)$ as shown in Fig.1.5. The naive propagator (1.91) for which $F_\mu(p) = \frac{1}{a} sin\ p_\mu a$ is an example with such an extra crossing. Such behaviour means there are extra excitations in the theory as we discussed for the naive propagator. So it is impossible to solve doubling problem for a chiral symmetric lattice action. If $F_\mu(p)$ does not cross p_μ axis between 0 and $\frac{2\pi}{a}$ then there must be a jump across this axis in this period as shown in Fig. 1.5. Such discontinuous propagators might solve the doubling problem but imply non-local lattice action [14].

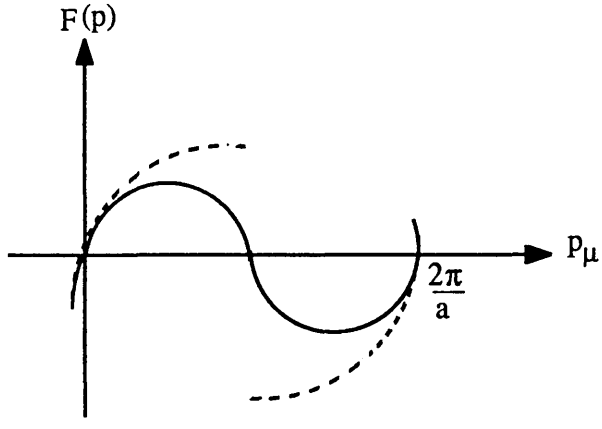

Fig. 1.5 The function $F(p)$ vs. p_μ : either an extra axis crossing (full curve) or a gap (dashed curve).

We can consider this problem from another point of view. If, around a corner of Brillouin zone, we write those components of momentum which are close to $\frac{\pi}{a}$ as $p_\mu = \frac{\pi}{a} + p'_\mu$ where p'_μ is very small, then the corresponding replica particle is described by the propagator $S(p')$ which is read from (1.91) as:

$$S(p') = \left[i \sum_\mu \gamma'_\mu \sin p'_\mu a + ma \right]^{-1} \qquad (1.94)$$

Eq. (1.94) is the same as Eq. (1.91) except $\gamma'_\mu = \pm\gamma_\mu$ depending whether $p_\mu \sim 0$ or $p_\mu \sim \frac{\pi}{a}$. As $\gamma_5 = \gamma_0 \gamma_1 \gamma_2 \gamma_3$ we have similar modification of γ_5 as $\gamma'_5 = \pm\gamma_5$. It is then clear that at half of the corners of Brillouin zone γ_5 changes sign. On the other hand we know that due to the presence of anomalous term in the continuum

QCD the chiral charge,

$$Q^5 = \int d^3x\, \bar{\psi}\, \gamma_0\, \gamma_5\, \psi \tag{1.95}$$

corresponding to $U(1)$ axial current $j^5_\mu = \bar{\psi}\gamma_\mu\gamma_5\psi$ is not conserved even in massless theory [15]. On the lattice each replica fermion contributes to the chiral charge. However due to the sign change of γ_5 these contributions cancel out, resulting in vanishing chiral charge and accordingly the anomaly $\partial^\mu j^5_\mu$. This is just an example of the general theorem by Nielsen and Ninomiya [16] that the chiral symmetry and chiral anomaly are not compatible on the lattice. Preserving the locality of the action, two major approaches have been proposed to remove this 16-fold degeneracy of the naive action and have a theory which describes one single fermion or at least a smaller set of fermionic modes.

1.12 Kogut-Susskind Fermions

We can spin-diagonalize the naive fermion action (1.25) by the following transformation of fermionic fields [17]:

$$\psi(n) \rightarrow T(n)\,\chi(n) \tag{1.96}$$

$$\bar{\psi}(n) \rightarrow \bar{\chi}(n)\,T^\dagger(n) \tag{1.97}$$

where

$$T(n) = \gamma_1^{n_1}\gamma_2^{n_2}\gamma_3^{n_3}\gamma_4^{n_4} \tag{1.98}$$

and

$$n = (n_1,n_2,n_3,n_4) \tag{1.99}$$

The fermion action in terms of χ-fields is then expressed as:

$$S_f = \sum_n \Big\{ \eta_\mu(n) \Big[\bar{\chi}(n)\, U_\mu(n)\, \chi(n+\hat{\mu}) - \bar{\chi}(n+\hat{\mu})\, U_\mu^\dagger(n)\, \chi(n) \Big] + 2ma\bar{\chi}(n)\chi(n) \Big\} \tag{1.100}$$

(the summation over repeated index μ is understood). Here $\eta_\mu(n)$ are phase factors

arising from commuting γ-matrices through one another and are evaluated for each flavour as:

$$\eta_1(n) = 1 \tag{1.101}$$

$$\eta_2(n) = (-1)^{n_1} \tag{1.102}$$

$$\eta_3(n) = (-1)^{n_1+n_2} \tag{1.103}$$

$$\eta_4(n) = (-1)^{n_1+n_2+n_3} \tag{1.104}$$

In the action (1.100) the 4 spin components of the so called *staggered* or *Kogut-Susskind fermions* $\chi(n)$ are manifestly decoupled, making the fermion matrix diagonal in spin space. One then may consider only one component and drop the other three. This reduces the number of fermions by a quarter, leaving only four fermions. Since the doubling problem is not solved completely in this formulation, the chiral symmetry is not violated totally either. The massless theory is invariant under the following transformations:

$$\left.\begin{aligned} \chi(n) &\rightarrow e^{i\alpha}\chi(n) \\ \overline{\chi}(n) &\rightarrow e^{-i\beta}\overline{\chi}(n) \end{aligned}\right\} \quad \text{at even sites}^{14} \tag{1.105}$$

$$\left.\begin{aligned} \chi(n) &\rightarrow e^{i\beta}\chi(n) \\ \overline{\chi}(n) &\rightarrow e^{-i\alpha}\overline{\chi}(n) \end{aligned}\right\} \quad \text{at odd sites} \tag{1.106}$$

where α and β are two independent phases. If $m \neq 0$ the theory is invariant under the above transformations only if $\alpha = \beta$. The broken symmetry turns out to be a remnant of $SU_A(4)$ chiral symmetry. The hidden chiral property of the above transformations can be attributed to the possibility of giving opposite phases to the χ-fields at different sites of the lattice [18].

[14] A site is called *even* (*odd*) if $\sum_\mu n_\mu$ is even (odd).

1.13 Wilson Fermions

We might remove the degeneracy of the naive action (1.25) by adding an irrelevant term to the action. To see how this comes about consider the term $-\frac{1}{2} ra\bar{\psi}\partial^2\psi$, the so called *Wilson term* [19]. Once discretized, the contribution of the the Wilson term to the action i.e.

$$-a^4\sum_n \frac{r}{2a}\,\bar{\psi}(n)\left[\psi(n+\hat{\mu}) - 2\psi(n)+\psi(n-\hat{\mu})\right] \tag{1.107}$$

clearly vanishes as $a \rightarrow 0$. Adding this term to the naive action in free case, the corresponding fermion matrix (1.89) will be modified as:

$$M_{nn'} = -\kappa\sum_\mu\left[(r-\gamma_\mu)\,\delta_{n+\mu,n'} + (r+\gamma_\mu)\,\delta_{n-\mu,n'}\right] + \delta_{n,n'} \tag{1.108}$$

where

$$\kappa = \frac{1}{2ma+8r} \tag{1.109}$$

κ is called *hopping parameter*. Transforming $M_{nn'}$ into momentum space, the corresponding massless fermion propagator $S(p)$ is obtained as:

$$S(p) = \left[\sum_\mu \frac{1}{a}(i\gamma_\mu \sin p_\mu a - r\cos p_\mu a) + 4\frac{r}{a}\right]^{-1} \tag{1.110}$$

For small momenta when $p_\mu a \rightarrow 0$ the propagator (1.110) recovers the correct continuum propagator and has a pole at the origin of the Brillouin zone $p_\mu = (0,0,0,0)$. At the other corners where some of the components of p_μ are $\frac{\pi}{a}$, $S(p)$ reduces to $(\frac{nr}{a})^{-1}$ where $n = 2, 4, 6, 8$. This means that $S(p)$ has only one pole at the origin and the replica fermions have disappeared in the continuum limit by acquiring masses $\frac{nr}{a}$. The doubling problem is completely solved, however with the expense of loss of chiral symmetry of the massless theory which is explicitly broken by the Wilson term.

For the interacting theory the gauge invariant Wilson term can be constructed by the same approach discussed in §1.3.1. This results in the interacting action,

$$S = \sum_n \Big\{ -\kappa \sum_\mu \Big[\bar{\psi}(n)(r-\gamma_\mu) U_\mu(n) \psi(n+\hat{\mu}) + \bar{\psi}(n+\hat{\mu})(r+\gamma_\mu) U_\mu^\dagger(n) \psi(n) \Big] + \bar{\psi}(n)\psi(n) \Big\} \quad (1.111)$$

and consequently the *Wilson fermion matrix* is obtained,

$$M_{nn'} = -\kappa \sum_\mu \left[(r-\gamma_\mu) U_\mu(n) \delta_{n+\hat{\mu},n'} + (r+\gamma_\mu) U_\mu^\dagger(n-\hat{\mu}) \delta_{n-\hat{\mu},n'} \right] + \delta_{n,n'} \quad (1.112)$$

Since chiral symmetry is explicitly broken in this formulation the fermion mass is not protected from renormalization. The κ at which the renormalized mass vanishes is called *critical hopping parameter* κ_c . In free case Eq. (1.109) gives $\frac{1}{8r}$ for κ_c . In the interacting theory however it depends on β in a complicated manner. In the next chapter we develop the algorithms suitable to study such dependences in the subsequent chapters.

Chapter 2

Lanczos And Conjugate Gradient Algorithms

Having regularized QCD by the lattices, one must be able to find the spectrum as well as the inverse of quantum operators such as fermion matrix in order to study strong interactions. Amongst the existing algorithms which could be applied to lattice field theories, we have studied Lanczos [20, 21] and conjugate gradient [22] algorithms. In this chapter we present these two algorithms and their results once applied to Wilson version of fermion matrix [23].

2.1 The Lanczos Algorithm

The eigenvalues of the matrices can be calculated by their diagonalization in the, usually large, basis of their eigenstates. In most practical cases, however, we are interested in only the small eigenvalues close to zero. Therefore, since the dimensions of the configuration space may be very large, it would be quite economic not to have to diagonalize the complete and large matrix if only the small eigenvalues are desired. Most procedures that are in use[1] do require such a complete diagonalization of the full matrix. An exception is the Lanczos iterative method of tridiagonalization, which permits one to obtain some eigenvalues quite accurately from only part of the full matrix. Although the method can be applied to any matrices, we only consider hermitian matrices.

Let H be an $N \times N$ hermitian matrix. Starting from any unit vector x_1, one

[1] E.g. the Householder method [24].

can generate a set of x_i, for $i = 1, 2, 3, ..., N$ by the following algorithm:

$$\alpha_i = x_i^\dagger H x_i \tag{2.1}$$

$$\beta_i = \| Hx_i - x_i\alpha_i - x_{i-1}\beta^\dagger_{i-1} \| \tag{2.2}$$

$$x_{i+1} = (Hx_i - x_i\alpha_i - x_{i-1}\beta^\dagger_{i-1})\beta_i^{-1} \tag{2.3}$$

where

$$\beta_0 = 0 \tag{2.4}$$

Properly sequenced, these formulae define the Lanczos iteration and x_i are called Lanczos vectors.

If x_1 happens to be orthogonal to an eigenstate of H, say ψ, though very unlikely to happen in practice, it is shown from procedure (2.3) that ψ is then orthogonal to all $x_1, x_2, x_3, ..., x_n$ and $\beta_n = 0$ for some $n < N$. In that case the algorithm terminates and if required it could be continued by constructing a new starting unit vector orthogonal to all the vectors already obtained.

The interesting feature of Lanczos algorithm is that H appears only in a matrix-vector product and is not altered during the entire process. In particular if H is a large sparse matrix, sparsity is preserved and one needs to store only the non-zero elements of H.

By induction it is easily checked that x_i form an orthonormal set and matrix elements of H in the basis $\{x_i / i = 1,2,3,...,N\}$ satisfy:

$$x_i^\dagger H x_j = \delta_{i\,j-1}\beta^\dagger_{j-1} + \delta_{ij}\alpha_j + \delta_{i\,j+1}\beta_j. \tag{2.5}$$

As the hermiticity of H ensures the reality of α_i, Eq. (2.5) indicates that H is a symmetric tridiagonal matrix in that basis. In other words, defining

$$X = [x_1, x_2, x_3, ..., x_N] \tag{2.6}$$

an $N \times N$ matrix, then X is unitary and symmetrizes and tridiagonalizes H via the unitary transformation,

$$X^\dagger H X = T \tag{2.7}$$

where

$$T = \begin{pmatrix} \alpha_1 & \beta_1^{\dagger} & & & & \\ \beta_1 & \alpha_2 & \beta_2^{\dagger} & & & \\ & \beta_2 & \alpha_3 & \beta_3^{\dagger} & & \\ & & \cdots\cdots & & & \\ & & & \cdots\cdots & & \\ & & & \cdots\cdots & & \\ & & & \beta_{N-2} & \alpha_{N-1} & \beta_{N-1}^{\dagger} \\ & & & & \beta_{N-1} & \alpha_N \end{pmatrix} \tag{2.8}$$

The eigenvalues of T are those of H because of unitary nature of X. In the next section the application of bisection method to *Sturm sequences* evaluates these eigenvalues in any desired interval.

2.2 Sturm Sequence

Let T_r be the leading $r \times r$ principal submatrix of an $N \times N$ hermitian matrix and define the polynomials $P_0(\lambda)$, ..., $P_N(\lambda)$, by:

$$P_0(\lambda) = 1 \tag{2.9}$$

$$P_r(\lambda) = \det(T_r - \lambda I) \tag{2.10}$$

for $r = 1, 2, 3, ..., N$. Then for any real value of λ the number of sign changes in the sequence S_1,

$$S_1 = \{P_0(\lambda), P_1(\lambda), ..., P_N(\lambda)\} \tag{2.11}$$

equals the number of eigenvalues of T less than λ [25]. Conventionally any zero terms in the sequence are considered as positive. For a tridiagonal matrix T a determinantal expansion can be used to derive the recurrence relation for $P_r(\lambda)$,

$$P_r(\lambda) = (\alpha_r - \lambda) P_{r-1}(\lambda) - \beta^{\dagger}_{r-1}\beta_{r-1} P_{r-2}(\lambda) \tag{2.12}$$

Alternatively one may form the ratios of successive determinants i.e.

$$d_{r-1}(\lambda) = \frac{P_r(\lambda)}{P_{r-1}(\lambda)} = \alpha_r - \lambda - \frac{\beta^{\dagger}_{r-1}\beta_{r-1}}{d_{r-1}(\lambda)} \tag{2.13}$$

where

$$d_0 = 1. \tag{2.14}$$

The number of sign changes in sequence S_1 is, then, the same as the number of negative terms in sequence S_2,

$$S_2 = \{ d_0(\lambda), d_1(\lambda), \ldots d_N(\lambda) \} \tag{2.15}$$

Once the number of eigenvalues in a specific interval is obtained one could home in on each one within any desired precision by bisecting the interval successively.

2.3 Rounding Errors

Theoretically, Lanczos iterations (2.1), (2.2) and (2.3) result in the exact tridiagonal form which is, in turn, diagonalized by Sturm sequences. However, the presence of rounding errors, destroys the orthogonality among the Lanczos vectors as the iterations proceed. This, as a result, complicates the relationship between the eigenvalues of T and H. To cope with this difficulty one might reorthogonalise the Lanczos vector to the previous vectors which are already obtained after each iteration. The reorthogonalisation procedure is obviously very time consuming and costly in storage space even if it is performed only once in each several iterations, or only to a small space of some selected vectors[2] which is usually much smaller than the set of previous Lanczos vectors.

The alternative approach which does not involve any kind of orthogonality enforcement focuses on the problem of ghost and spurious eigenvalues of tridiagonal matrices. To outline this method let $\tilde{X}$ be an $\tilde{N} \times \tilde{N}$ matrix formed by the first $\tilde{N}$ Lanczos vectors and $T_{\tilde{N}}$ an $\tilde{N} \times \tilde{N}$ tridiagonal matrix formed by the first $\tilde{N}$ α's and $\tilde{N}$-*1* β's. Then we define R, the remainder $\tilde{N} \times \tilde{N}$ matrix as:

$$R = H\tilde{X} - \tilde{X}T_{\tilde{N}} \tag{2.16}$$

Writing the matrices explicitly in terms of column vectors,

---

[2] The interested reader may refer to [26] for further discussion on this so called *Selective Reorthogonalisation.*

$$\tilde{X} = \left[x_1, x_2, x_3, \ldots, x_{\tilde{N}}\right] \tag{2.17}$$

$$T_{\tilde{N}} = \left[t_1, t_2, \ldots, t_{\tilde{N}}\right] \tag{2.18}$$

where

$$t_1 = \begin{pmatrix} \alpha_1 \\ \beta_1 \\ 0 \\ \vdots \\ 0 \end{pmatrix} \quad t_i = \begin{pmatrix} 0 \\ \vdots \\ \beta^{\dagger}_{i-1} \\ \alpha_i \\ \beta_i \\ \vdots \\ 0 \end{pmatrix} \quad t_N = \begin{pmatrix} 0 \\ \vdots \\ 0 \\ \beta^{\dagger}_{\tilde{N}-1} \\ \alpha_{\tilde{N}} \end{pmatrix} \tag{2.19}$$

and

$$R = \left[r_1, r_2, \ldots, r_{\tilde{N}}\right] \tag{2.20}$$

then Eq. (2.16) is written,

$$r_i = Hx_i - \tilde{X}t_i = \begin{cases} Hx_1 - x_1\alpha_1 - x_2\beta_1 & \text{if } i = 1 \\ Hx_i - x_{i-1}\beta^{\dagger}_{i-1} - x_i\alpha_i - x_{i+1}\beta_i & \text{if } 1 < i < \tilde{N} \\ Hx_{\tilde{N}} - x_{\tilde{N}-1}\beta^{\dagger}_{\tilde{N}-1} - x_{\tilde{N}}\alpha_{\tilde{N}} & \text{if } i = \tilde{N} \end{cases} \tag{2.21}$$

Using Eq. (2.3), Eq. (2.21) reads,

$$r_i = \begin{cases} 0 & \text{if } 1 \le i \le \tilde{N}-1 \\ x_{\tilde{N}+1}\beta_{\tilde{N}} & \text{if } i = \tilde{N} \end{cases} \tag{2.22}$$

i.e.

$$R = \left[0, 0, \ldots, x_{\tilde{N}+1}\beta_{\tilde{N}}\right] \tag{2.23}$$

Now let $T_{\tilde{N}}$ have an eigenvalue λ with eigenstate Φ. Applying both sides of Eq. (2.16) to Φ one obtains,

$$R\Phi = H\tilde{X}\Phi - \tilde{X}T_{\tilde{N}}\Phi \tag{2.24}$$

and since

$$R\Phi = \left[0, 0, \ldots, x_{\tilde{N}+1}\beta_{\tilde{N}}\right]\Phi = x_{\tilde{N}+1}\beta_{\tilde{N}}\Phi_{\tilde{N}} \tag{2.25}$$

where $\Phi_{\tilde{N}}$ is the $\tilde{N}^{\text{th}}$ component of Φ, Eq. (2.24) reads,

$$H\tilde{X}\Phi = \lambda\tilde{X}\Phi + x_{\tilde{N}+1}\beta_{\tilde{N}}\Phi_{\tilde{N}} \tag{2.26}$$

Eq. (2.26) indicates that λ, the eigenvalue of $T_{\tilde{N}}$ is also an eigenvalue of H with the eigenstate $\tilde{X}\,\Phi$ provided that $\Phi_{\tilde{N}} = 0$.

In practice rounding errors alter the remainder terms slightly and Eq. (2.23) holds only approximately i.e.

$$R \approx \left[\, 0,0,\ldots,x_{\tilde{N}+1}\beta_{\tilde{N}} \right] \tag{2.27}$$

This, in turn, affects Eq. (2.26), however it still holds within the machine precision i.e.

$$H\tilde{X}\Phi \approx \lambda\tilde{X}\Phi + x_{\tilde{N}+1}\beta_{\tilde{N}}\Phi_{\tilde{N}} \tag{2.28}$$

Accordingly, it would be enough for $\Phi_{\tilde{N}}$ to be very small so that the correspondence between the eigenvalues of $T_{\tilde{N}}$ and H remains valid. Actually we do not need to calculate $\Phi_{\tilde{N}}$ to decide if λ is an eigenvalue of H. Instead, we consider the reduced tridiagonal matrix $T_{\tilde{N}-1}$. Let Φ be an eigenstate of $T_{\tilde{N}}$ with corresponding λ, then

$$T_{\tilde{N}}\Phi = \lambda\Phi \tag{2.29}$$

or in terms of components,

$$\sum_{j=1}^{\tilde{N}} \left(T_{\tilde{N}}\right)_{ij} \Phi_j = \lambda\Phi_i \qquad i = 1, 2, 3, \ldots, \tilde{N} \tag{2.30}$$

which may be equivalently written as:

$$\sum_{j=1}^{\tilde{N}-1} \left(T_{\tilde{N}}\right)_{ij} \Phi_j + \left(T_{\tilde{N}}\right)_{i\tilde{N}} \Phi_{\tilde{N}} = \lambda\Phi_i \qquad i = 1, 2, 3, \ldots, \tilde{N} \tag{2.31}$$

If $\Phi_{\tilde{N}} \approx 0$ then Eq. (2.31) yields:

$$\sum_{j=1}^{\tilde{N}-1} \left(T_{\tilde{N}}\right)_{ij} \Phi_j \approx \lambda\Phi_i \qquad i = 1, 2, 3, \ldots, \tilde{N} \tag{2.32}$$

The first $\tilde{N}$ *-1* equations in system (2.32) could be combined to give:

$$T_{\tilde{N}-1}\hat{\Phi} = \lambda\hat{\Phi} \tag{2.33}$$

where $\hat{\Phi}$ is the reduced vector formed by removing the last component of Φ. The presence of $\left(T_{\tilde{N}}\right)_{i\tilde{N}} \Phi_{\tilde{N}}$ term in Eq. (2.31) indicates that the eigenvalues of $T_{\tilde{N}}$ undergo large shifts by removing $\alpha_{\tilde{N}}$ and $\beta_{\tilde{N}-1}$ unless $\Phi_{\tilde{N}} \approx 0$ in which case Eq. (2.33) shows that true eigenvalues of H are then the common eigenvalues of $T_{\tilde{N}}$ and $T_{\tilde{N}-1}$.

Once an eigenvalue of $T_{\tilde{N}}$ is known to be in the interval $(\lambda-\delta,\lambda+\delta)$, one can easily check if the corresponding eigenvalue of $T_{\tilde{N}-1}$ is in the same interval by checking the sign of $d_{\tilde{N}}$ at the end points of that interval. If either $d_{\tilde{N}}$ $(\lambda-\delta)$ is negative or $d_{\tilde{N}}$ $(\lambda+\delta)$ is positive, sequence S_2 confirms that λ is also an eigenvalue of the reduced matrix $T_{\tilde{N}-1}$ within the same precision δ. The smallest δ for which this condition holds fixes a measure of shift between the corresponding eigenvalues of $T_{\tilde{N}}$ and $T_{\tilde{N}-1}$. For a given λ large shift signals that the corresponding eigenvalue is a *spurious*[3] eigenvalue while a small shift singles out the true eigenvalue of H.

Due to the presence of rounding errors the complete spectrum of H can not be obtained from the eigenvalues of its tridiagonal form $T_{\tilde{N}}$. However the computed value of β_N which, in an exact arithmetic, vanishes, is no longer vanishing as a result of rounding errors. Consequently there is nothing to stop one from continuing the Lanczos iterations beyond N. We have observed that for large enough $\tilde{N}$ all the eigenvalues of H converge as the eigenvalues of $T_{\tilde{N}}$. The extreme eigenvalues in the spectrum of H converge faster and appear many times. These so called *ghosts* are recognized as H is assumed to be non-degenerate[4]. In practice one is only interested in particular eigenvalues, usually small ones. These could be obtained when $\tilde{N}$ is still much less than N. The rate of convergence of any eigenvalue depends on the absolute value of the eigenvalue, the density of the

---

[3] In our calculations we have recognized the spurious eigenvalues as those which shift by more than 10^{-10}.

[4] In practice we have recognized the ghosts as those eigenvalues which differ from each other by less than 10^{-13}.

eigenvalues in that region, and finally its location in the spectrum of H [27].

It is important to determine when to terminate the iterating process so that the desired eigenvalues are converged [28]. We discuss this problem later when we deal with matrix inversion. In fact the inverse of the matrix and its rate of convergence are mainly dominated by the smallest eigenvalues. We will see that the convergence of matrix inverse implies the convergence of small eigenvalues [29] and these are the ones which are of great interest in QCD studies.

2.4 Inversion

The problem of calculating columns of the inverse of a matrix, say H, is equivalent to solving the equation:

$$H\psi = \eta \tag{2.34}$$

for some vector η. The m^{th} column of H^{-1} is the solution $\psi = H^{-1}\eta$ if one chooses $\eta_i = \delta_{im}$. Letting η be the first Lanczos vector x_1, the Lanczos equations (2.1), (2.2) and (2.3) can be applied iteratively to calculate $H^{-1}x_1$. After K iterations $H^{-1}x_1$ is calculated as:

$$H^{-1}x_1 = V_K + H^{-1}x_K a_K + H^{-1}x_{K+1}b_K \tag{2.35}$$

where

$$V_K = \sum_{i=1}^{K} c_i x_i \tag{2.36}$$

for some coefficients a_K, b_K, c_1, c_2, c_3, ..., c_K. The series V_1, V_2, V_3, ..., V_K converges to $H^{-1}x_1$ as both a_K and b_K tend to zero. Using Eq. (2.3) for $i = k+1$ and eliminating $H^{-1}x_K$ between that and Eq. (2.35), $H^{-1}x_1$ is obtained as:

$$H^{-1}x_1 = V_K + x_{K+1}\left(\beta_K^{-1}\right)^{\dagger}a_K + H^{-1}x_{K+1}\left[b_K - \alpha_{K+1}\left(\beta_K^{-1}\right)^{\dagger}a_K\right]$$

$$- H^{-1}x_{K+2}\beta_{K+1}\left(\beta_K^{-1}\right)^{\dagger}a_K \tag{2.37}$$

Changing K to $K+1$ Eq. (2.35) can be written as:

$$H^{-1}x_1 = V_{K+1} + H^{-1}x_{K+1}a_{K+1} + H^{-1}x_{K+2}b_{K+1} \tag{2.38}$$

Having compared Eq. (2.37) with Eq. (2.38) the following recurrence relations are obtained for a's, b's and V's:

$$V_{K+1} = V_K + x_{K+1}\left(\beta_K^{-1}\right)^{\dagger} a_K \tag{2.39}$$

$$a_{K+1} = b_K - \alpha_{K+1}\left(\beta_K^{-1}\right)^{\dagger} a_K \tag{2.40}$$

$$b_{K+1} = -\beta_{K+1}\left(\beta_K^{-1}\right)^{\dagger} a_K \tag{2.41}$$

It is more convenient to rewrite these relations in matrix form as:

$$V_{K+1} = V_K + \left[x_{K+1}\left(\beta_K^{-1}\right)^{\dagger}, 0 \right] \begin{pmatrix} a_K \\ b_K \end{pmatrix} \tag{2.42}$$

$$\begin{pmatrix} a_{K+1} \\ b_{K+1} \end{pmatrix} = \begin{bmatrix} -\alpha_{K+1}\left(\beta_K^{-1}\right)^{\dagger} & 1 \\ -\beta_{K+1}\left(\beta_K^{-1}\right)^{\dagger} & 0 \end{bmatrix} \begin{pmatrix} a_K \\ b_K \end{pmatrix} \tag{2.43}$$

To obtain a_K and b_K from Eq. (2.43) iteratively it is essential to know the initial values, a_i and b_i for some i. If i iterations are already performed one might construct $H^{-1}x_I$ from a proper but arbitrary linear combination of Lanczos equations (2.3). Comparing the result with Eq. (2.35) at $K = i$ could provide one with the most general initial conditions on the a and b parameters. The most convenient initial conditions to apply to the Wilson fermion matrix are set up from the first two Lanczos equations:

$$Hx_1 = x_1\alpha_1 + x_2\beta_1 \tag{2.44}$$

$$Hx_2 = x_1\beta_1^{\dagger} + x_2\alpha_2 + x_3\beta_2 \tag{2.45}$$[5]

[5] Usually the equation $Hx_I = Hx_I$ is used instead of Eq. (2.45). However, as we will see later, it results in the failure of the algorithm in hadron spectroscopy with Wilson fermions.

Multiplying both sides of Eq. (2.44) by H^{-1} on the left and $\beta_1^{-1}R$ on the right and both sides of Eq. (2.45) by H^{-1} on the left and $\beta_2^{-1}S$ on the right, where R and S are arbitrary, $H^{-1}x_1$ is obtained as:

$$H^{-1}x_1 = \left(x_1\beta_1^{-1}R + x_2\beta_2^{-1}S\right)\left(\alpha_1\beta_1^{-1}R + \beta_1^{\dagger}\beta_2^{-1}S\right)^{-1}$$

$$-H^{-1}x_2\left(R + \alpha_2\beta_2^{-1}S\right)\left(\alpha_1\beta_1^{-1}R + \beta_1^{\dagger}\beta_2^{-1}S\right)^{-1}$$

$$-H^{-1}x_3S\left(\alpha_1\beta_1^{-1}R + \beta_1^{\dagger}\beta_2^{-1}S\right)^{-1} \qquad (2.46)$$

Comparing Eq. (2.46) with Eq. (2.35) for $k = 2$, a_2, b_2, and v_2 are obtained to be:

$$V_2 = \left(x_1\beta_1^{-1}R + x_2\beta_2^{-1}S\right)\left(\alpha_1\beta_1^{-1}R + \beta_1^{\dagger}\beta_2^{-1}S\right)^{-1} \qquad (2.47)$$

$$a_2 = -\left(R + \alpha_2\beta_2^{-1}S\right)\left(\alpha_1\beta_1^{-1}R + \beta_1^{\dagger}\beta_2^{-1}S\right)^{-1} \qquad (2.48)$$

$$b_2 = -S\left(\alpha_1\beta_1^{-1}R + \beta_1^{\dagger}\beta_2^{-1}S\right)^{-1} \qquad (2.49)$$

The last two relations are more conveniently written as:

$$\begin{pmatrix} a_2 \\ b_2 \end{pmatrix} = -\begin{pmatrix} R + \alpha_2\beta_2^{-1}S \\ S \end{pmatrix}\left(\alpha_1\beta_1^{-1}R + \beta_1^{\dagger}\beta_2^{-1}S\right)^{-1} \qquad (2.50)$$

Also one might define σ_2, an $N \times N$ matrix as:

$$\sigma_2 = \left[-x_1\beta_1^{-1},\ x_1\beta_1^{-1}\alpha_2\beta_2^{-1} - x_2\beta_2^{-1}\right] \qquad (2.51)$$

to rewrite Eq. (2.47) more conveniently as:

$$V_2 = \sigma_2\begin{pmatrix} a_2 \\ b_2 \end{pmatrix} \qquad (2.52)$$

Now that the starting conditions are known (2.43) can be used iteratively to yield:

$$\begin{pmatrix} a_K \\ b_K \end{pmatrix} = \begin{bmatrix} -\alpha_K \left(\beta_{K-1}^{-1}\right)^{\dagger} & 1 \\ -\beta_K \left(\beta_{K-1}^{-1}\right)^{\dagger} & 0 \end{bmatrix} \cdots \begin{bmatrix} -\alpha_3 \left(\beta_2^{-1}\right)^{\dagger} & 1 \\ -\beta_3 \left(\beta_2^{-1}\right)^{\dagger} & 0 \end{bmatrix} \begin{pmatrix} a_2 \\ b_2 \end{pmatrix} \tag{2.53}$$

and for obvious definition for π_K,

$$\begin{pmatrix} a_K \\ b_K \end{pmatrix} = \pi_K \begin{pmatrix} a_2 \\ b_2 \end{pmatrix} \tag{2.54}$$

where

$$\pi_2 = \begin{bmatrix} 1 & 0 \\ 0 & 1 \end{bmatrix} \tag{2.55}$$

and

$$\pi_K = \begin{bmatrix} -\alpha_K \left(\beta_{K-1}^{-1}\right)^{\dagger} & 1 \\ -\beta_K \left(\beta_{K-1}^{-1}\right)^{\dagger} & 0 \end{bmatrix} \pi_{K-1} \tag{2.56}$$

Using Eq. (2.54), Eq. (2.42) can be written in terms of initial conditions as:

$$V_{K+1} = V_K + \left[x_{K+1} \left(\beta_K^{-1}\right)^{\dagger}, 0 \right] \pi_K \begin{pmatrix} a_2 \\ b_2 \end{pmatrix} \tag{2.57}$$

It is more useful if we write Eq. (2.57) in a more closed form. Using Eq. (2.52) for V_2 and defining σ_3 as:

$$\sigma_3 = \sigma_2 + \left[x_3 \left(\beta_2^{-1}\right)^{\dagger}, 0 \right] \pi_2 \tag{2.58}$$

we get for V_3,

$$V_3 = \sigma_3 \begin{pmatrix} a_2 \\ b_2 \end{pmatrix} \tag{2.59}$$

One might obtain similar relations for V_4, V_5, ..., and in general V_K could be obtained as:

$$V_K = \sigma_K \begin{pmatrix} a_2 \\ b_2 \end{pmatrix} \tag{2.60}$$

where

$$\sigma_{K+1} = \sigma_K + \left[x_{K+1} \left(\beta_K^{-1} \right)^{\dagger}, 0 \right] \pi_K \tag{2.61}$$

Returning to the question of convergence of $H^{-1} x_1$, we required $\begin{pmatrix} a_K \\ b_K \end{pmatrix}$ to vanish for some K. Eq. (2.54) translates this problem to whether π_K has a zero eigenvalue in which case $\begin{pmatrix} a_2 \\ b_2 \end{pmatrix}$ or equivalently $\begin{pmatrix} R+\alpha_2\beta_2^{-1}S \\ S \end{pmatrix}$ can be considered as the corresponding eigenstate. However, Eq. (2.56) shows that:

$$\det \pi_K = \prod_{i=2}^{k-1} \beta_{i+1} \left(\beta_i^{-1} \right)^{\dagger} \tag{2.62}^{6}$$

We have already seen that due to rounding errors β_i do not vanish and accordingly *det* π_K fluctuate about a finite value. As a result, if one of the eigenvalues of π_K converges to zero the other one diverges. This in turn reflects the divergence of elements of π_K due to rounding errors as the algorithm proceeds. We are interested to find a condition among the elements of π_K which reflects the convergence of one of its eigenvalues to zero. It is difficult to search for such a condition while the π_K elements are too large. However, this difficulty could be avoided if we write π_K, without loss of generality, in the following representation:

$$\pi_K = \begin{bmatrix} A_K & A_K y_K \\ B_K & B_K y_K + t_K \end{bmatrix} \tag{2.63}$$

Written in this form, π_K has a zero eigenvalue if and only if $A_K t_K$ converges to zero, even if A_K, B_K and y_K diverge.

Let, after K_0 iterations, $A_{K_0} t_{K_0}$ become arbitrarily small. Then as we have seen $\begin{pmatrix} a_{K_0} \\ b_{K_0} \end{pmatrix} \to 0$ and Eqs. (2.50) and (2.54) fix the parameters R and S as:

---

6 In single Lanczos algorithm where, according to Eq. (2.2), the β 's are real numbers (contrary to the block algorithm discussed in §2.10) Eq. (2.62) is simplified to $\beta_K \beta_2^{-1}$.

$$\begin{pmatrix} R \\ S \end{pmatrix} = C \begin{pmatrix} \alpha_2 \beta_2^{-1} + y_{K_0} \\ -1 \end{pmatrix} \tag{2.64}$$

where C is a constant which can be set to unity without loss of generality. Moreover they yield:

$$\begin{pmatrix} a_{K_0} \\ b_{K_0} \end{pmatrix} = \begin{pmatrix} 0 \\ -t_{K_0} \end{pmatrix} \left(-\alpha_1 \beta_1^{-1} y_{K_0} - \alpha_1 \beta_1^{-1} \alpha_2 \beta_2^{-1} + \beta_1^{\dagger} \beta_2^{-1} \right)^{-1} \tag{2.65}$$

As the elements of π_K grow large the elements of σ_K will grow as well according to Eq. (2.61). As for π_K, one can separate the error built divergent part of σ_K if it is written in a similar fashion,

$$\sigma_K = \left[U_K , U_K y_K + W_K \right] \tag{2.66}$$

where U_K and W_K are N-component vectors. Written in this form and incorporating Eqs. (2.50) and (2.64) in Eq. (2.60) the convergent solution, $H^{-1}x_1$ is achieved after K_0 iterations even if U_K and W_K diverge, as:

$$V_{K_0} = -W_{K_0} \left(-\alpha_1 \beta_1^{-1} y_{K_0} - \alpha_1 \beta_1^{-1} \alpha_2 \beta_2^{-1} + \beta_1^{\dagger} \beta_2^{-1} \right)^{-1} \tag{2.67}$$

and Eqs. (2.35) and (2.65) evaluate the residue term after K_0 iterations, i.e. $//x_1 - HV_{k_0}//$, as:

$$\mathrm{Res}_{K_0} = \left\| -t_{K_0} \left(-\alpha_1 \beta_1^{-1} y_{K_0} - \alpha_1 \beta_1^{-1} \alpha_2 \beta_2^{-1} + \beta_1^{\dagger} \beta_2^{-1} \right)^{-1} \right\| \tag{2.68}$$

In Eqs. (2.65) and (2.67) the remainder term and the solution are given in terms of t_{K_0}, y_{K_0} and W_{K_0}. So it is necessary to translate the recursive relations for π_K and σ_K into the relations for t_{K_0}, y_{K_0} and W_{K_0}. Eqs. (2.56) and (2.63) result in:

$$A_{K+1} = -\alpha_{K+1} \left(\beta_K^{\dagger} \right)^{-1} A_K + B_K \tag{2.69}$$

$$B_{K+1} = -\beta_{K+1} \left(\beta_K^{\dagger} \right)^{-1} A_K \tag{2.70}$$

$$y_{K+1} = y_K + \left(A_{K+1}\right)^{-1} t_K \tag{2.71}$$

$$t_{K+1} = -B_{K+1}\left(A_{K+1}\right)^{-1} t_K \tag{2.72}$$

Similarly Eqs. (2.61), (2.63) and (2.66) will result in:

$$U_{K+1} = U_K + x_{K+1}\left(\beta_K^{\dagger}\right)^{-1} A_K \tag{2.73}$$

$$W_{K+1} = W_K - U_{K+1}\left(A_{K+1}\right)^{-1} t_K \tag{2.74}$$

Being evaluated after K_0 iterations, when $A_{K_0} t_{K_0} \rightarrow 0$, the above equations provide us with the converged solution and the residue term. In practice one might monitor the residue and the solution after each step by the following algorithm:

$$A_{i+1} = -\alpha_{i+1}\left(\beta_i^{\dagger}\right)^{-1} A_i + B_i \tag{2.75}$$

$$B_{i+1} = -\beta_{i+1}\left(\beta_i^{\dagger}\right)^{-1} A_i \tag{2.76}$$

$$y_{i+1} = y_i + \left(A_{i+1}\right)^{-1} t_i \tag{2.77}$$

$$t_{i+1} = -B_{i+1}\left(A_{i+1}\right)^{-1} t_i \tag{2.78}$$

$$U_{i+1} = U_i + x_{i+1}\left(\beta_i^{\dagger}\right)^{-1} A_i \tag{2.79}$$

$$W_{i+1} = W_i - U_{i+1}\left(A_{i+1}\right)^{-1} t_i \tag{2.80}$$

$$V_{i+1} = -W_{i+1}\left(-\alpha_1\beta_1^{-1} y_{i+1} - \alpha_1\beta_1^{-1}\alpha_2\beta_2^{-1} + \beta_1^{\dagger}\beta_2^{-1}\right)^{-1} \tag{2.81}$$

$$\text{Res}_{i+1} = \left\| -t_{i+1}\left(-\alpha_1\beta_1^{-1} y_{i+1} - \alpha_1\beta_1^{-1}\alpha_2\beta_2^{-1} + \beta_1^{\dagger}\beta_2^{-1}\right)^{-1} \right\| \tag{2.82}$$

where the initial values A_2, B_2, y_2 and t_2 are obtained from Eqs. (2.55) and (2.63) and U_2 and W_2 from Eqs. (2.51) and (2.66) as:

$$A_2 = 1 \tag{2.83}$$

$$B_2 = 0 \tag{2.84}$$

$$y_2 = 0 \tag{2.85}$$

$$t_2 = 1 \tag{2.86}$$

$$U_2 = -x_1\beta_1^{-1} \tag{2.87}$$

$$W_2 = -x_2\beta_2^{-1} + x_1\beta_1^{-1}\alpha_2\beta_2^{-1} \tag{2.88}$$

$$V_2 = \left(x_2 - x_1\beta_1^{-1}\alpha_2\right)\left(-\alpha_1\beta_1^{-1}\alpha_2 + \beta_1^{\dagger}\right)^{-1} \tag{2.89}$$

In hadron propagator calculations, as discussed in Chapter 4, the first Lanczos vector must be a δ-function located at a certain site to calculate the appropriate column of the inverse of $\gamma_5 M$ where M is the fermion matrix. For Wilson fermions where M is given by Eq. (1.112) it is easily shown that the Lanczos equations (2.1) to (2.3) result in $\alpha_2 = 0$ for such an initial Lanczos vector. If the algorithm had initially fixed A_1, B_1, etc. rather than A_2, B_2, etc. then A_2 would have vanished which in turn would have resulted in divergent y_2, t_2, etc. and consequently the failure of the algorithm to converge. This is the case for the algorithm given in [30] and that is the reason why we modified the standard algorithm.

2.5 Convergence Of Eigenvalues And Inversion

The convergence of eigenvalues of H in a given neighborhood around λ can be related to the convergence of $(H-\lambda\mathbb{1})^{-1}x_1$ in the Lanczos algorithm. To see this consider $P_K(\lambda)$, the $det\,(T_K-\lambda\mathbb{1})$ where T_K is the tridiagonal form of H after K iterations, given by Eq. (2.12) as:

$$P_K(\lambda) = (\alpha_K - \lambda)\, P_{K-1}(\lambda) - \beta^{\dagger}_{K-1}\beta_{K-1}\, P_{K-2}(\lambda) \tag{2.90}$$

Defining:

$$\bar{C}_K(\lambda) = \frac{(-1)^{K+1} P_K(\lambda)}{\prod_{i=1}^{K} \beta_i} \tag{2.91}$$

where

$$\bar{C}_0(\lambda) = -1 \tag{2.92}$$

then we get:

$$\bar{C}_K(\lambda) = -\frac{\alpha_K - \lambda}{\beta_K} \bar{C}_{K-1}(\lambda) - \frac{\beta^{\dagger}_{K-1}}{\beta_K} \bar{C}_{K-2}(\lambda) \tag{2.93}$$

or

$$\left(\bar{C}_K(\lambda), \bar{C}_{K+1}(\lambda)\right) = \left(\bar{C}_{K-1}(\lambda), \bar{C}_K(\lambda)\right) \begin{pmatrix} 0 & -\frac{\beta^{\dagger}_K}{\beta_{K+1}} \\ 1 & -\frac{\alpha_{K+1} - \lambda}{\beta_{K+1}} \end{pmatrix} \tag{2.94}$$

We had previously defined π_{K+1} in Eq. (2.56) for H. Changing α_{K+1} to $\alpha_{K+1}-\lambda$ in π_{K+1} would define π_{K+1} for $H-\lambda \mathbf{1}$ as:

$$\pi_{K+1}(\lambda) = \begin{pmatrix} -(\alpha_{K+1} - \lambda)(\beta^{\dagger}_K)^{-1} & 1 \\ -\beta_{K+1}(\beta^{\dagger}_K)^{-1} & 0 \end{pmatrix} \pi_K(\lambda) \tag{2.95}$$

Eqs. (2.94) and (2.95) result in:

$$\left(\bar{C}_K(\lambda), \bar{C}_{K+1}(\lambda)\right)\pi_{K+1}(\lambda) = \left(\bar{C}_{K-1}(\lambda), \bar{C}_K(\lambda)\right)\pi_K(\lambda) = \cdots$$

$$= \left(\bar{C}_1(\lambda), \bar{C}_2(\lambda)\right) = \omega(\lambda) \tag{2.96}$$

where $\omega(\lambda)$ is independent of K. Eq. (2.96) yields:

$$\bar{C}_K(\lambda) = \omega(\lambda)\pi_k^{-1}(\lambda) \begin{pmatrix} 0 \\ 1 \end{pmatrix} \tag{2.97}$$

Therefore Eq. (2.91) gives for determinant $P_K(\lambda)$,

$$P_K(\lambda) = (-1)^{K+1}\left(\prod_{i=1}^{K}\beta_i\right)\omega(\lambda)\pi_K^{-1}(\lambda)\begin{pmatrix}0\\1\end{pmatrix} \tag{2.98}$$

Let λ_T and λ_H be some eigenvalues of T_K and H, respectively, in the interesting neighborhood around λ. We are interested to study the behaviour of $P_K(\lambda)$ at these values of λ. Let us first consider $P_K(\lambda_H)$. We expand x_{K+1}, the $K+1^{st}$ Lanczos vector in terms of ψ_h, the eigenstates of H:

$$x_{K+1} = \sum_{h=1}^{N} C_{Kh}\psi_h \qquad K = 0, 1, 2, \ldots \tag{2.99}$$

The Lanczos equations (2.3), could then imply:

$$C_{0h}\lambda_h = C_{0h}\alpha_1 + C_{1h}\beta_1 \tag{2.100}$$

$$C_{Kh}\lambda_h = C_{K-1\,h}\,\beta^{\dagger}_{K} + C_{Kh}\alpha_{K+1} + C_{K+1\,h}\,\beta_{K+1} \tag{2.101}$$

where λ_h are eigenvalues of H. Eq. (2.101) results in:

$$C_{Kh} = -\frac{\alpha_K - \lambda_h}{\beta_K}C_{K-1\,h} - \frac{\beta^{\dagger}_{K-1}}{\beta_K}\,C_{K-2\,h} \tag{2.102}$$

where

$$C_{1h} = -\frac{\alpha_1 - \lambda_h}{\beta_1}C_{0h} \tag{2.103}$$

Eq. (2.102) has exactly the same form as Eq. (2.93) for $\bar{C}_K(\lambda)$. By the same approach we deduce an equation similar to Eq. (2.97) for C_{Kh} as:

$$C_{K\,h} = -\,C_{0h}\,\omega(\lambda_h)\,\pi_K^{-1}(\lambda_h)\begin{pmatrix}0\\1\end{pmatrix} \tag{2.104}$$

Comparing Eq. (2.104) with Eq. (2.98) we get:

$$P_K(\lambda_h) = (-1)^{K+1}\left(\prod_{i=1}^{K}\beta_i\right)C_{Kh} \tag{2.105}$$

As the Lanczos vectors are unit vectors Eq. (2.99) imposes the constraint:

$$\sum_{h=1}^{N} C_{Kh}^{\,2} = 1 \tag{2.106}$$

on the C_{Kh}'s. Accordingly none of C_{Kh}'s diverge. On the other hand if x_1 is not normal to ψ_h then β_i are non-vanishing. Even if x_1 is perpendicular to ψ_h in which case $C_{0h} = 0$, then as we had discovered before one of the β's, say β_j, would converge to zero and it is easy to show that $\frac{\beta_j}{C_{0h}}$ and consequently $\beta_j\, \omega(\lambda_h)$ would remain finite. These considerations imply that $P_K(\lambda_h)$ is different from zero and $O(1)$. On the other hand the $det\,(T_K - \lambda \mathbb{1})$ must vanish for all eigenvalues of T_K. We summarize these results as:

$$P_K(\lambda_H) \approx O(1) \tag{2.107}$$

$$P_K(\lambda_T) = 0 \tag{2.108}$$

Eqs. (2.107) and (2.108) show that as λ_H converges i.e. as $\lambda_T \rightarrow \lambda_H$, $P_K(\lambda)$ changes rapidly from zero to a non-zero value. This sudden jump is an indication of the same behaviour in $\pi_K^{-1}(\lambda)$ once viewed through Eq. (2.98). The large value of $\pi_K^{-1}(\lambda)$ is in turn the sign of convergence of one of the eigenvalues of $\pi_K(\lambda)$ to zero which is necessary and sufficient condition for the convergence of $(H - \lambda \mathbb{1})^{-1} x_1$. Conversely convergence of $(H - \lambda \mathbb{1})^{-1} x_1$ implies the divergence of $\pi_K^{-1}(\lambda)$ which in turn implies that $P_K(\lambda)$ picks up a non-zero value in Eq. (2.98). In particular $P_K(\lambda)$ remains non-zero even if λ is an eigenvalue of T_K. So λ must be close to one of eigenvalues of H. For example $H^{-1}x_1$ converges whenever the small eigenvalues of H are converged and conversely small eigenvalues of H are converged as $A_{K_0} t_{K_0} \rightarrow 0$ (i.e. as $H^{-1}x$ converges). In our calculations we terminate the algorithm when $A_{K_0} t_{K_0}$ (or practically t_{K_0}) falls below 10^{-12}. This proved to guarantee the convergence of the closest eigenvalues to zero. The same stopping condition is sufficient to converge the closest eigenvalues to λ provided we change α's to $\alpha - \lambda$.

2.6 Lanczos Algorithm Results

We will present our results on the application of Lanczos algorithm for eigenvalue calculations in the next chapter where we directly deal with fermion matrix spectrum. In the present chapter we concentrate on the inversion applications. To investigate the practical aspects of the hermitian Lanczos algorithm and the subsequent algorithms discussed in this chapter we have always worked solely with $\gamma_5 M$ where M is the Wilson fermion matrix given by Eq. (1.112). Though M is not hermitian, $\gamma_5 M$ is[7] and this is what we intend to invert to calculate meson propagators later on in Chapter 4.

We work with 4^4 and 8^4 lattices. As the results are similar we outline the findings on the latter. For this lattice we generated a gauge field configuration in the confining phase at $\beta = 5.8$ (see Fig. 3.9) obtained by 13300 sweeps from a hot start. As we shall describe in Chapter 3 there are values of κ at which $\gamma_5 M$ has a zero eigenvalue. The corresponding eigenstate is called a zero mode. For the above gauge configuration the $\gamma_5 M$ matrix spectrum indicates that the first two values of hopping parameter corresponding to the first two zero modes i.e. κ_z's, are 0.1619 and 0.1649 with the minimum modulus eigenvalues λ_z of 0.1820E-3 and 0.8898E-5 respectively[8] when antiperiodic boundary conditions are imposed on fermion fields. We have also studied the effects of boundary conditions on the algorithms. Since their general qualitative features do not alter, we work with antiperiodic boundary conditions on the fermion fields throughout; otherwise indicated explicitly.

As we tune κ, the convergence rate of the inversion is observed to be governed by $/\lambda/_{min}$ and its density and slows down as we approach κ_z from either side as seen in Table 2.1 where the minimum number of iterations, N_{it}, so that the norm of residue falls below 10^{-8} is given as κ changes. The corresponding

---

[7] See §3.7.

[8] A number followed by a letter E (or D) and an integer exponent represents a power of 10 held with a precision of about 7 (or 14) decimal digits.

Table 2.1

Convergence rate of the Lanczos algorithm for an 8^4 lattice at $\beta = 5.8$. The number of eigenvalues with moduli less than 0.05 is found to be 7 for all the κ's listed.

κ	$\lvert\lambda\rvert_{min}$	N_{it}
0.1590	0.1206E-1	918
0.1619	0.1820E-3	*
0.1630	0.3765E-2	1078
0.1649	0.8898E-5	*
0.1650	0.1279E-3	1156
0.1670	0.2223E-2	1048

* No inversions were performed at the corresponding κ_c.

behaviour is plotted in Fig. 2.1 for 2 values of κ.

Although the solution vectors have converged and their norms have reached plateaus long before residues fall below 10^{-8} as shown in Fig. 2.2, it is a direct check of legitimacy of the converged solution ψ_c, if we check whether η-$H\psi_c$ i.e. the real residue vector vanishes. It is also interesting to see the behaviour of Res_n

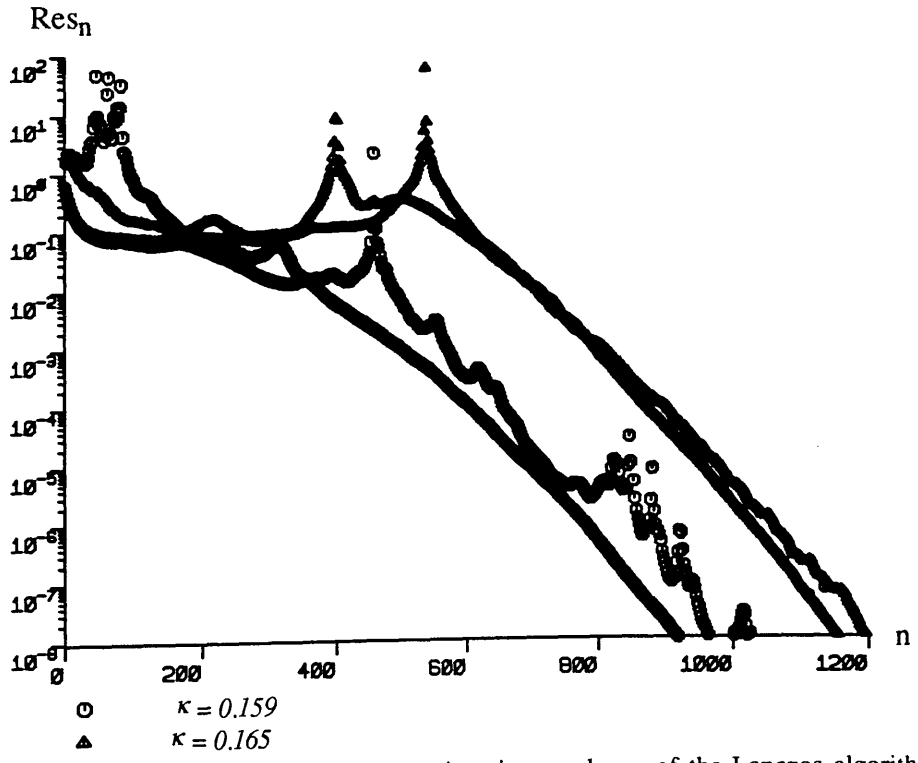

Fig. 2.1 The norm of residue Res_n vs. iteration number n of the Lanczos algorithm for an 8^4 lattice at $\beta = 5.8$.

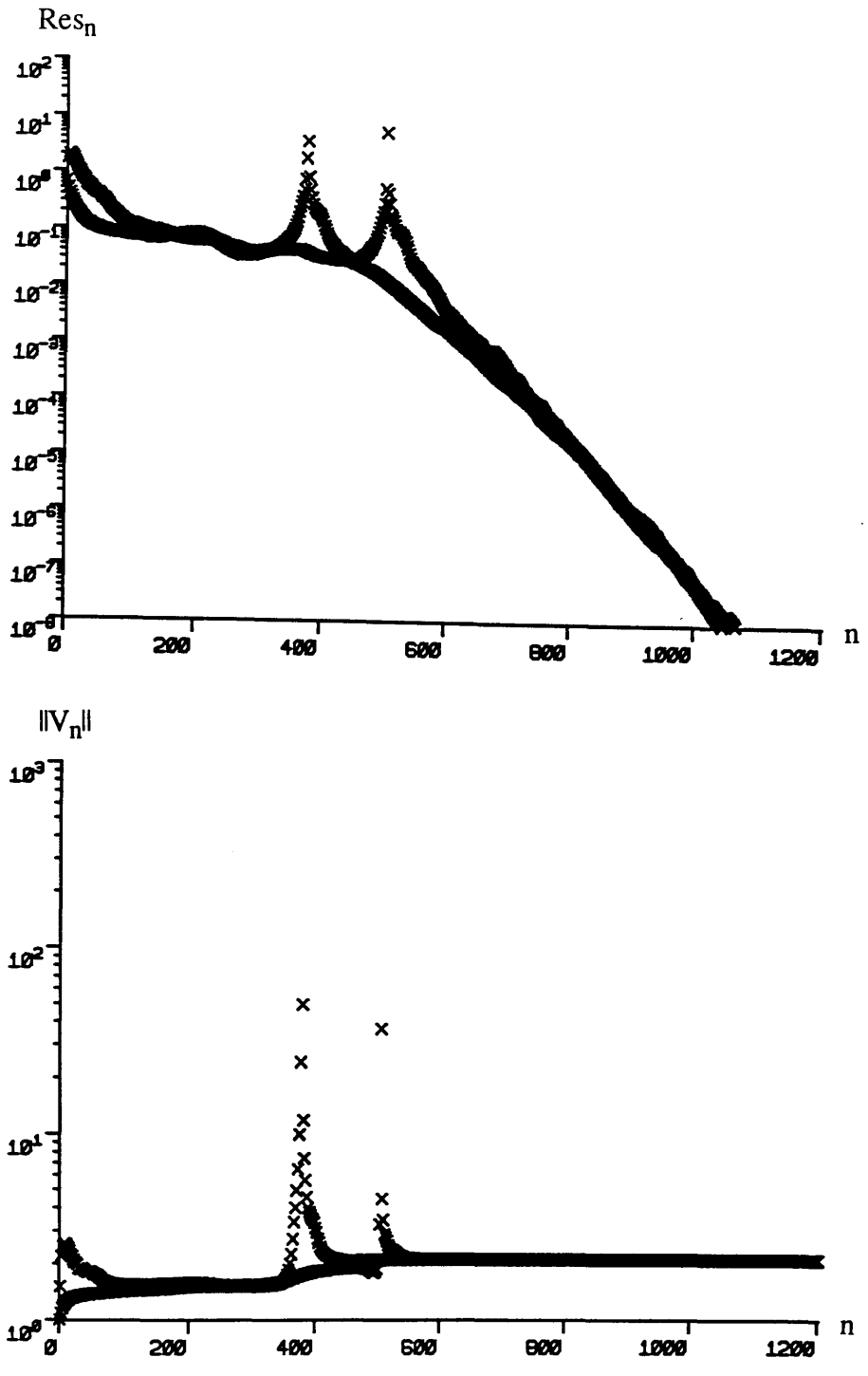

Fig. 2.2 The norms of residue Res_n (top) and solution vectors (above) vs. iteration number n of the Lanczos algorithm for an 8^4 lattice at $\beta = 5.8$ and $\kappa = 0.163$.

compared with the norm of the real residue as the algorithm proceeds. We found, in exact arithmetic, that Res_n as shown in Eq. (2.82) is exactly the same as real residue norm $//x_1\text{-}HV_n//$ in each step. However our results show that as one approaches very close to κ_z the very small Res_n's tend to vanish slightly faster

than the real residue as indicated in Table 2.2 for $\kappa = 0.165$. This can be interpreted as the limitation of the machine precision.

It is interesting to see that both norms of residue and solution vector behave as if they are superpositions of two independent residues or solution vectors, obtained from the odd and even iteration numbers respectively as in Fig. 2.3.

2.7 Conjugate Gradient Algorithm

2.7.1 Positive Definite Matrices

An alternative approach to solve Eq. (2.34) when H is an $N \times N$ positive definite hermitian matrix is the conjugate gradient iterative algorithm. The idea is based on a procedure that produces a sequence of residue vectors, r's, that are all mutually orthogonal and a sequence of p vectors that are all mutually conjugate [31]. Defining ψ_i to be the approximation to ψ after i iterations and $r_i \equiv \eta - H\psi_i$ as the corresponding residue vector, the algorithm is outlined as follows:

$$a_i = \left(p_i^\dagger H p_i\right)^{-1}\left(r_i^\dagger r_i\right) \tag{2.109}$$

$$\psi_{i+1} = \psi_i + p_i a_i \tag{2.110}$$

$$r_{i+1} = r_i - H p_i a_i \tag{2.111}$$

$$b_i = \left(r_i^\dagger r_i\right)^{-1}\left(r_{i+1}^\dagger r_{i+1}\right) \tag{2.112}$$

$$p_{i+1} = r_{i+1} + p_i b_i \tag{2.113}$$

Table 2.2

The difference between Res_n and $//x_1 - HV//$.

N_{it}	Res	$\|x_1 - HV\|$
1150	0.1201E-07	0.1201E-07
1250	0.2658E-09	0.5706E-09
1350	0.5163E-11	0.5048E-09

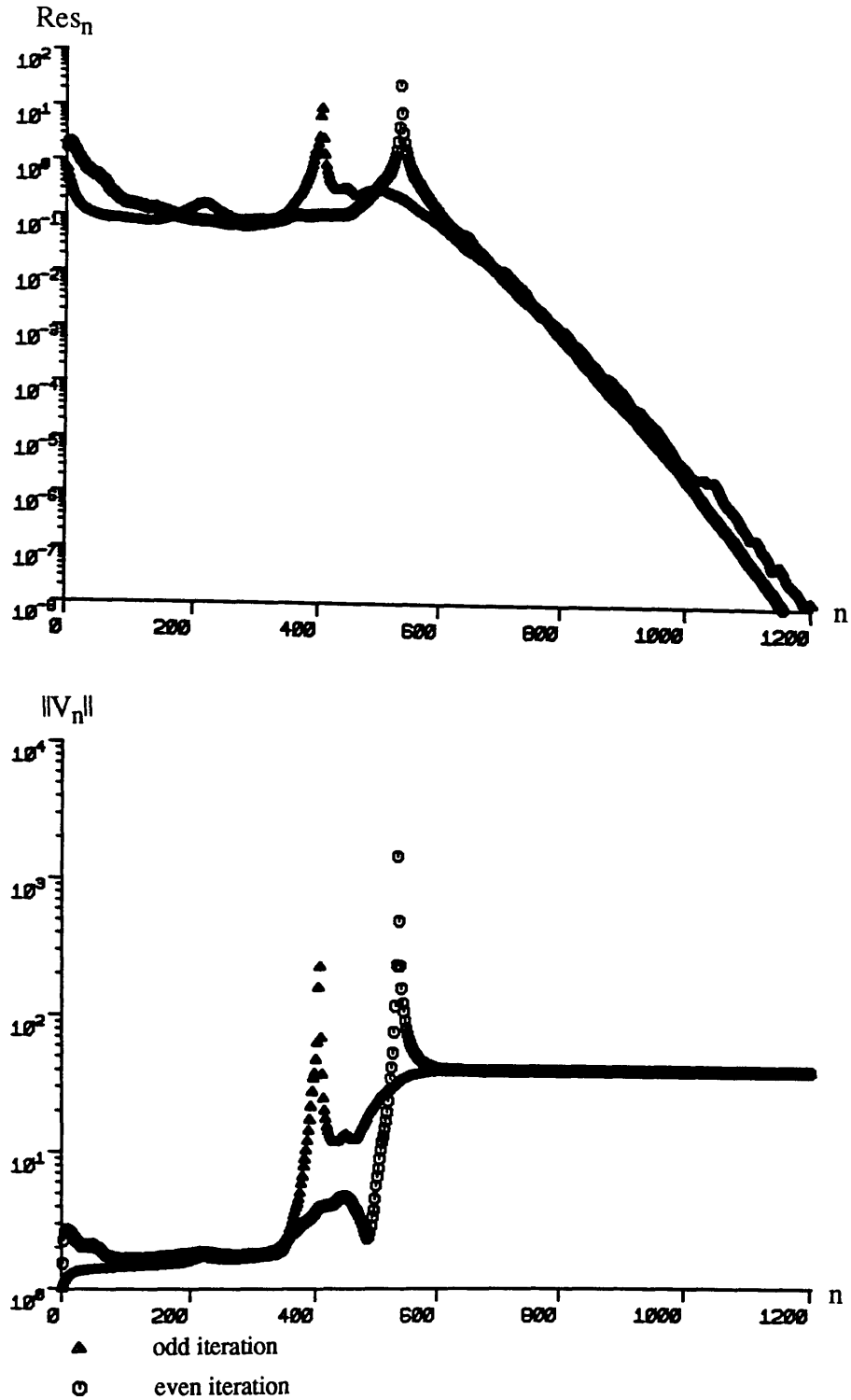

Fig. 2.3 The norm of residue vector Res_n (top) and the norm of solution vector (above) vs. iteration number n of the Lanczos algorithm for an 8^4 lattice at $\beta = 5.8$ and $\kappa = 0.165$.

where

$$p_1 = r_1 = \eta - H\Psi_1 \tag{2.114}$$

and ψ_1 is an arbitrary vector taken to be the null vector.

The orthogonality of $\{r_i / i = 1, 2, 3, ..., N\}$ and the H-conjugacy of $\{ p_i / i = 1,2,3,...,N\}$ i.e.

$$r_i r_j = 0 \qquad \text{if } i \neq j \leq N \tag{2.115}$$

and

$$p_i H p_j = 0 \qquad \text{if } i \neq j \leq N \tag{2.116}$$

could be proved by straight forward induction [32]. As there are at most only N linearly independent orthogonal vectors in an N-dimensional complete set, Eq. (2.115) implies that r_{N+1} vanishes. This in turn means that we have reached the solution of Eq. (2.34) because:

$$\eta - H\psi_{N+1} = r_{N+1} = 0 \tag{2.117}$$

To reflect the geometrical content of the conjugate gradient algorithm we review alternative approach to prove its convergence. Define the functional:

$$F[\psi] = \frac{1}{2}\psi^{\dagger} H \psi - \psi^{\dagger}\eta \tag{2.118}$$

in the space spanned by $\{p_i\}$. It is obvious that the problem of solving Eq. (2.34) is identical to minimizing the functional F. In other words the solution ψ to Eq. (2.34) is the point at which F is minimum (maximum if H is negative definite). We can calculate all the N components of ψ in this space in N steps if we minimize F in the n-dimensional hyperplane spanned by the subspace $\{ p_i / i = 1,2,3,...,n\}$ through ψ_1 in the n^{th} step. This is equivalent to starting from ψ_1 and minimizing F along conjugate direction p_1 to arrive at ψ_2 and then starting from ψ_2 and minimizing F along conjugate direction p_2 to arrive at ψ_3 and so forth. The general form of ψ in the n^{th} step, i.e. ψ_{n+1}, can be written in terms of its components along p_i as:

$$\psi_{n+1} = \psi_1 + \sum_{i=1}^{n} p_i a_i = \psi_1 + PA \tag{2.119}$$

where

$$A=\left(a_1,a_2,a_3,\ldots,a_n\right) \tag{2.120}$$

and

$$P=\left[p_1,p_2,p_3,\ldots,p_n\right] \tag{2.121}$$

For this value of ψ_{n+1}, F is evaluated to be:

$$F\left[\psi_{n+1}\right]=F\left[\psi_1\right]+\frac{1}{2}A^{\dagger}P^{\dagger}HPA+A^{\dagger}P^{\dagger}r_1 \tag{2.122}$$

We are interested in such a vector A which translates ψ_1 to the minimum of F in the subspace $\{ p_i / i = 1,2,3,\ldots,n\}$. This is obtained by setting the functional derivative of F with respect to A equal to zero i.e.:

$$P^{\dagger}HPA - P^{\dagger}r_1 = 0 \tag{2.123}$$

The i^{th} component of Eq. (2.123) reads:

$$\sum_{j=1}^{n}\left(p_i^{\dagger}Hp_j\right)a_j = p_i^{\dagger}r_1 \tag{2.124}$$

The H-conjugacy of p's reduces Eq. (2.124) to:

$$a_i=\left(p_i^{\dagger}Hp_i\right)^{-1}p_i^{\dagger}r_1 \qquad i = 1, 2, 3, \ldots n \tag{2.125}$$

On the other hand taking the orthogonality of r's into account Eq. (2.113) can be manipulated to yield:

$$p_i^{\dagger}r_1 = r_i^{\dagger}r_i \tag{2.126}$$

Then a_i is rewritten as:

$$a_i=\left(p_i^{\dagger}Hp_i\right)^{-1}r_i^{\dagger}r_i \qquad i = 1, 2, 3, \ldots n \tag{2.127}$$

These values of a_i are exactly those used in the course of the algorithm to build up ψ through Eqs. (2.109) and (2.110). This means that after at most N iterations of the conjugate gradient algorithm we achieve the minimum of F or equivalently the exact solution of Eq. (2.34). Moreover, in the intermediate stages the residue vectors are:

$$r_{i+1} = \eta - H\psi_{i+1} = \eta - H\psi_i - Hp_ia_i = r_i - Hp_ia_i \qquad (2.128)$$

as stated by Eq. (2.111) in the algorithm.

2.7.2 Non-Definite Matrices

As discussed in the previous section the conjugate gradient algorithm is applicable to solve Eq. (2.34) only when H has definite positiveness or negativeness (in which case $-H$ is positive definite). In the absence of such definitness or even when H is not hermitian one might multiply both sides of Eq. (2.34) by $H^\dagger$ to replace H by $H^\dagger H$ which is a positive definite matrix. This multiplication does not change the solution to Eq. (2.34). Changing η to $H^\dagger\eta$ and H to $H^\dagger H$ and as a result r_i to $H^\dagger r_i$, the modified algorithm would read as follows:

$$a_i = \left[\left(Hp_i\right)^\dagger\left(Hp_i\right)\right]^{-1}\left(H^\dagger r_i\right)^\dagger\left(H^\dagger r_i\right) \qquad (2.129)$$

$$\psi_{i+1} = \psi_i + p_ia_i \qquad (2.130)$$

$$r_{i+1} = r_i - Hp_ia_i \qquad (2.131)$$

$$b_i = \left[\left(H^\dagger r_i\right)^\dagger\left(Hr_i\right)\right]^{-1}\left(H^\dagger r_{i+1}\right)^\dagger\left(H^\dagger r_{i+1}\right) \qquad (2.132)$$

$$p_{i+1} = H^\dagger r_{i+1} + p_ib_i \qquad (2.133)$$

where $p_1 = H^\dagger r_1$ and $r_1 = \eta - H\psi_1$ and as before ψ_1 is taken to be the null vector. Since in this algorithm, which we call $H^\dagger H$ algorithm, a's, b's and p's are defined differently, the r's and ψ's in each step would now differ from the corresponding values in original algorithm, which we will call H algorithm. Moreover since there are two matrix-vector multiplications, each step takes twice longer than it does for the H algorithm.

2.8 Rounding Errors And Convergence

In the previous section we saw that the conjugate gradient algorithm converges in at most N iterations in exact arithmetic. However the rounding errors developed in calculating r and p vectors make the algorithm fail in preserving the orthogonality among the r vectors and H-conjugacy among the p vectors. Also, for large enough number of iterations the accumulation of rounding errors in the residual vector may become very large when we need the residue to be negligible. This might hamper the convergence of the algorithm in applications such as eigenvalue calculations at the presence of almost zero modes. In this case any large enough residue corresponds to a set of solution vectors differing from each other by the zero mode. The right solution can be detected only if extremely small residue norms of the order of the corresponding eigenvalue of the zero mode are achievable. This in turn requires an extremely large number of iterations before the right solutions can converge. However, as stated above, here is a situation where the rounding errors become considerably large. The situation, here, is more serious than in the case of the Lanczos algorithm. There we did not need to store the residual vectors to which the solution is highly sensitive. Moreover the Lanczos vectors would essentially remain as unit vectors though not orthogonal. Due to these considerations it can be concluded that the Lanczos algorithm is more stable to rounding errors than the conjugate gradient algorithm. However, it must be noted that the Lanczos algorithm is known to be exactly equivalent to conjugate gradient algorithm in exact arithmetic. The most direct connection between the two algorithms in terms of vectors generated is that the Lanczos vectors are parallel to the residue vectors of the conjugate gradient algorithm [33].

Regardless of cases such as the one discussed above, conjugate gradient algorithm can still converge despite the presence of rounding errors. In fact since in this algorithm each vector is directly obtained from the previous neighbouring one, it is fair enough to assume that H-conjugacy of p's and orthogonality of r's are locally nearly preserved. This assumption is enough to demonstrate that all

conjugate gradient equations are still approximately valid. As r_{N+1} does not necessarily vanish one might continue the iterations beyond N so that small enough residues are obtained. As was the case for the Lanczos algorithm, the rate of convergence is controlled by the nature of the spectrum of H.

2.9 Conjugate Gradient Algorithm Results

Under the same conditions that we investigated the Lanczos algorithm, we implemented both versions of the conjugate gradient algorithm to invert $H = \gamma_5 M$. The H conjugate gradient algorithm still converges despite the fact that $\gamma_5 M$ is not positive definite. Moreover our results strongly confirm the equivalence of the H conjugate gradient to the Lanczos algorithm. However, the two-valued behaviour of norms of residue and solution vectors disappears once the $H^\dagger H$ version of the conjugate gradient algorithm is applied as shown in Fig. 2.4. Taking into account the fact that each iteration of $H^\dagger H$ conjugate gradient algorithm takes almost twice as long as the H algorithm, Table 2.3 compares the convergence rate e of the H relative to $H^\dagger H$ conjugate gradient algorithm as the residue norms fall below 10^{-8}. As shown in Table 2.3, despite the stability of $H^\dagger H$ conjugate gradient compared with the fluctuating behaviour of H algorithm, it is slower and slower as κ_z is approached. The reason for this slowing down is that the eigenvalues of $H^\dagger H$ are the square of those of H. In other words the least modulus eigenvalues are much smaller for $H^\dagger H$ compared with the corresponding least modulus eigenvalues of H specially when κ_z is approached. On the other hand, as shown in §2.6, the rate of convergence is controlled by the least modulus eigenvalue as well as its density. Accordingly the slow rate of convergence of $H^\dagger H$ is expected.

Since we have already seen that the non-definiteness of $\gamma_5 M$ does not hamper the convergence of H algorithms, we will be therefore most concerned about the improvement factor in rate of convergence rather than the convergence alone. Accordingly the above results emphasize that H algorithms are more

efficient to use than $H^{\dagger}H$ ones.

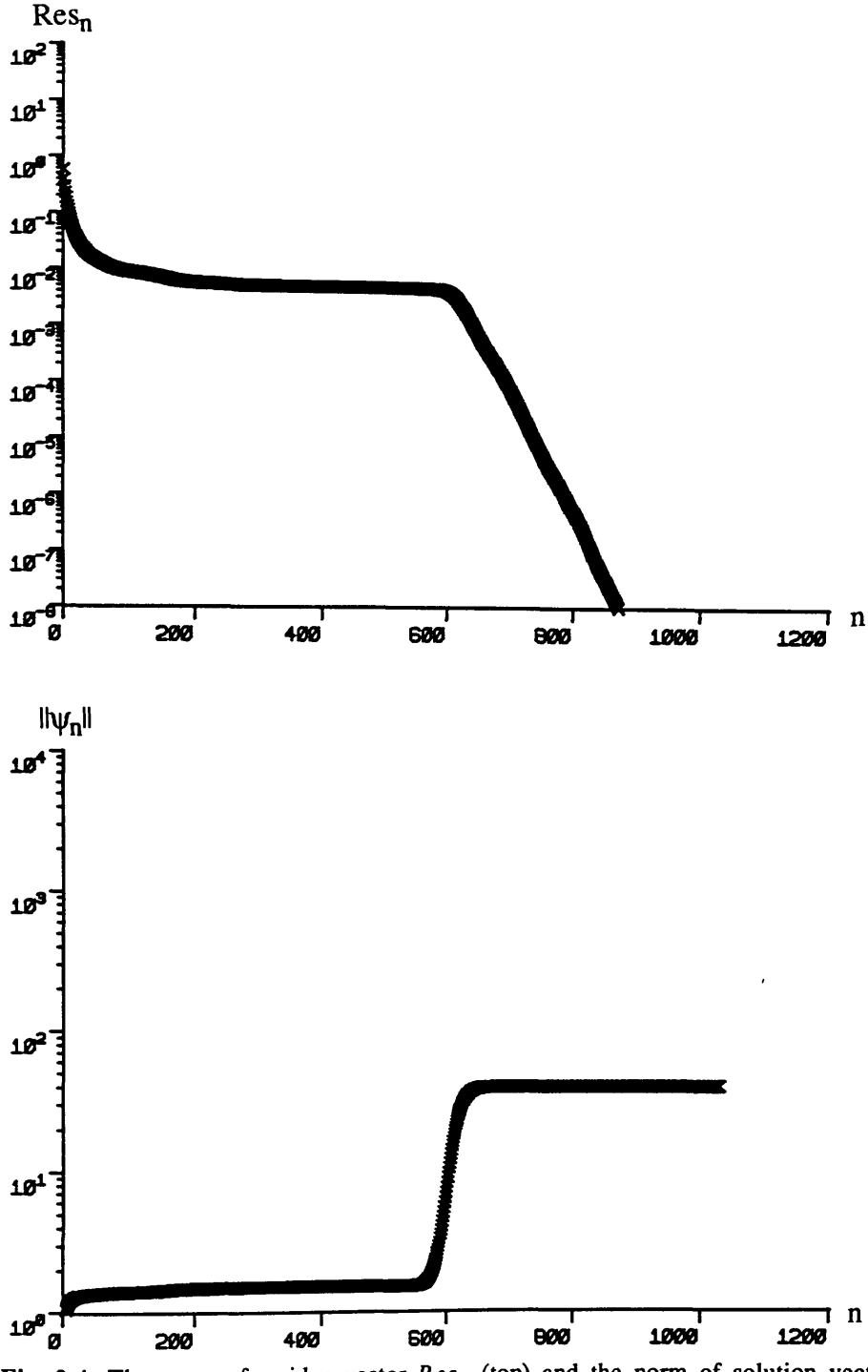

Fig. 2.4 The norm of residue vector Res_n (top) and the norm of solution vector (above) vs. iteration number n of $H^{\dagger}H$ conjugate gradient algorithm for an 8^4 lattice at $\beta = 5.8$ and $\kappa = 0.165$.

Table 2.3

Convergence rate e of the H conjugate gradient algorithm compared with its $H^{\dagger}H$ version for an 8^4 lattice at $\beta = 5.8$. N_1 and N_2 are the corresponding iteration numbers.

κ	N_1	N_2	e
0.159	0918	608	1.32
0.165	1156	872	1.51
0.167	1048	729	1.39

2.10 Block Algorithms

Matrix inversion calculations are among the most time consuming calculations we encounter in lattice QCD. This problem becomes more serious when we have to calculate several columns of the inverse simultaneously. Two examples are, all the columns affected by a change to one gauge field link in an updating algorithm, or the columns corresponding to different spins on the starting site of a hadron propagator. Accordingly improving the convergence rate of the algorithm by some factor seems inevitable. One successful step towards this goal is to modify the algorithm to its blocked form [23, 34]. To do this we construct blocks of N rows by N_B columns to represent N_B vectors of dimension N. Then generalizing all our N-dimensional vectors to such $N \times N_B$ matrix-like vectors we can end up with the blocked versions of the algorithm. Under such blocking procedure the scalar quantities turn out to become $N_B \times N_B$ square full matrices. Now if we begin the algorithm with an initial η block containing N_B orthogonal vectors then, in exact arithmetic, we span the whole space of x vectors (in the Lanczos algorithm) or r vectors (in the conjugate gradient algorithm) in $\frac{N}{N_B}$ iterations because in each step N_B orthogonal vectors are generated and there are only N such vectors in an N-dimensional space. On the other hand since the main computation tasks are matrix-vector multiplications, each iteration takes almost N_B times longer than for the single algorithm. As a result the whole space is generated almost in the same time as

for the single algorithm but during the same time we have obtained a matrix-like solution vector which contains N_B columns of inverse i.e. we have improved the algorithm by a factor of N_B. In practice, however, due to rounding errors more iterations are required for convergence. In previous sections we saw that the convergence is somehow proportional to the extent the orthogonality and/or H-conjugacy is preserved among the relevant vectors at the presence of rounding errors. One plausible way to improve the rate of convergence is, then, to maintain orthogonality and/or H-conjugacy among as many vectors as possible. The above described block algorithm works well in this aspect because approximate local orthogonality and/or conjugacy is extended to a larger range in the blocks. So we expect a good improvement factor over single algorithms once block versions are applied. To apply block algorithms one is required to invert the $N_B \times N_B$ matrices which appear in each iteration. This is normally carried out by *Gaussian elimination* [35]. Moreover in the block Lanczos algorithm β's are square roots of $N_B \times N_B$ hermitian matrices. The hermicity of such matrices imposes $\frac{1}{2} N_B(N_B+1)$ constraints on the elements of each β. This lets one construct β's as triangular matrices whose elements can easily be calculated from the original matrices. In practice the overhead computation time required to invert and/or to calculate square roots of such $N_B \times N_B$ matrices is negligible for practically possible block sizes.[9]

2.11 Block Algorithm Results

In studying the convergence properties of blocked algorithms one faces a serious storage problem in large lattices if the blocks are large enough. To see the real effect of blocking on the algorithms one might begin with a modest lattice size in favour of reasonably larger blocks. In the following we present our results obtained from 4^4 and 8^4 lattices.

[9] See Fig. 2.16.

2.11.1 4^4 Lattices

I Strong Coupling Limit

We have found that on finite-size lattices the first zero modes at $\beta = 0$ appear just above $\kappa = 0.25$.[10] The exact value of κ_z depends on the configuration as well as the lattice size. For the configuration that we have generated by 20 sweeps from a hot start, the $\gamma_5 M$ spectra at $\kappa = 0.23$ and $\kappa = 0.25$ are shown in Fig. 2.5.

Block Conjugate Gradient Algorithm

The largest blocks used to study the block H conjugate gradient algorithm are $N_B = 32$ and the norm of residue is monitored as it falls down to 10^{-12}.

At $\kappa = 0.23$ the algorithm behaves well up to $N_B = 4$. For $N_B = 8$ the norm of residue goes down to about 10^{-11} but then gradually goes up again to 10^{-7} and does not change considerably anymore. This deficiency is partially developed by the errors in inverting the $N_B \times N_B$ matrices in each iteration. However this

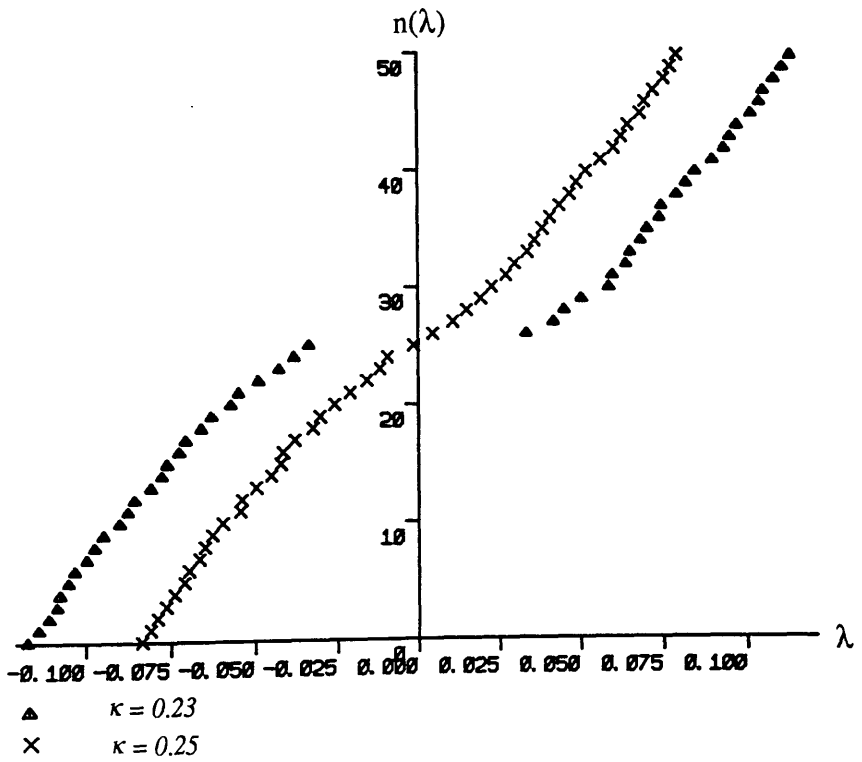

Fig. 2.5 The eigenvalues of $\gamma_5 M$ with smallest modulus for a 4^4 lattice at $\beta = 0.0$. The eigenvalue number $n(\lambda)$ (with arbitrary origin) is plotted against the eigenvalue λ.

[10] See §3.9.1.

unpleasant behaviour does not harm the convergence of the solution vector as long as the attainable minimum residue norm is about 10^{-4} or less, as is the case for $N_B = 32$ for which residue goes down to 10^{-5} first and then goes up to 10^{-2} and stays there as shown in Fig. 2.6. The algorithm fails to converge for $N_B = 16$ for which

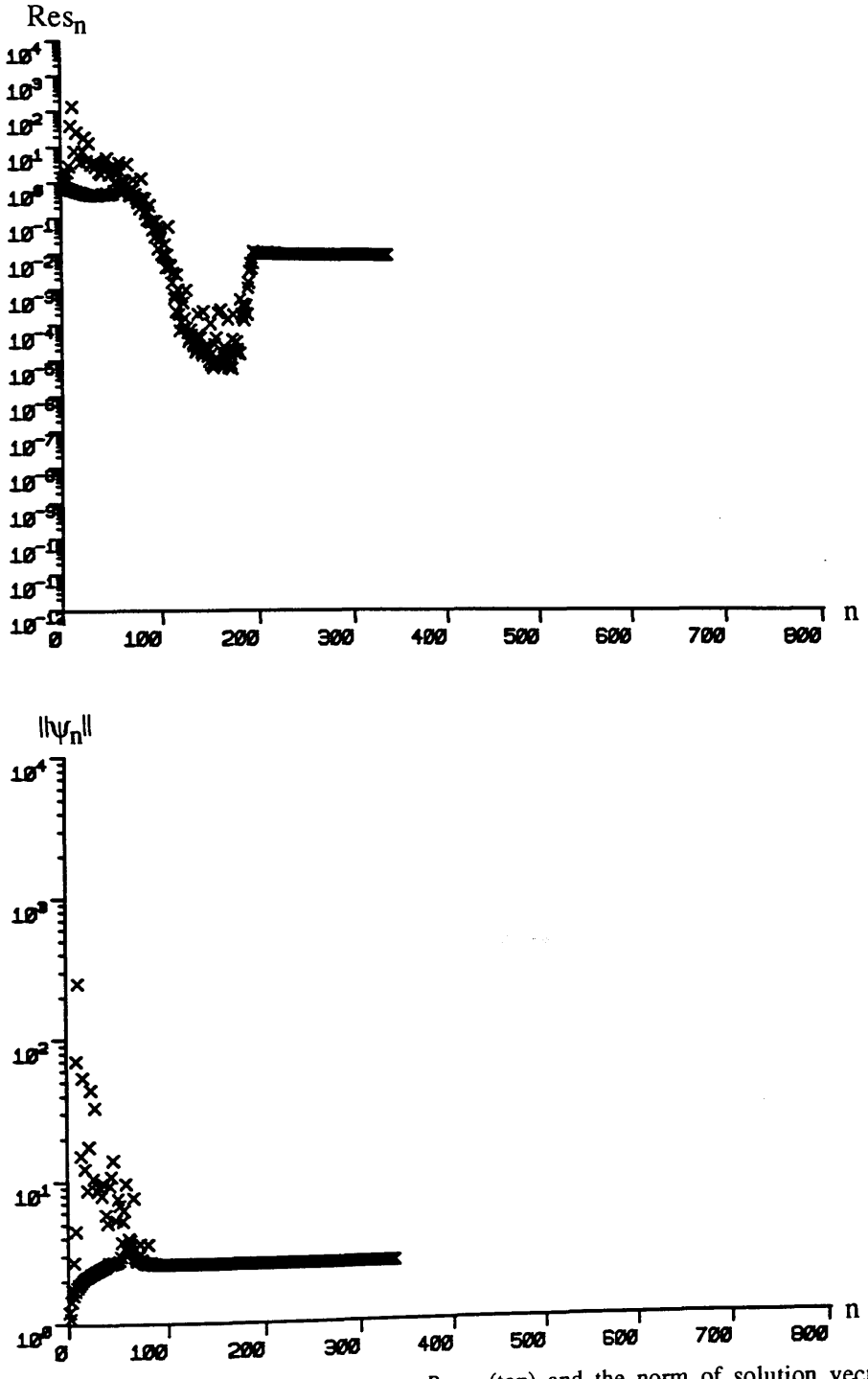

Fig. 2.6 The norm of residue vector Res_n (top) and the norm of solution vector (above) vs. iteration number n of block conjugate gradient algorithm with $N_B = 32$ for a 4^4 lattice at $\beta = 0.0$ and $\kappa = 0.23$.

the minimum residue norm is just about 10^{-1}! Fig. 2.7 shows the corresponding behaviour.

Knowing that the time per iteration for block algorithm is almost N_B times as much as the corresponding time for single algorithm, the improvement factor, e,

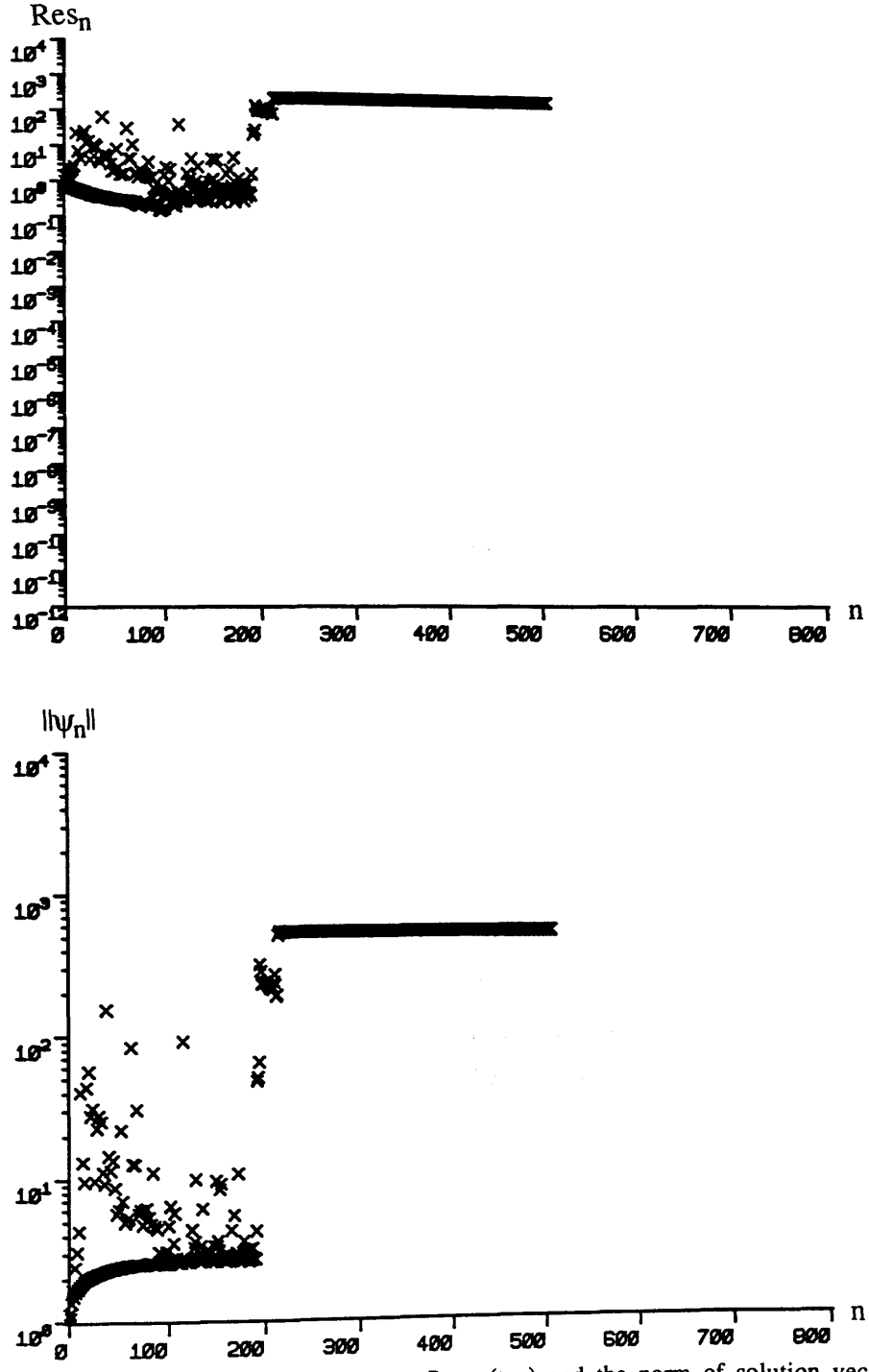

Fig. 2.7 The norm of residue vector Res_n (top) and the norm of solution vector (above) vs. iteration number n of block conjugate gradient algorithm with $N_B = 16$ for a 4^4 lattice at $\beta = 0.0$ and $\kappa = 0.23$.

of block algorithm relative to single algorithm in calculating one column of the inverse when the residue norm falls below 10^{-5} is given in Table 2.4. This table clearly indicates that larger blocks result in more efficient algorithms.

Approaching κ_z, not only the algorithm slows down, but rounding errors overcome it and the algorithm fails to converge as it is the case for $\kappa = 0.25$ at which the algorithm does not converge except for $N_B = 1$ and 2. This behaviour is indicated in Fig. 2.8 for $N_B = 4$.

Contrary to the H algorithm, the $H^\dagger H$ algorithm works well for all N_B's at both $\kappa = 0.23$ and $\kappa = 0.25$. However it must be pointed out that residue norms at $\kappa = 0.25$ do not fall below certain minima and these minimum values grow larger as N_B increases so that for $N_B = 32$ it reaches about 10^{-2} as shown in Fig. 2.9.

In Table 2.5 the improvement factors of block algorithm over the single version of $H^\dagger H$ conjugate gradient algorithm are given for the two κ's used as residue norms fall below 10^{-5}. Comparing the iteration numbers N_I in Table 2.5 with the corresponding values in Table 2.4 we again see that, as was the case for single algorithms, the block H conjugate gradient algorithm is faster (and comparable only for $N_B = 1$) than the corresponding block version of $H^\dagger H$ conjugate gradient algorithm. Also the e's in the two tables show that the blocking

Table 2.4

Improvement factor e of the block compared with the single H conjugate gradient algorithm for a 4^4 lattice at $\beta = 0.0$ and $\kappa = 0.23$.

N_B	N_{it}	e
1	705	1.00
2	587	1.20
4	457	1.54
8	327	2.15
16	*	*
32	149	4.75

* Convergence is not achieved.

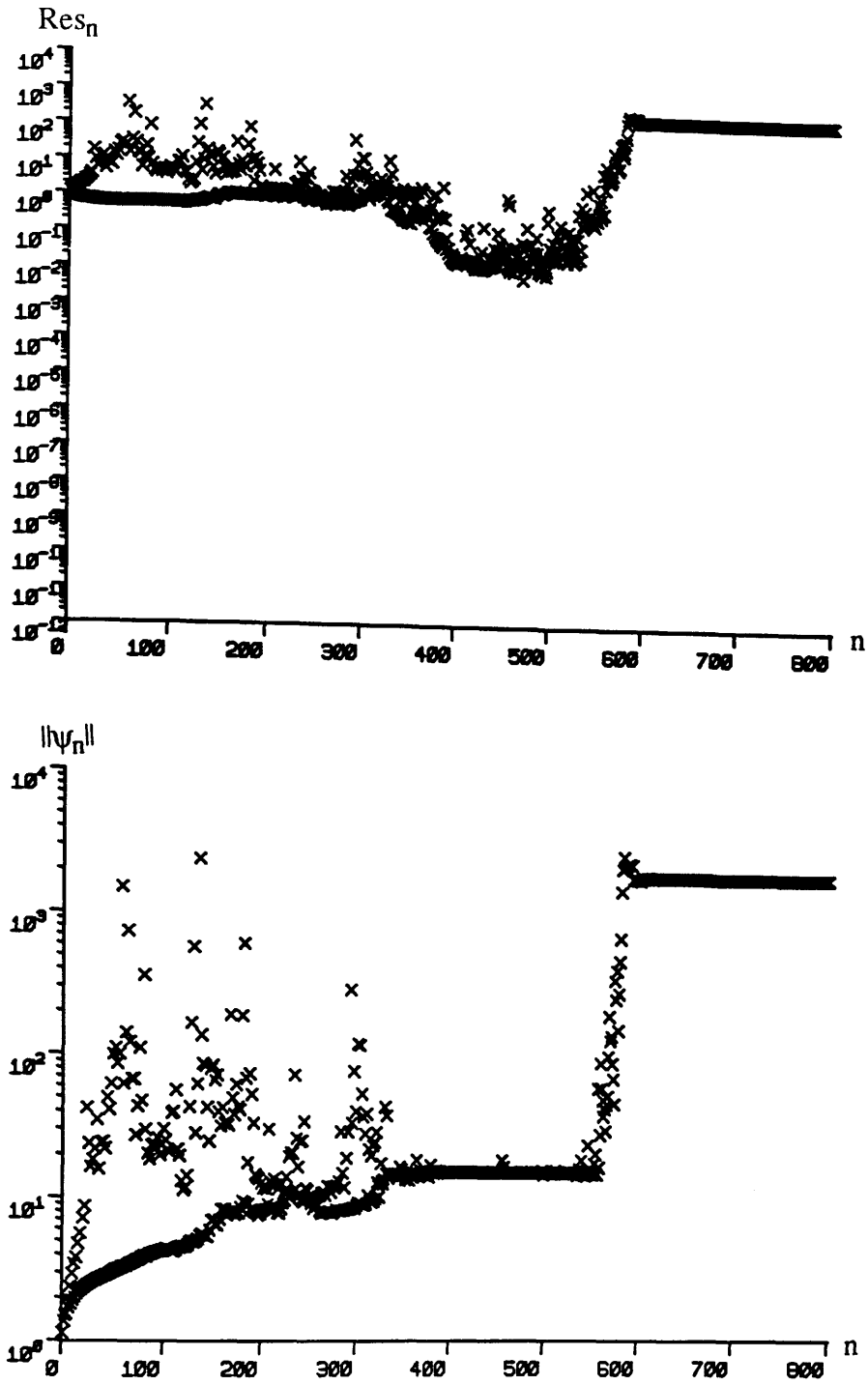

Fig. 2.8 The norm of residue vector Res_n (top) and the norm of solution vector (above) vs. iteration number n of block conjugate gradient algorithm with $N_B = 4$ for a 4^4 lattice at $\beta = 0.0$ and $\kappa = 0.25$.

procedure has a better performance once applied to the H conjugate gradient rather than to the $H^\dagger H$ conjugate gradient algorithm. On the other hand, comparing e_1 with e_2 shows that the block algorithms are even more promising as one

approaches the zero modes at hopping parameters κ_z.

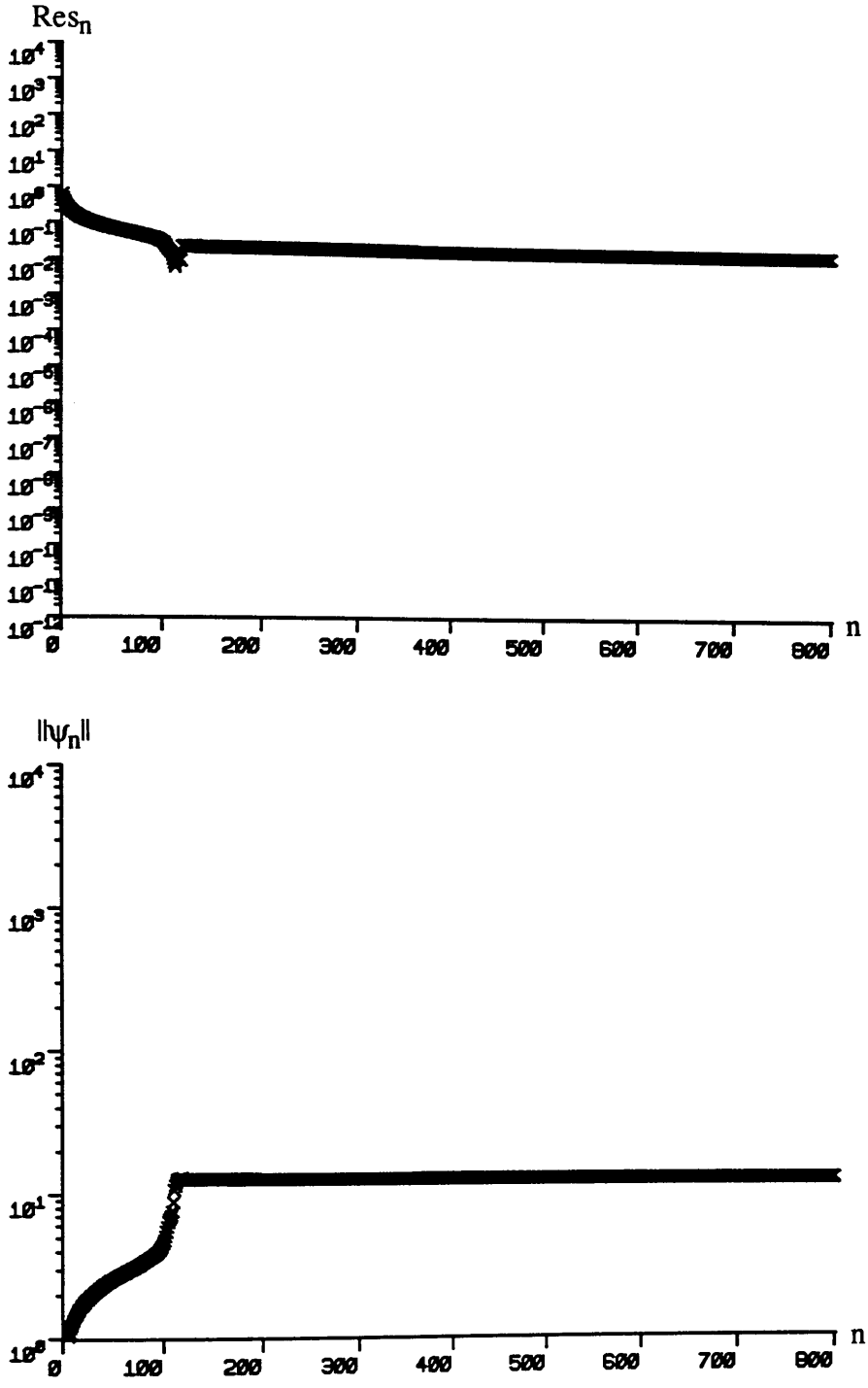

Fig. 2.9 The norm of residue vector Res_n (top) and the norm of solution vector (above) vs. iteration number n of block $H^\dagger H$ conjugate gradient algorithm with N_B = *32* for a 4^4 lattice at $\beta = 0.0$ and $\kappa = 0.25$.

Table 2.5

Improvement factors e_1 and e_2 of the block compared with the single $H^\dagger H$ conjugate gradient algorithm at $\beta = 0.0$ for a 4^4 lattice. N_1 and N_2 are the iteration numbers.

	$\kappa = 0.23$		$\kappa = 0.25$	
N_B	N_1	e_1	N_2	e_2
1	357	1.00	1790	1.00
2	318	1.06	1129	1.58
4	279	1.21	681	2.63
8	217	1.55	395	4.53
16	155	2.17	331	5.41
32	99	3.40	*	*

* Norm of residue does not reach to 10E-5.

Block Lanczos Algorithm

Under the same conditions as before blocked version of Lanczos algorithm was worked out. The storage limitation which was imposed as we decided to compare $//x_1\text{-}HV_n//$ with Res_n in each step does not now allow to work for $N_B = 32$. Accordingly we did not proceed beyond $N_B = 16$. Though our previous results showed that the single version of Lanczos and conjugate gradient algorithms are essentially identical, however their blocked forms gradually begin to behave differently as we increase the block size. Fig. 2.10 which shows the behaviours of the two algorithms at $\kappa = 0.23$ for $N_B = 8$ shows this discrepancy. The corresponding solution vectors are plotted in Fig. 2.11.

It is remarkable that the block Lanczos algorithm does not suffer from the growth of residue norm after it reaches a minimum as was the case for the block conjugate gradient. One might compare Fig. 2.12 which shows the behaviour of the block Lanczos algorithm at $\kappa = 0.23$ for $N_B = 16$ with Fig. 2.7 for the corresponding conjugate gradient results as an example of a better behaviour of the block Lanczos algorithm over the conjugate gradient algorithm. The reason for this is that the vectors in the Lanczos algorithm are orthonormal, and hence the elements of the vectors and the expansion matrices constructed from them are always much

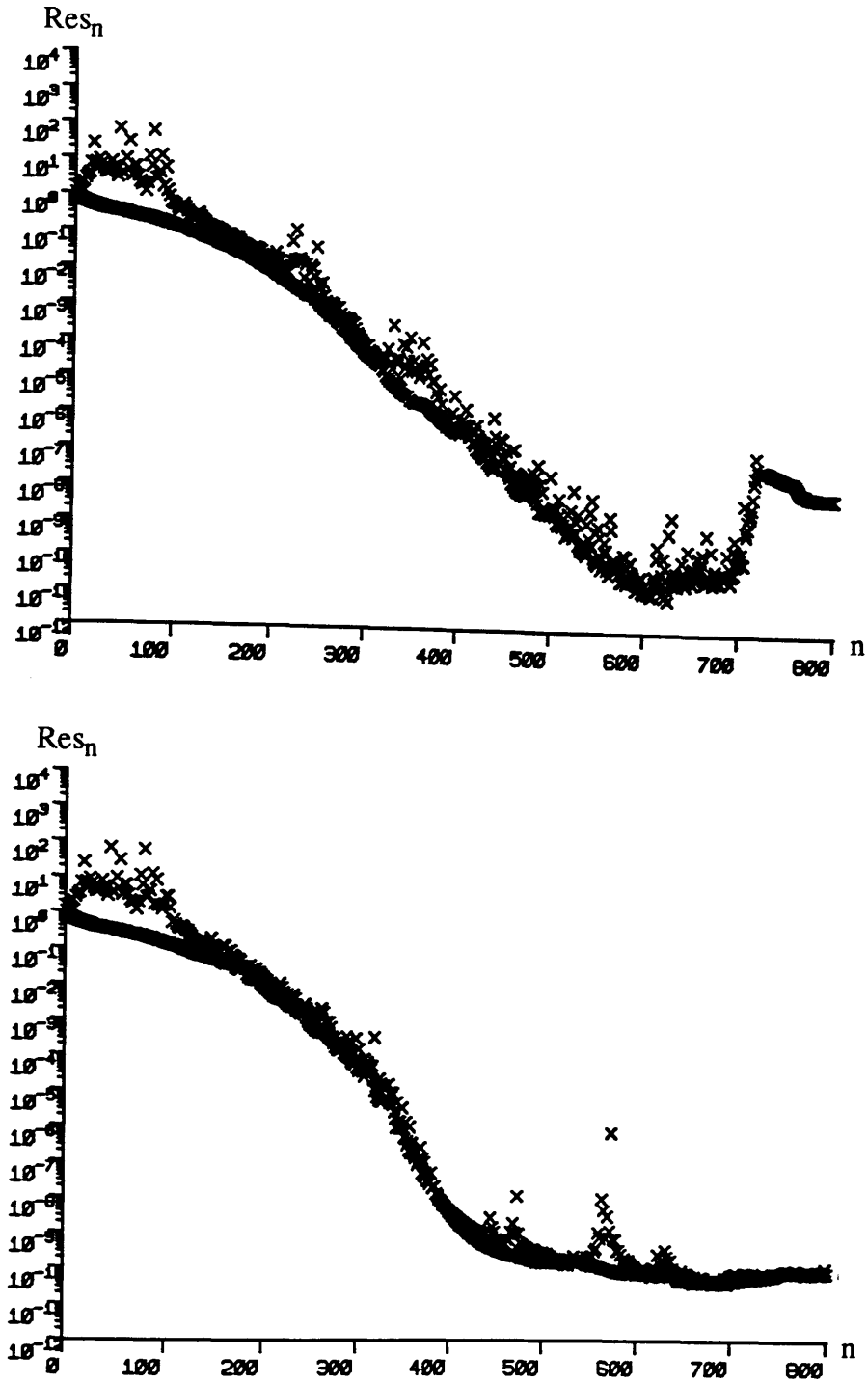

Fig. 2.10 The norm of residue vector Res_n of the block conjugate gradient (top) and the block Lanczos (above) algorithms with $N_B = 8$ for a 4^4 lattice at $\beta = 0.0$ and $\kappa = 0.23$.

larger in magnitude than machine precision. However, in the conjugate gradient algorithm our expansion vectors are the residue vectors themselves which are orthogonal but not normalized. When the residue becomes very small the expansion

matrices will have very small elements. For large block sizes, inverting these matrices with some exact algorithm to calculate the parameters a_i and b_i in Eqs. (2.109) and (2.112) introduces large relative errors and prevents reliable convergence.

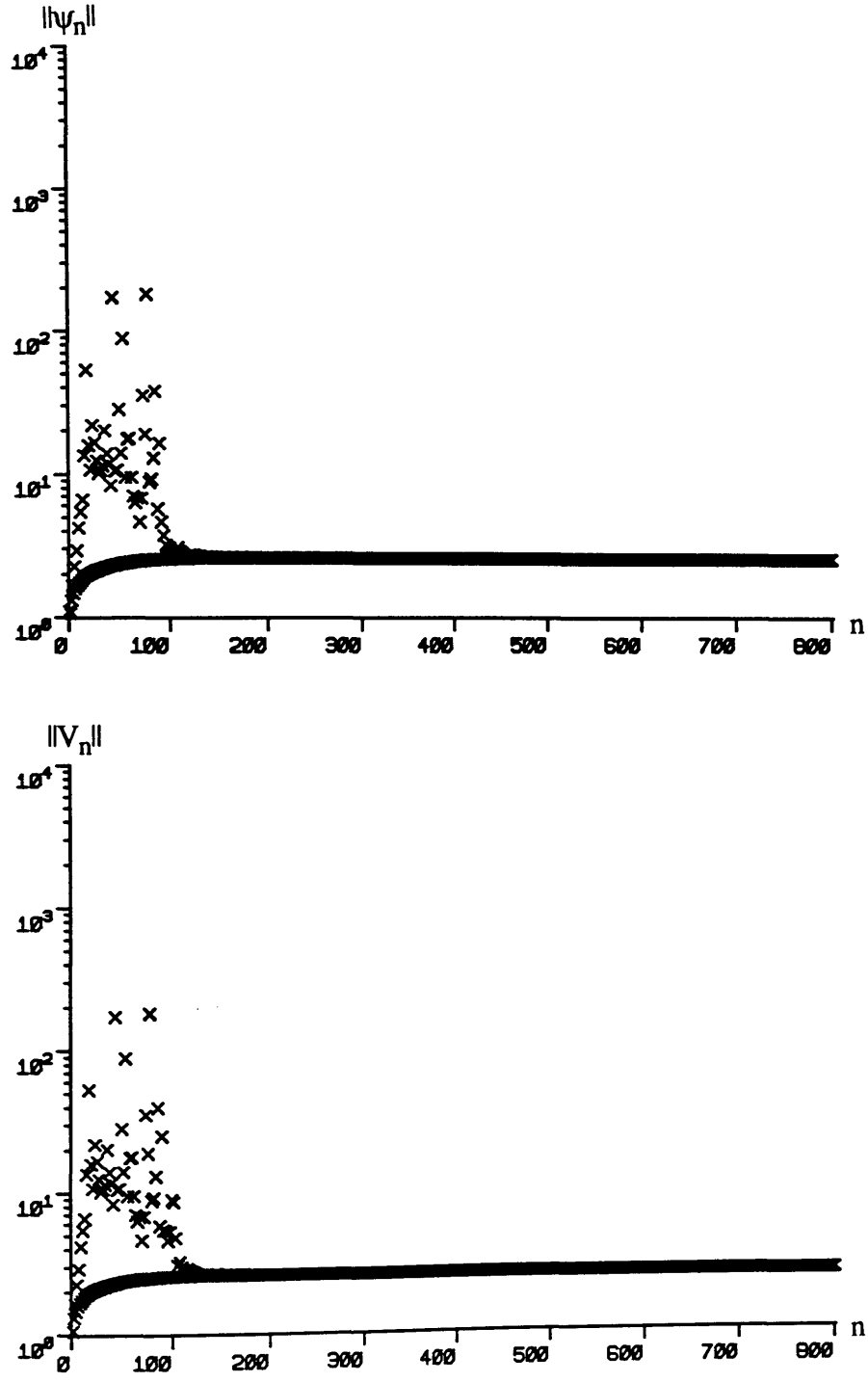

Fig. 2.11 The norm of solution vector of the block conjugate gradient (top) and the block Lanczos (above) algorithms with $N_B = 8$ for a 4^4 lattice at $\beta = 0.0$ and $\kappa = 0.23$.

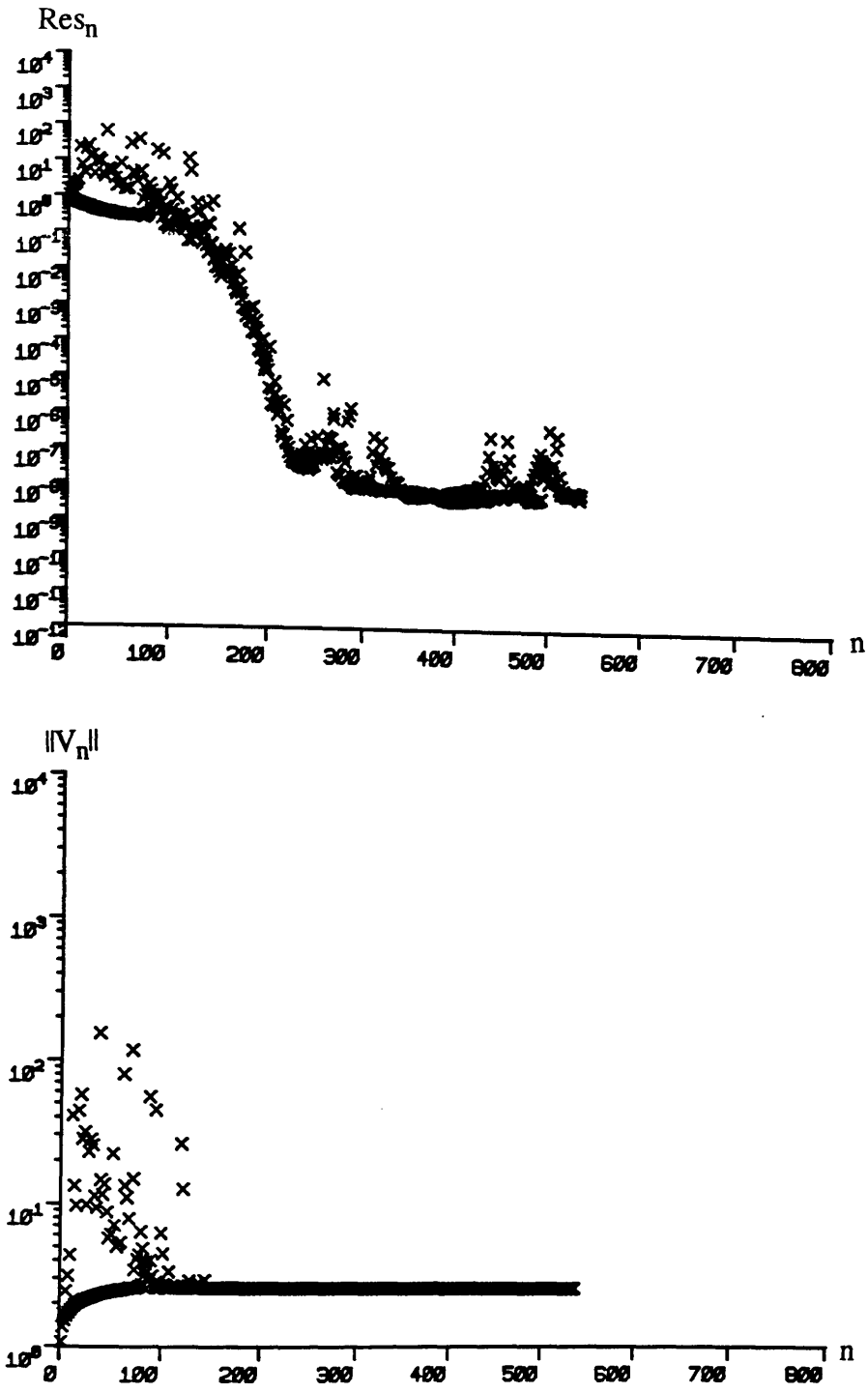

Fig. 2.12 The norm of residue vector Res_n (top) and the norm of solution vector (above) vs. iteration number n of the block Lanczos algorithm with $N_B = 16$ for a 4^4 lattice at $\beta = 0.0$ and $\kappa = 0.23$.

However, it is worth pointing out that the least attainable residue norm increases as one approaches κ_z and/or increases N_B. So, accordingly, it is quite probable that the algorithm fails to converge for large enough blocks, though it

converges for all N_B's and κ's we used and even its behaviour at $\kappa = 0.25$, i.e. close to κ_z, proved much better and faster than the block conjugate gradient algorithm as shown in Fig. 2.13 which is the block Lanczos version of Fig. 2.8. Our results when residue norms fall below 10^{-5} are outlined in Table 2.6. In

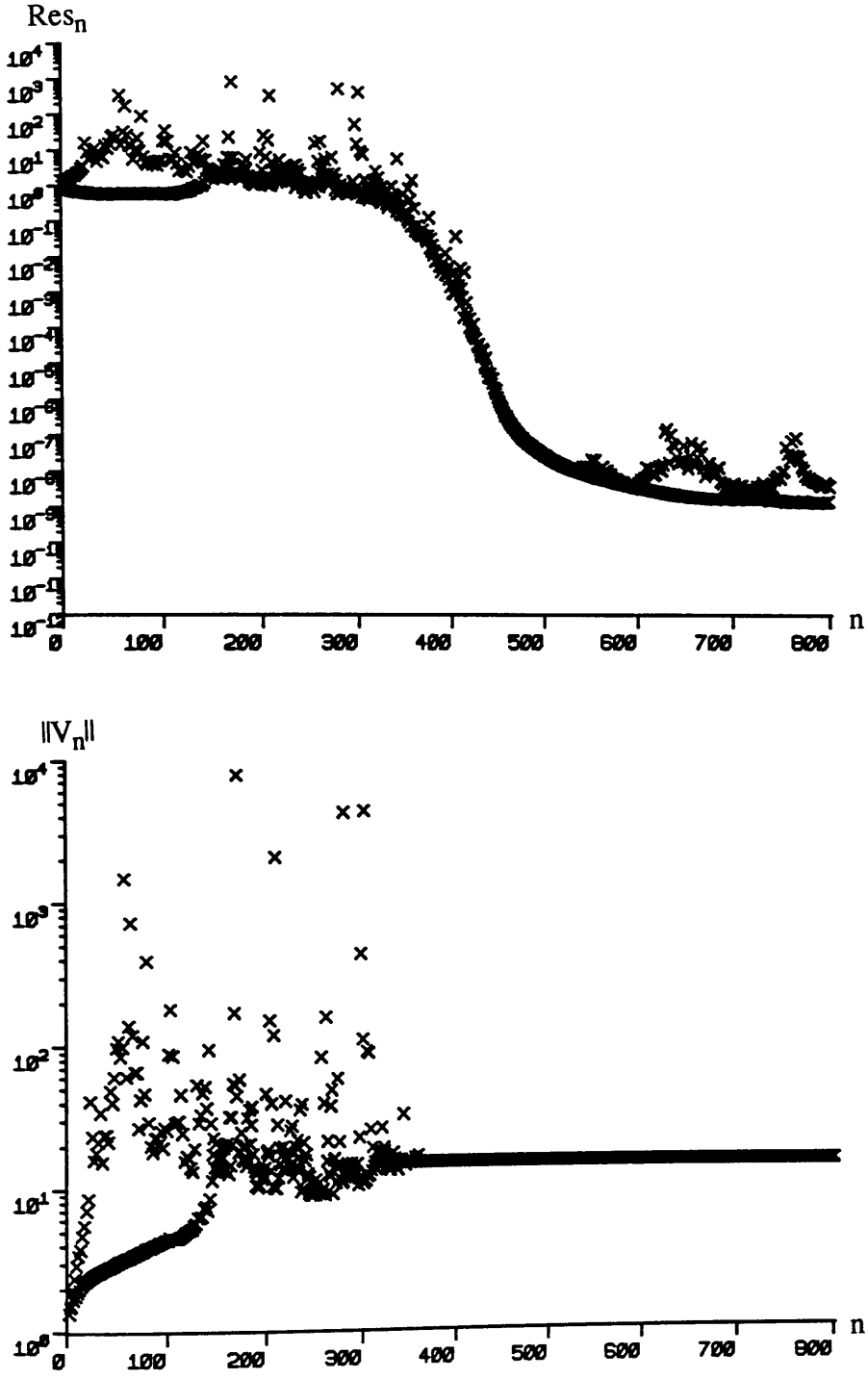

Fig. 2.13 The norm of residue vector Res_n (top) and the norm of solution vector (above) vs. iteration number n of block Lanczos algorithm with $N_B = 4$ for a 4^4 lattice at $\beta = 0.0$ and $\kappa = 0.25$.

Table 2.6

Improvement factors e_1 and e_2 of the block compared with the single H Lanczos algorithm at $\beta = 0.0$ for a 4^4 lattice. N_1 and N_2 are the iteration numbers.

	$\kappa = 0.23$		$\kappa = 0.25$	
N_B	N_1	e_1	N_2	e_2
1	707	1.00	2185	1.00
2	579	1.22	1302	1.68
4	451	1.57	765	2.86
8	322	2.20	438	4.99
16	202	3.50	233	9.38

addition to the confirmation of the general qualitative statements we made about the nature of blocking in previous section, once compared with Table 2.4, Table 2.6 shows stability of the block Lanczos algorithm over the block conjugate gradient algorithm which failed at $\kappa = 0.23$ for $N_B = 16$ and at $\kappa = 0.25$ for $N_B > 2$. Also, they show the speed of the block Lanczos over block $H^\dagger H$ conjugate gradient algorithm once compared with Table 2.5.

All our results single out the block Lanczos algorithm from different algorithms that we studied as the most efficient algorithm at strong coupling limit. Moreover it is worth to mention that the presence of approximate zero modes at κ' s very close to κ_z on one hand and the high density of such modes at strong coupling limit on the other, as shown in Table 2.7, make our fermion matrix (or $\gamma_5 M$) at $\kappa = 0.25$ the most difficult one to invert. While the successful performance of the block Lanczos algorithm in this ordeal gives it special superiority, the failure of block conjugate algorithm excludes it from our further investigations.

II Weak Coupling

We have generated two gauge configurations, one in the confining phase at $\beta = 5.3$ obtained by 35000 sweeps from a hot start and the other above the deconfining

Table 2.7

Smallest modulus eigenvalue and eigenvalue density for a 4^4 lattice.

β	κ	$\lvert\lambda\rvert_{min}$	N_λ
5.7	0.145	0.1079	7
5.7	0.164	0.6557E-1	17
5.3	0.184	0.3489E-1	42
5.3	0.198	0.1683E-2	51
5.3	0.1991*	0.1144E-6	51
0.0	0.230	0.3340E-1	127
0.0	0.250	0.1355E-2	157
0.0	0.266 *	0.9911E-5	174

*Approximate κ_z.

phase transition point at $\beta = 5.7$ obtained by 55000 sweeps from a hot start. As we will see later in §3.9.2, where the spectra of 4^4 lattices at weak coupling constants are discussed in more detail, at $\beta = 5.3$ the first zero mode is found to be at $\kappa_z = 0.1991$. In this configuration we have worked at $\kappa = 0.184$ and $\kappa = 0.198$, both below κ_z. At $\beta = 5.7$ where there are, of course, no zero modes we have chosen $\kappa = 0.145$ and $\kappa = 0.164$. The spectra of $\gamma_5 M$ at these values of κ and β are shown in Fig. 2.14 and the eigenvalues with smallest modulus as well as the number of eigenvalues whose moduli are less than 0.2, N_λ, are given in Table 2.7 for each case. The largest block tried is $N_B = 25$.

Block $H^\dagger H$ Conjugate Gradient Algorithm

$H^\dagger H$ conjugate gradient algorithm works well when $|\lambda|_{min}$ is not too small. However, it fails as one approaches κ_z in large blocks e.g. at $\beta = 5.3$ and $\kappa = 0.198$ the residue norm slowly falls below 10^{-10} for $N_B \leq 4$. It does never fall below 10^{-7} for $N_B = 6$. For $8 \leq N_B \leq 16$ the minimum attainable residue norm is of the order of 10^{-4} while it is only of the order or 10^{-3} for $18 \leq N_B \leq 25$. The minimum number of iterations required to converge to a solution with residue norm less than 10^{-10} is given in Table 2.8 in terms of β, κ and N_B.

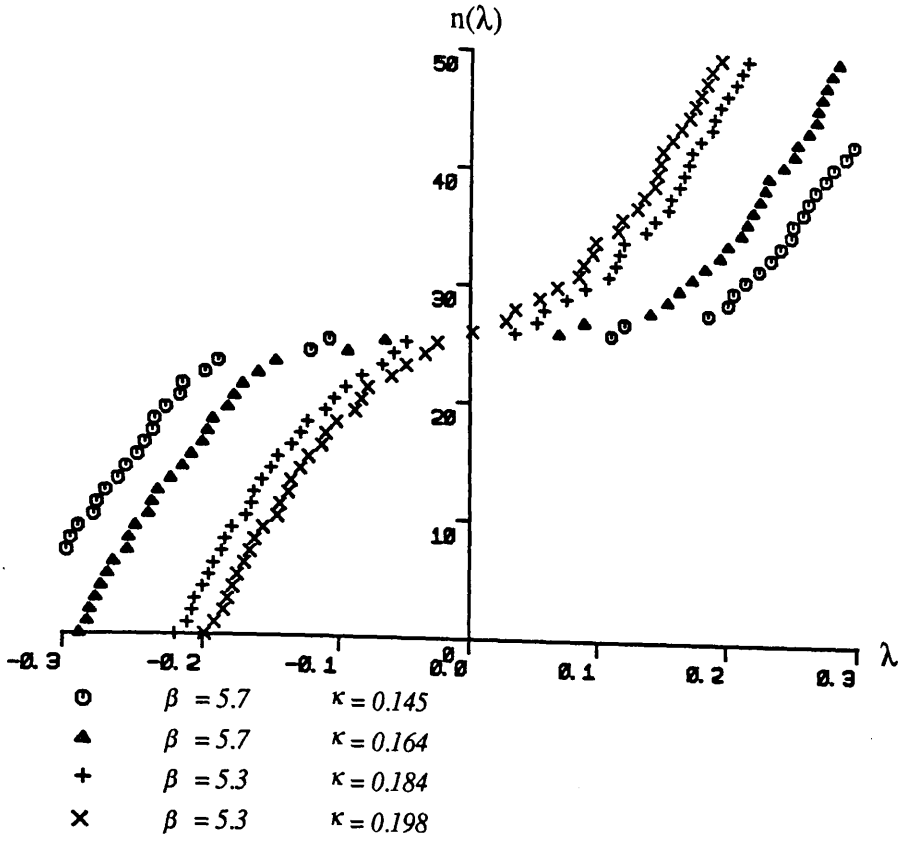

Fig. 2.14 The eigenvalues of $\gamma_5 M$ with smallest modulus for a 4^4 lattice at weak coupling constants. The eigenvalue number $n(\lambda)$ (with arbitrary origin) is plotted against the eigenvalue λ.

Table 2.8

The minimum number of iterations to achieve residues of less than 10^{-10} with block $H^\dagger H$ conjugate gradient algorithm for a 4^4 lattice at weak coupling constants.

	β = 5.7		β = 5.3	
N_B	κ = 0.145	κ = 0.164	κ = 0.184	κ = 0.198
1	160	228	438	675
2	132	182	323	644
4	112	146	233	752
6	101	130	192	*
8	92	117	168	*
10	86	109	151	*
12	82	101	138	*
14	77	96	126	*
16	75	91	119	*
18	72	87	112	*
22	66	79	101	*
25	63	76	94	*

* Residue norm does not reach to 1.0E-10.

The Block Lanczos Algorithm

Under the same conditions as for $H^{\dagger}H$ conjugate gradient algorithm, we studied the block Lanczos algorithm. It works very well for all cases. Although, as we have already seen, the algorithms slow down to converge as one decreases β and/or approaches κ_z (in the confining phase), however they tend to behave more independently of details of fermion matrix such as hopping parameter or gauge configuration as one increases block size. In other words convergence is achieved almost at the same time (or iteration number) for large blocks. This makes it feasible to study cases such as hadron propagators in the vicinity of κ_z where critical slowing-down is a problem for the single algorithm. The actual computation time plot of Fig. 2.15, obtained from the block Lanczos results when residues fall below 10^{-10}, shows this interesting feature of block algorithms. Fig. 2.15 also shows an improvement factor of 3.75 near κ_z.

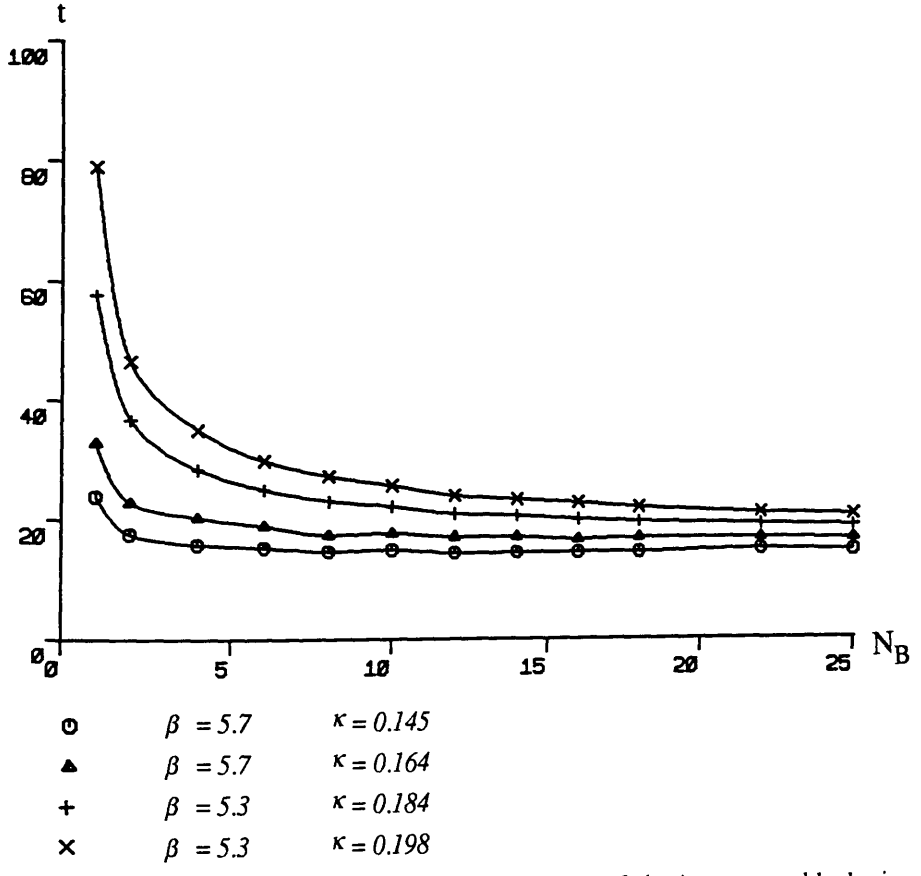

Fig. 2.15 The actual computation time t per column of the inverse vs. block size N_B for block H Lanczos algorithm for a 4^4 lattice.

One might be interested to compare the real time per iteration as block size increases. Due to the overheads from inverting $N_B \times N_B$ matrices, this computation time grows slightly more than linearly with N_B as shown in Fig. 2.16.

Comparing our results on the block Lanczos algorithm in Table 2.9, with those of $H^\dagger H$ conjugate gradient algorithm in Table 2.8 emphasizes the superiority of the block Lanczos over $H^\dagger H$ conjugate gradient algorithm in convergence and speed.

III Precision Considerations

We have always worked in double precision arithmetic. It is worth to see how the employed precision affects the rate of convergence of our algorithms. As an example once again we have investigated the single versions of the Lanczos and $H^\dagger H$ conjugate gradient algorithms for a 4^4 lattice at $\beta = 5.3$ and $\kappa = 0.198$ while the arithmetic has been performed in single precision. As shown in Fig. 2.17 convergence rate of $H^\dagger H$ conjugate gradient algorithm slows down once single

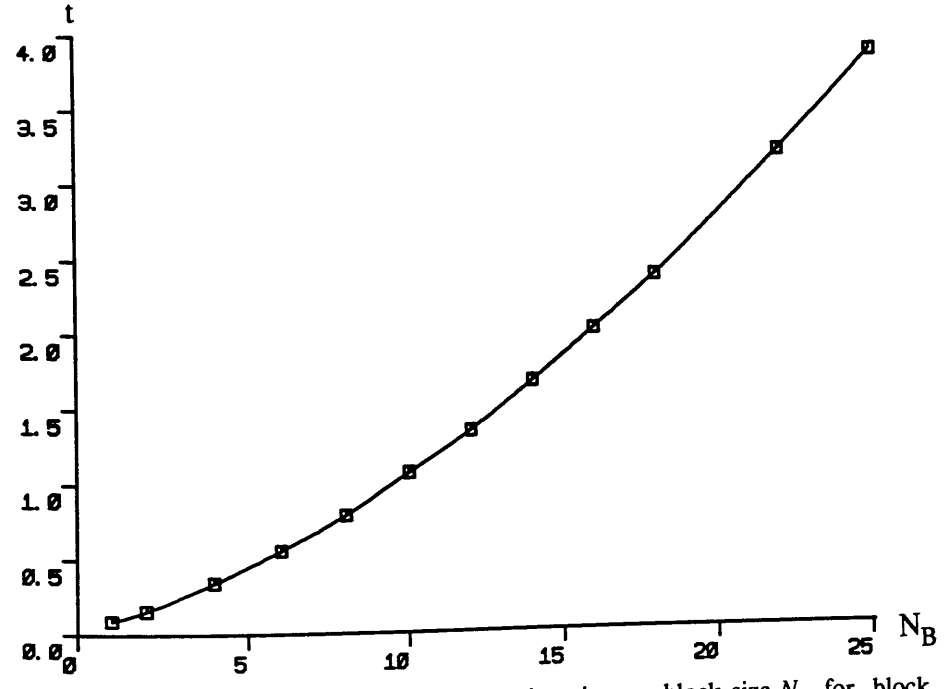

Fig. 2.16 The actual computation time t per iteration vs. block size N_B for block H Lanczos algorithm for a 4^4 lattice.

Table 2.9

The minimum number of iterations to achieve residues of less than 10^{-10} with block *H* Lanczos algorithm for a 4^4 lattice at weak coupling constants.

N_B	$\beta = 5.7$		$\beta = 5.3$	
	$\kappa = 0.145$	$\kappa = 0.164$	$\kappa = 0.184$	$\kappa = 0.198$
1	265	365	639	875
2	223	290	466	589
4	183	235	329	405
6	165	204	270	322
8	149	177	235	277
10	140	166	208	241
12	129	153	188	215
14	122	144	174	197
16	116	133	160	182
18	111	129	150	168
22	104	117	133	146
25	96	109	123	135

precision arithmetic is used. However the norm of solution remains practically stable against the precision used. In Figs. 2.18 and 2.19 we have presented computed residue norm Res_n, real residue norm $//x_1\text{-}HV_n//$ and the norm of solution vector for the Lanczos algorithm in double and single precision respectively. Comparing Figs. 2.18 and 2.19, we observe that Res_n, and $//x_1\text{-}HV_n//$ are exactly the same in double precision arithmetic while they gradually differ from each other in single precision arithmetic. Moreover the rate of convergence of both quantities slows down in single precision arithmetic. In particular $//x_1\text{-}HV_n//$ does not fall below a certain minimum. Anyway, regardless of some minor differences the norm of solution vector in both cases converges almost similarly.

2.11.2 8^4 Lattices

So far we have practically observed that block Lanczos algorithm is a more successful algorithm in lattice field theories. Accordingly we do not need any longer to compare it with both versions of conjugate gradient algorithm. Therefore we now

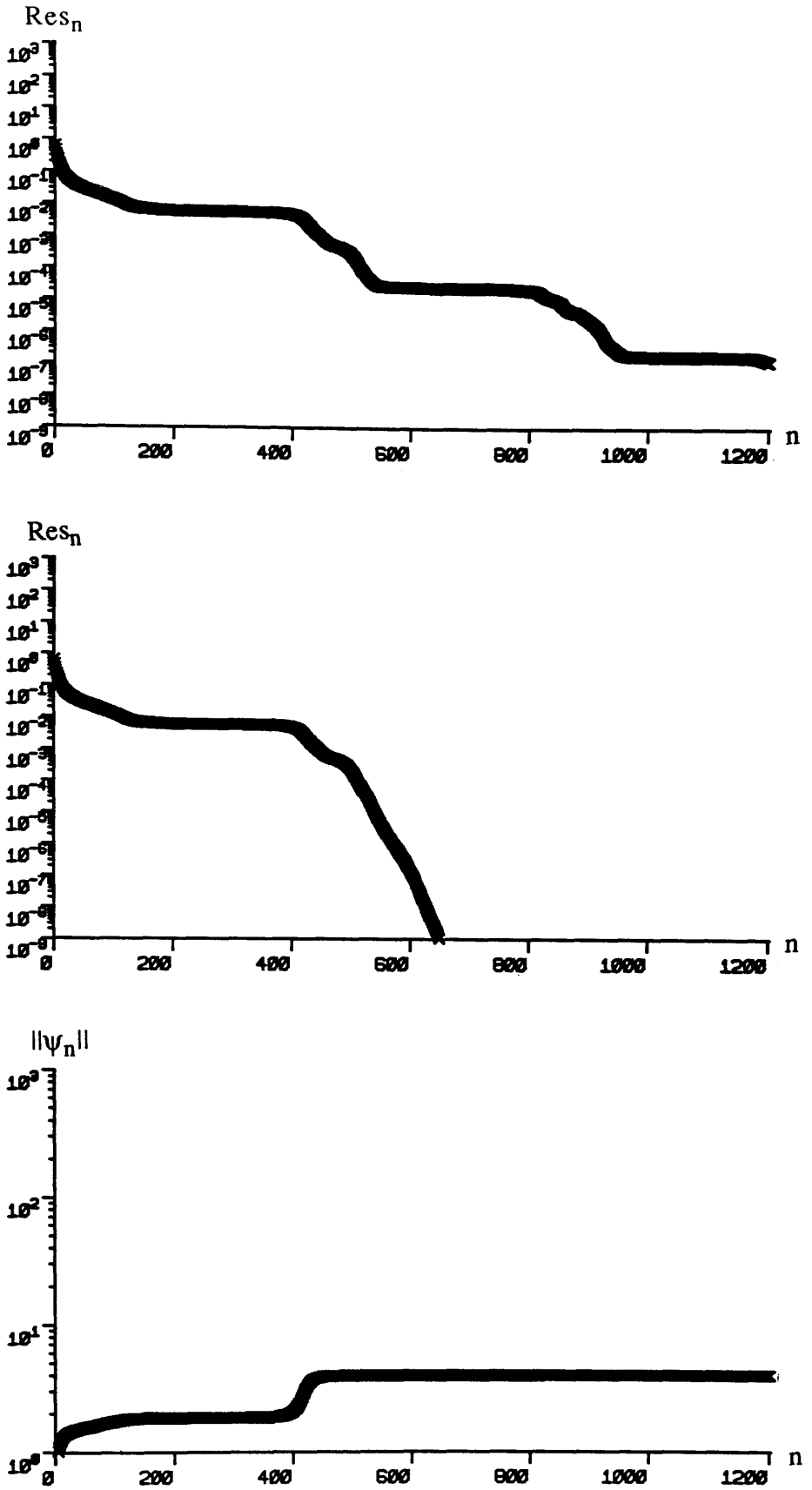

Fig. 2.17 The norm of residue vector Res_n in single precision (top) and in double precision (middle) and the norm of solution vector (above) vs. iteration number n of $H^{\dagger}H$ conjugate gradient algorithm for a 4^4 lattice at $\beta = 5.3$ and $\kappa = 0.198$.

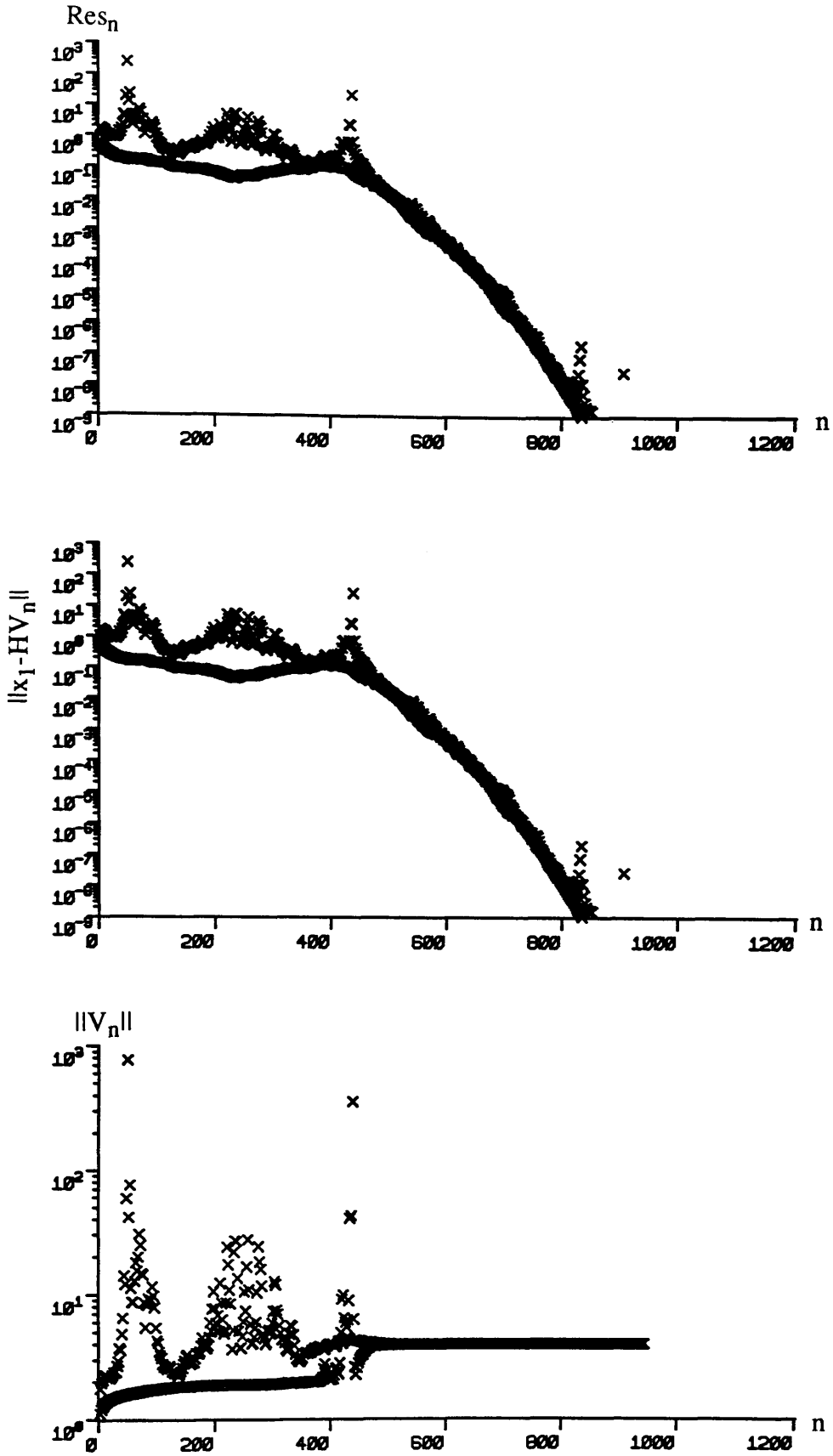

Fig. 2.18 The norm of residue vector Res_n (top), the real residue $//x_1\text{-}HV_n//$ (middle) and the norm of solution vector (above) vs. iteration number n for the Lanczos algorithm for a 4^4 lattice at $\beta = 5.3$ and $\kappa = 0.198$ in double precision.

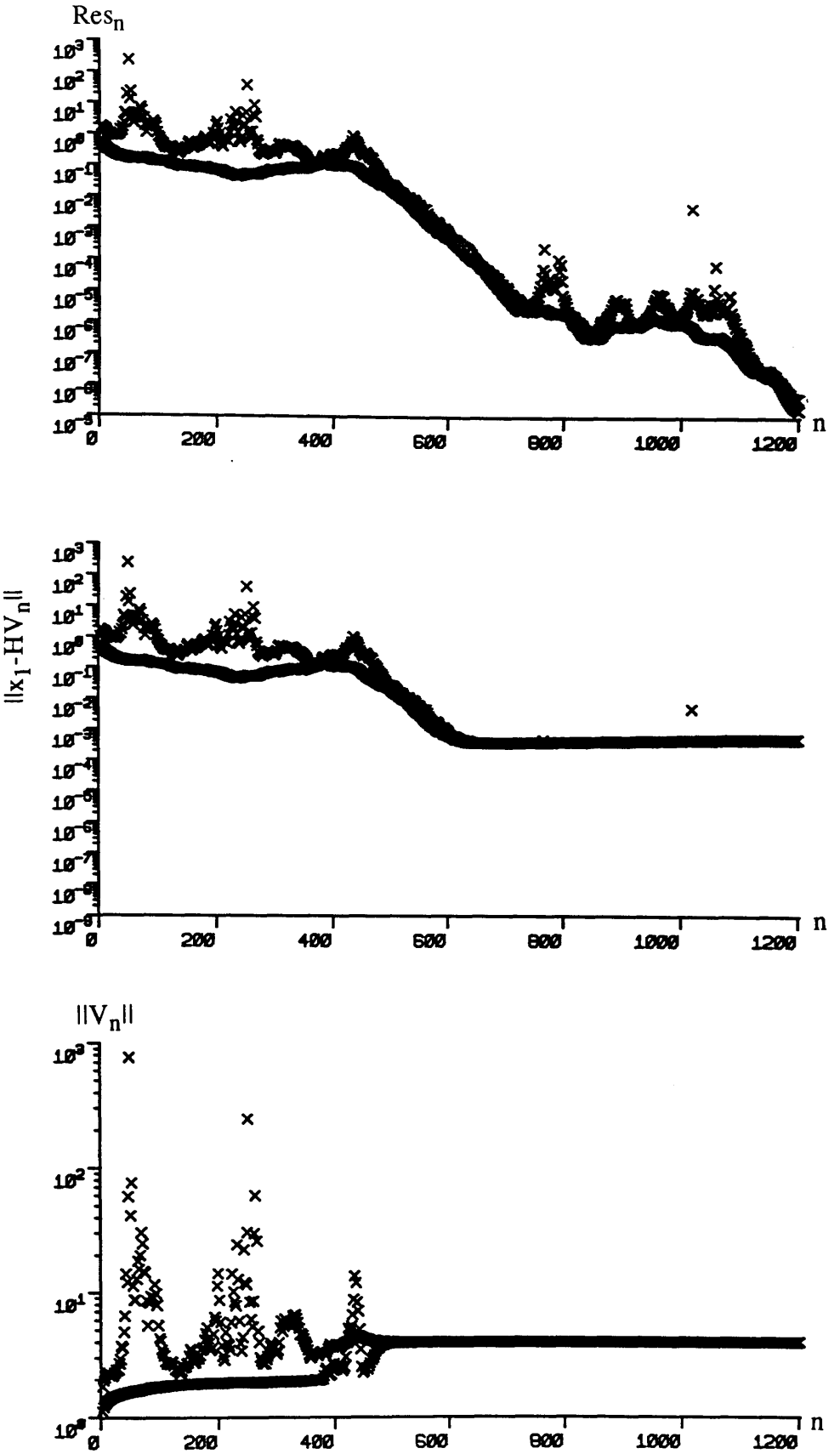

Fig. 2.19 The norm of residue vector Res_n (top), the real residue $//x_1\text{-}HV_n//$ (middle) and the norm of solution vector (above) vs. iteration number n for the Lanczos algorithm for a 4^4 lattice at $\beta = 5.3$ and $\kappa = 0.198$ in single precision.

only work with block Lanczos algorithm to see how it handles larger lattices. Moreover we investigate our algorithm in only more physically interesting cases i.e. at weak coupling constants in the confining phase rather than at strong coupling limit. For an 8^4 lattice, we generated two gauge configurations, at $\beta = 5.8$ and $\beta = 5.5$ both in the confining phase. For the first configuration, which is obtained by 16300 sweeps from a hot start, we worked at $\kappa = 0.1650$ and $\kappa = 0.1677$ and for the second configuration, obtained by 13302 sweeps from a hot start, we worked at $\kappa = 0.1820$ and $\kappa = 0.1827$ both below κ_z and at $\kappa = 0.1940$ above κ_z. The corresponding eigenvalues with least moduli and the number of eigenvalues whose moduli are less than 0.1 are listed in Table 2.10. The $\gamma_5 M$ spectrum at these values of β and κ are plotted in Fig. 2.20. Due to storage limitation we can not work beyond $N_B = 8$. The results of our block Lanczos algorithm to converge to solutions with residues less than 10^{-10}, summarized in Table 2.11, confirm our previous statements made about the Lanczos algorithm and the blocking effect on that. The actual computation time per column of inverse is plotted in Fig. 2.21 for each case. Depending on β and κ, they indicate speed up factors of 4.38 are achievable.

To summarize, our studies show clearly that the block version of algorithms are more efficient than the corresponding single algorithms. Moreover the Lanczos algorithm is more stable than both versions of the conjugate gradient algorithm and in particular faster than $H^\dagger H$ conjugate gradient algorithm. As a result, the block Lanczos algorithm with a considerable improvement factor is recommended for updating dynamical fermions and studying hadron propagators. Moreover as the computation time becomes roughly independent of κ and β for large block sizes, the block Lanczos algorithm is less subject to critical slowing down. Therefore, the use of the block Lanczos algorithm offers the opportunity of increasing the speed of many calculations particularly those which are hampered by critical slowing down.

Table 2.10

Smallest modulus eigenvalue and eigenvalue density for an 8^4 lattice

β	κ	$\lvert\lambda\rvert_{min}$	N_λ
5.8	0.16500	0.6562E-2	43
5.8	0.16770	0.1069E-3	44
5.8	0.16775	0.2435E-6	*
5.5	0.18200	0.1096E-2	128
5.5	0.18270	0.1238E-3	132
5.5	0.18280	0.4337E-5	*
5.5	0.19400	0.5888E-3	161

* No inversions were performed at the corresponding κ_c.

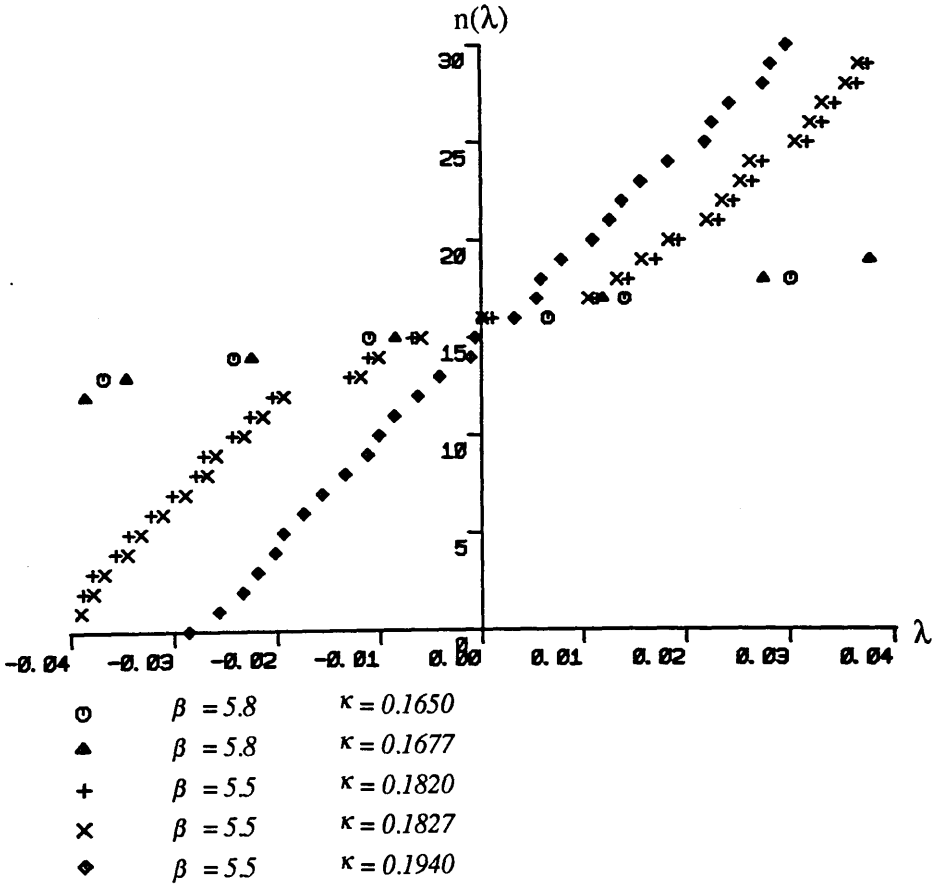

Fig. 2.20 The eigenvalues of $\gamma_5 M$ with smallest modulus for an 8^4 lattice at weak coupling constants.

Table 2.11

The minimum number of iterations to achieve residues of less than 1.0E-10 with block H Lanczos algorithm for an 8^4 lattice at weak coupling constants.

	$\beta = 5.8$		$\beta = 5.5$		
N_B	$\kappa = 0.165$	$\kappa = 0.1677$	$\kappa = 0.182$	$\kappa = 0.1827$	$\kappa = 0.194$
1	1307	1917	2969	3217	4845
2	964	1070	1981	2099	2858
3	808	896	1563	1647	2110
4	720	813	1350	1408	1738
5	649	732	1167	1223	1500
6	624	676	1075	1016	1322
7	584	634	970	1130	1225
8	547	604	898	946	1130

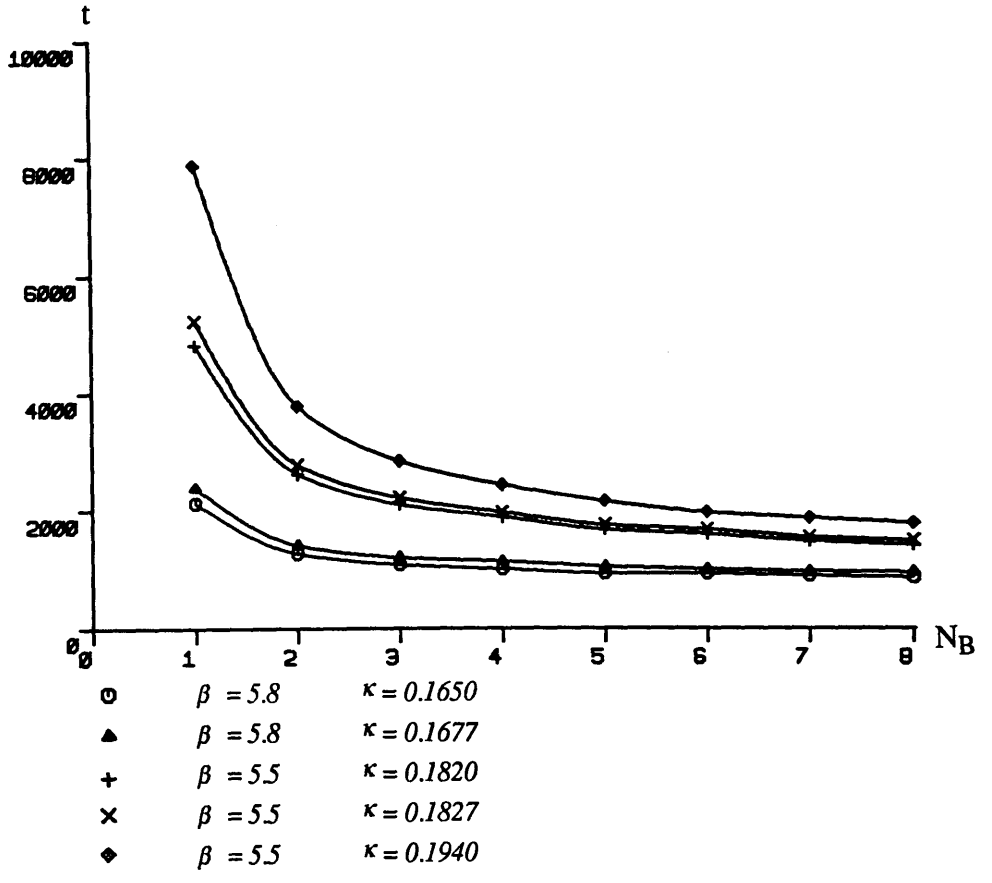

Fig. 2.21 The actual computation time t per column of the inverse vs. block size N_B for H block Lanczos algorithm for an 8^4 lattice.

Chapter 3

Fermion Matrix Spectrum

In the last chapter we saw how Lanczos algorithm could be applied to large sparse matrices to calculate their eigenvalue spectra. In this chapter, we use that algorithm specifically to study the Wilson fermion spectrum. The results will provide us with a suitable ground to probe QCD phase structure.

3.1 Symmetries Of Strong Interaction

The QCD Lagrangian Eq. (1.1) has certain symmetries which play an important role in the strong interaction. As discussed in §1.2 it is *SU(3)* colour gauge invariant. Moreover it is conserving charge conjugation and parity, and because the gluons are flavour independent it conserves strangeness etc. In particular, if different quark flavours are degenerate in mass, then n_f-flavour QCD Lagrangian is also invariant under global phase transformations $U_V(n_f)$ defined by:

$$U_V(n_f) \equiv SU_V(n_f) \times U_V(1) \tag{3.1}$$

where

$$SU_V(n_f): \qquad \psi \rightarrow \exp(i\alpha^a\tau^a)\,\psi \tag{3.2}$$

$$U_V(1): \qquad \psi \rightarrow \exp(i\alpha\mathbb{1})\,\psi \tag{3.3}$$

Here ψ is an n_f-component column vector in the flavour space, $\mathbb{1}$ is an $n_f \times n_f$ unit matrix, τ^a are the generators of $SU(n_f)$ gauge group and $a = 1, 2, ..., n_f^2 - 1$. Both $\mathbb{1}$ and τ^a act on the flavour index of fermion field ψ. In the limit of vanishing quark mass, the so called *massless theory* becomes symmetric under one more

transformation i.e. the *chiral symmetry* $U_A(n_f)$ defined as:

$$U_A(n_f) \equiv SU_A(n_f) \times U_A(1) \tag{3.4}$$

where

$$SU_A(n_f): \qquad \psi \rightarrow \exp(i\alpha^a \tau^a \gamma_5)\,\psi \tag{3.5}$$

$$U_A(1): \qquad \psi \rightarrow \exp(i\alpha \mathbf{1} \gamma_5)\,\psi, \tag{3.6}$$

and γ_5 acts on spin index. As the masses of u and d and to a lesser extent the mass of s quarks[1] are much smaller than a typical hadronic mass scale of $1Gev$, one expects to observe $U_V(n_f)$ and $U_A(n_f)$ flavour symmetries in the light hadron spectrum for $n_f = 2$ and 3. However, only the vector sector of the above symmetry is observed in the real world. This leads to the idea that $U_V(3) \times U_A(3)$ symmetry is spontaneously broken to $U_V(3)$. The lack of $U_A(3)$ implies no parity doublets of the particles we do see. The spontaneous breakdown of global chiral symmetry $SU_A(3)$ results in the almost massless pseudoscalar mesons 3π's, $4K$'s and η i.e. the Goldstone bosons of this symmetry breaking. On the other hand one expects one more massless pseudoscalar meson corresponding to $U_A(1)$ spontaneous symmetry breaking. But η' is too heavy to be identified as the Goldstone mode of this symmetry breakdown. In fact in perturbative calculation, as mentioned in §1.11, the presence of anomaly in the singlet axial current $j^5_\mu = \bar{\psi}\gamma_\mu\gamma_5\psi$ which couples to gluons gives non-zero divergence to this current. Thus, this anomaly means that the $U_A(1)$ chiral symmetry, present in the theory at the classical level, disappears at the quantum level. Following this idea it was proposed by 't Hooft that the topologically non-trivial gauge configurations in massless QCD gives mass to the singlet meson through anomaly [37]. Despite these theoretical suggestions, no successful perturbative calculations have been so far performed to show explicitly that the singlet meson becomes heavier than the other mesons and that chiral symmetry breaks down spontaneously in QCD. Due to the nature of these problems, a non-perturbative calculation is required to treat them.

[1] $m_u \approx 4\ Mev$, $m_d \approx 7\ Mev$, $m_s \approx 130\ Mev$ [36].

Lattice gauge theory, as discussed at the end of §1.5, provides an efficient regularization scheme to study such non-perturbative aspects of QCD. This could be achieved if the lattice theory possesses the formal properties of the corresponding continuum theory. As far as the hadronic spectrum is concerned, this means that the lattice action must have the above said symmetries. Wilson fermion action, Eq. (1.111), has most of these symmetries but unfortunately, as we saw in §1.13, due to the presence of the Wilson term, it breaks axial chiral symmetry $SU_A(n_f) \times U_A(1)$ explicitly even at the limit of vanishing quark bare mass. This symmetry must be recovered in the continuum limit and be broken spontaneously to provide the observed hadron spectrum with massless pions. However despite the lack of chiral symmetry it turns out that we can tune the hopping parameter κ, for a fixed β, to a critical value κ_c, such that the pion becomes massless. This intuition is supported by strong coupling expansion [38], as well as our Monte Carlo simulations.[2] This very existence of massless pion and in general the light hadrons on a lattice can not be identified as the Goldstone modes of spontaneous chiral symmetry breaking as the Wilson fermion action does not have this symmetry. So there must be a mechanism different from spontaneous chiral symmetry breaking to explain the presence of massless pion on a lattice. Moreover this mechanism should be able to convert its massless mode to a Goldstone boson associated with the spontaneous breakdown of chiral symmetry in the continuum limit of lattice QCD. In the following we review such an alternative mechanism proposed by Aoki [39].

3.2 Parity-Violation In Single Flavour Lattice QCD

Let $\varphi(n)$ be a local operator having the same quantum numbers as a massless particle. As the inverse of mass gap m_Φ associated with $\varphi(n)$ is identified as the correlation length ξ, the correlation length or equivalently correlation function $<\phi(n)\,\phi(0)>$ diverges in the limit where $m_\phi \to 0$. The divergence of correlation

[2] See §4.5.1.

function, in turn implies a phase transition i.e. a transition from a phase where a certain symmetry (not necessarily continuous) is sustained to a phase where this symmetry is violated. Then the massless particle is identified as massless mode associated with this phase transition. One should note that the massless mode occurs only at a critical value of a free parameter of the theory. In other words m_{Φ} becomes non-zero as we tune that parameter above its critical value unless there exists a dense region of such critical values.

Finally if the vacuum expectation value of $\varphi(n)$, $<\varphi(n)>$, in symmetric phase vanishes as a consequence of that symmetry then $<\varphi(n)>$ is a good order parameter to signal the spontaneous break down of the symmetry of the system [40]. To apply these general remarks to lattice QCD with one flavour we note that the Wilson fermion action (1.111) is invariant under the following parity transformations:

$$\overline{\Psi}(x) \rightarrow \overline{\Psi}(-\underline{x},t)\,\gamma_0 \tag{3.7}$$

$$\psi(x) \rightarrow \gamma_0\,\psi(-\underline{x},t) \tag{3.8}$$

$$\psi(x+\hat{\mu}) \rightarrow \begin{cases} \gamma_0\psi(-\underline{x},t+1) & \text{if } \mu = 4 \\ \gamma_0\psi(-\underline{x}-\hat{\mu},t) & \text{if } \mu \neq 4 \end{cases} \tag{3.9}$$

$$U_\mu(x) \rightarrow \begin{cases} U_\mu(-\underline{x},t) & \text{if } \mu = 4 \\ U_{-\mu}(-\underline{x},t) = U_\mu^\dagger(-\underline{x}-\hat{\mu},t) & \text{if } \mu \neq 4 \end{cases} \tag{3.10}$$

$$U_\mu^\dagger(x-\hat{\mu}) \rightarrow \begin{cases} U_\mu^\dagger(-\underline{x},t-1) & \text{if } \mu = 4 \\ U_{-\mu}^\dagger(-\underline{x}+\hat{\mu},t) = U_\mu(-\underline{x},t) & \text{if } \mu \neq 4 \end{cases} \tag{3.11}$$

Under the same transformations, the pseudoscalar field $\pi(x) = i\,\overline{\psi}(x)\gamma_5\psi(x)$ changes sign. So as the consequence of the parity invariance of the action:

$$<\pi(x)> = 0 \tag{3.12}$$

Therefore $<\pi(x)> \neq 0$ signals the spontaneous breaking of (discrete) parity symmetry. In this mechanism $\pi(x)$ is the massless mode associated with

spontaneous parity violating phase transition on a lattice provided that this transition is second order. It should be emphasized that it is not a Goldstone boson as parity is not continuous and it is massless only at the transition point i.e. at the critical hopping parameter κ_c. The above mechanism implies an effective potential $V(\pi)$ for the pion with the properties outlined in Fig. 3.1.

3.3 Parity-Flavour-Violation In 2-Flavour Lattice QCD

In 2-flavour continuum QCD, the members of triplet of pseudoscalar mesons i.e.

$$\pi^0 = \bar{\psi} i\gamma_5 \tau^3 \psi = \bar{u}\gamma_5 u - \bar{d}\gamma_5 d \tag{3.13}$$

$$\pi^{\pm} = \bar{\psi} i \gamma_5 \tau^{\pm} \psi = \begin{cases} \bar{u}\,\gamma_5\, d \\ \bar{d}\,\gamma_5\, u \end{cases} \tag{3.14}$$

appear as massless Goldstone bosons. Here

$$\tau^{\pm} = \frac{1}{2}\,(\tau^1 \pm i\tau^2), \tag{3.15}$$

and τ^1, τ^2 and τ^3 are generators of $SU(2)$ Lie algebra acting on flavour indices. On the other hand the singlet pseudoscalar meson i.e.

$$\eta = \bar{\psi} i\gamma_5 \mathbf{1} \psi = \bar{u}\gamma_5 u + \bar{d}\gamma_5 d \tag{3.16}$$

where $\mathbf{1}$ is a $SU(2)$ unit matrix, remains massive. Taking account of these experimental facts and generalizing the arguments of the last section will suggest to choose the neutral pion condensation $<\bar{\psi} i\gamma_5 \tau^3 \psi>$ as the right order parameter. This requires $\bar{u}\gamma_5 u$ and $\bar{d}\gamma_5 d$ to be in opposite vacua otherwise it is clear from Eq. (3.13) that $<\pi^0(x)>$ vanishes identically. As we saw before, in addition to discrete parity symmetry, the Wilson fermion action has also continuous flavour symmetry. Consequently the expectation value of $\pi^0(x)$ vanishes in the symmetric phase. In this phase $m_{\pi^0} = m_{\pi^+} = m_{\pi^-}$ as a result of states degeneracy. At κ_c, π^0, π^+ and π^- become massless. In particular π^0 is the massless mode associated with the

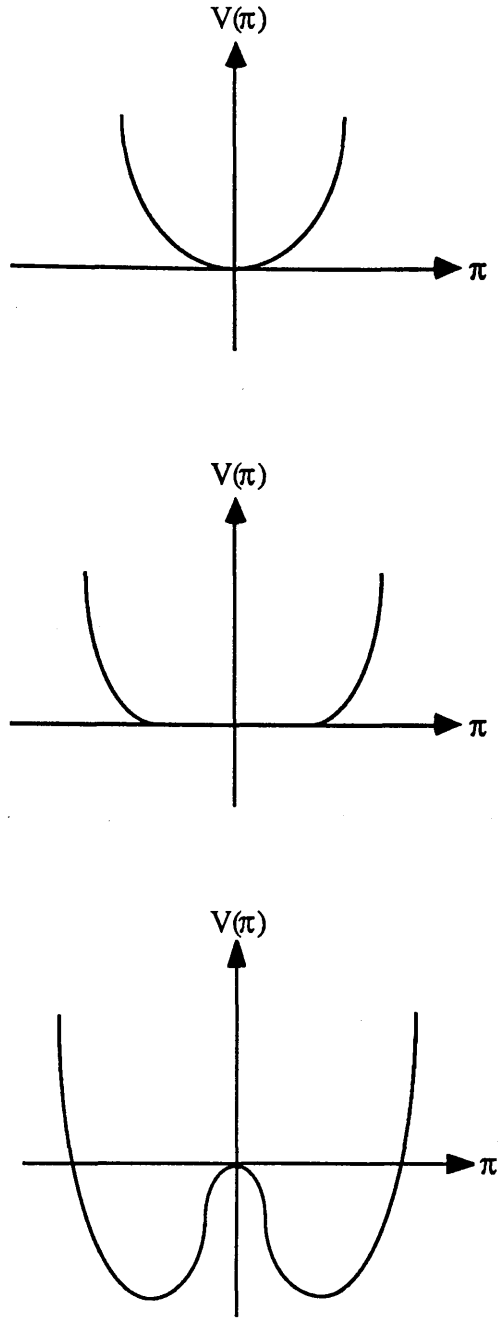

Fig. 3.1 Pion effective potential $V(\pi)$ vs. π field as κ increases; (top) at $\kappa < \kappa_c$ the phase is symmetric under $\pi \rightarrow -\pi$ and $<\pi> = 0$, (middle) at $\kappa = \kappa_c$ the π direction becomes flat and $m_\pi \rightarrow 0$, (above) at $\kappa > \kappa_c$ the symmetry is broken and $<\pi> = \pm c$, going to one another under $\pi \rightarrow -\pi$. The resulting massless mode is not a Goldstone particle since the broken symmetry is discrete.

phase transition from symmetric phase to a phase where both parity and flavour symmetries are broken spontaneously. Just above this phase transition point π^0 becomes massive again while π^+ and π^- remain as massless Goldstone bosons of (continuous) flavour symmetry breaking. On the other hand Eq. (3.16) indicates that η remains massive in the whole region of parameter space as $<\eta(x)>$ is always zero because $\bar{u}\gamma_5 u$ and $\bar{d}\gamma_5 d$ are in opposite vacua as mentioned above.

The existence of spontaneously parity-violating phase in single flavour lattice QCD and parity-flavour-violating phase in more than one flavour as well as the vanishing of m_{π^0} at κ_c, the masslessness of m_{π^+} and m_{π^-} in the symmetry broken phase and vanishing of η condensation at all κ's must be confirmed by analytic calculations and/or by Monte Carlo simulations. In the following sections we only review the results of such investigations in single-flavour case with a view to apply them to construct the QCD phase structure in κ-g^2 space.

Some theoretical arguments regarding lattice QCD with more than one flavour and in particular with two flavours can be found in [41] for the special case of strong coupling limit. Monte Carlo simulations of lattice QCD with more than one flavour which require the application of dynamical fermions can be the subject of further works in this context.

3.4 Free Fermion Theory

Analytic calculations can be performed at weak coupling and strong coupling cases. In the first case where $g \to 0$ the β $(\sim \frac{1}{g^2})$ factor in gauge action (1.26) becomes very large which suppresses the fluctuations in the plaquette variable i.e. the only non-zero contribution to the partition function comes from those configurations where $\frac{1}{N_c} Tr\ U_p \to 1$. The fluctuations around this trivial limit can be treated perturbatively, resulting in an expansion completely analogous to the perturbation theory of the continuum formulation. Having expanded the gauge variable (1.24) as:

$$U_\mu(n) = e^{-igaA_\mu(n)} = 1\text{-}igaA_\mu(n) \tag{3.17}$$

and rewriting the measure $\mathcal{D}U$ and the action in terms of vector potential $A_\mu(n)$ an ordinary perturbation theory can be set up [38]. In this section we consider special case of weak coupling limit i.e. $g = 0$ (free fermions). Because of the vanishing of gauge interaction, this case is equivalent to $U_\mu(n) = \mathbb{1}\ \forall\ n,\mu$. In this case the fermion matrix (1.112) reduces to Eq. (1.108) and one may Fourier transform it to obtain M in momentum space as:

$$M_{pq} = \left[1+2\kappa\sum_\mu (i\gamma_\mu \sin p_\mu - r\cos p_\mu) \right] \delta(p-q) \tag{3.18}$$

M is, then, diagonal in momentum space (but not in spin space) with the diagonal elements:

$$M(p) = 1+2\kappa\sum_\mu (i\gamma_\mu \sin p_\mu - r\cos p_\mu) \tag{3.19}$$

We are interested in the poles of fermion propagator $M(p)^{-1}$. As any zero eigenvalues of M are also zero eigenvalues of $M^\dagger M$ and vice versa, we work with $M^\dagger M$. Using the formal properties of γ-matrices[3] $M^\dagger M$ is diagonalized not only in momentum space but also in spin space with the diagonal elements (i.e. the eigenvalues):

$$M^\dagger M(p) = (1-2\kappa r\sum_\mu \cos p_\mu)^2 + 4\kappa^2 \sum_\mu \sin^2 p_\mu \tag{3.20}$$

As hopping parameter is real the zero eigenvalues are obtained from Eq. (3.20) if and only if

$$\sin p_\mu = 0 \qquad \mu = 1, ..., 4 \tag{3.21}$$

and

$$1-2\kappa r\sum_\mu \cos p_\mu = 0 \tag{3.22}$$

for real values of momenta. The constraints (3.21) and (3.22) would restrict the critical hopping parameters to the following at the corresponding momenta,

[3] See Appendix.

$$\frac{1}{\kappa_c} = \begin{cases} 8 & \text{at} \quad p = (0,0,0,0) \\ 4 & \text{at} \quad p = (\pi,0,0,0),\ ...,\ (0,0,0,\pi) \\ 0 & \text{at} \quad p = (\pi,\pi,0,0),\ ...,\ (0,0,\pi,\pi) \\ -4 & \text{at} \quad p = (\pi,\pi,\pi,0),\ ...,\ (0,\pi,\pi,\pi) \\ -8 & \text{at} \quad p = (\pi,\pi,\pi,\pi) \end{cases} \tag{3.23}$$

where we have let $r = 1$. Eq. (3.23) locates the κ_c's at the corners of the first Brillouin zone where the fermion doublers, in the naive action, sit.[4] From the poles of the fermion propagator the quark mass is obtained by letting the particle be at rest, i.e. $p = (0,0,0,im_q)$. Using Eq. (3.20) this results in:

$$\cosh m_q = 1 + \frac{(1-8\kappa)^2}{4\kappa(1-6\kappa)} \tag{3.24}$$

It is interesting to review the above considerations at the limiting case where $p_\mu \to 0$ i.e. the actual continuum limit. In this limit the fermion matrix $M(p)$ given by Eq. (3.19) reduces to:

$$M(p) \to M_{cont}(p) = 2\kappa\left(i\not{p} + \frac{1-8\kappa}{2\kappa}\right) \tag{3.25}$$

Following the same approach as before the quark mass m_q is calculated to be $\frac{1-8\kappa}{2\kappa}$ and then $M_{cont}(p)$ becomes identical with the continuum equation of free fermion Dirac operator. This κ dependence of m_q is now, of course, consistent with our previous definition of hopping parameter κ in Eq. (1.109). Moreover the fermion propagator has a pole at $\kappa_c = \frac{1}{8}$ at which the continuum limit of free theory becomes massless i.e. the quark mass vanishes.

Introducing the gauge fields in fermion matrix complicates the calculation of the poles of the fermion propagator. However, in weak coupling region the perturbative analysis shows a development in the singularity of the fermion propagator in the vicinity of free fermion singular point at $\kappa_c = \frac{1}{8}$ [38] as:

---

[4] See §1.11.

$$\kappa_c \approx \frac{1}{8}\,(1+0.095 N_c g^2) \tag{3.26}$$

for large N_c limit of $SU(N_c)$ gauge group. It is of interest to note that the sign of coefficient $N_c g^2$ is positive. This indicates that κ_c is increasing as g increases in the weak coupling region.

3.5 Strong Coupling Limit

In the last section it was confirmed that there exists a critical value of κ in free fermion theory at which quark mass vanishes. In the strong coupling region where $g \to \infty$ because of the smallness of β in gauge action, Eq. (1.26), the Boltzmann factor can be expanded and a systematic expansion in β can be constructed. The strong coupling expansion is in complete analogy with the high-temperature expansion in statistical physics. The large N_c strong coupling expansion techniques accompanied by the introduction of effective Lagrangian [42] can be applied to calculate meson propagators. As before, the pole of the meson propagator would give the meson mass in terms of hopping parameter. Much information can be obtained in the limiting case where $\beta = 0$. In this case [43],

$$\cosh m_\pi = \begin{cases} 1 + \dfrac{(1-16\kappa^2)(1-4\kappa^2)}{8\kappa^2(1-6\kappa^2)} & \text{at } \kappa \le \dfrac{1}{4} \\ 1 + \dfrac{(16\kappa^2-1)(64\kappa^2-1)(32\kappa^2+1)}{64\kappa^2\left(\frac{15}{32} - 8\kappa^2 + 128\kappa^4\right)} & \text{at } \kappa \ge \dfrac{1}{4} \end{cases} \tag{3.27}$$

therefore pion mass vanishes at $\kappa_c = \frac{1}{4}$.

Under the same conditions pion vacuum expectation value as an order parameter is calculated to be:

$$\frac{\langle \bar{\psi}\, i\gamma_5 \psi \rangle}{4N_c} = \begin{cases} 0 & \text{at } \kappa \le \dfrac{1}{4} \\ \dfrac{4\kappa\sqrt{3(16\kappa^2-1)}}{64\kappa^2 - 1} & \text{at } \kappa \ge \dfrac{1}{4} \end{cases} \tag{3.28}$$

This shows that parity-violating phase transition occurs at $\kappa_c = \frac{1}{4}$ and that parity-violating phase exists at $\kappa \geq \frac{1}{4}$. Moreover the pion which becomes massless only at $\kappa_c = \frac{1}{4}$ is the massless mode associated with this spontaneous parity-violating phase transition.

Introducing the gauge field terms in the strong coupling region does not alter the above qualitative properties of $\beta = 0$ case. Now the singularity in pion propagator develops [38] as:

$$\kappa_c = \frac{1}{4}\left(1 - \frac{3}{32N_c g^2}\right) \tag{3.29}$$

The important point is that the sign of the coefficient of $(N_c g^2)^{-1}$ in Eq. (3.29) is negative which means that κ_c is reducing as β increases in the strong coupling region. This property alongside with the corresponding result in weak coupling region, Eq. (3.26), will, in some extent, justify the phase diagram discussed in the following section.

3.6 QCD Phase Structure

To construct the QCD phase diagram in κ-g^2 plane at least some knowledge of intermediate-coupling region is required. Although no such analytic information is available for QCD, one still might be inspired from a relatively similar model i.e. the Gross-Neveu model [44] to construct such a phase diagram. This model is a two-dimensional massless fermion field theory with quartic interactions described by the Lagrangian,

$$\mathcal{L} = \bar{\psi}(i\not{\partial})\psi + \frac{1}{2}g^2(\bar{\psi}\psi)^2 \tag{3.30}$$

Its importance is that it is the only known soluble model with the distinctive properties of asymptotic freedom and chiral symmetry breaking as QCD. Lattice Gross-Neveu model with Wilson term behaves similar to QCD in the strong and weak coupling limits except there are only three continuum limits as compared to

five continuum limits of lattice QCD distinguished by five κ_c's in Eq. (3.23). Moreover it has been shown that the broken chiral symmetry by the Wilson term is recovered near the continuum limit in lattice Gross-Neveu model [45]. The phase diagram of lattice Gross-Neveu model is given in Fig. 3.2.

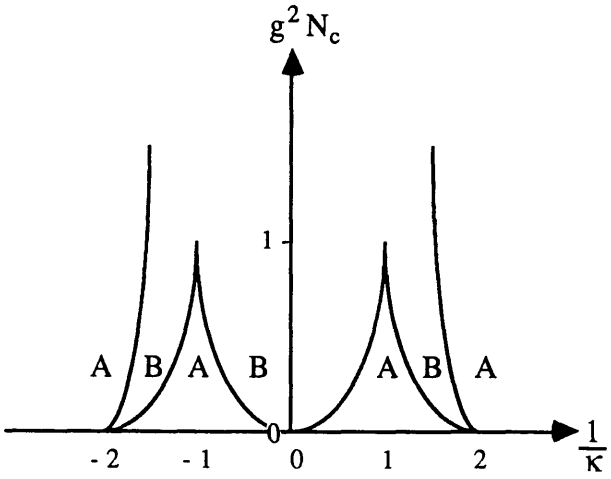

Fig. 3.2 Phase diagram of lattice Gross-Neveu model in g^2N_c-κ^{-1} plane.

From our review in the previous sections we already know that there are two phases in the strong coupling region: one is the phase with $<\bar{\psi}i\gamma_5\psi> = 0$ and the other is the phase with $<\bar{\psi}i\gamma_5\psi> \neq 0$. Furthermore the phase transition line which divides κ^{-1}-g^2 plane into the two domains exists also in the weak coupling region as we saw the appearance of massless quark in free case.

Based on the above considerations a lattice QCD phase diagram has been proposed by Aoki [46, 47, 48]. This phase diagram which is reproduced in Fig. 3.3 reflects the following properties for lattice QCD:

I There are five continuum limits corresponding to different regions in momentum space at weak coupling limit. These momentum regions and the corresponding critical values of κ where quark mass vanishes were given in Eq. (3.23). The true continuum limit is, of course, at low momentum where $\kappa_c = \frac{1}{8}$.

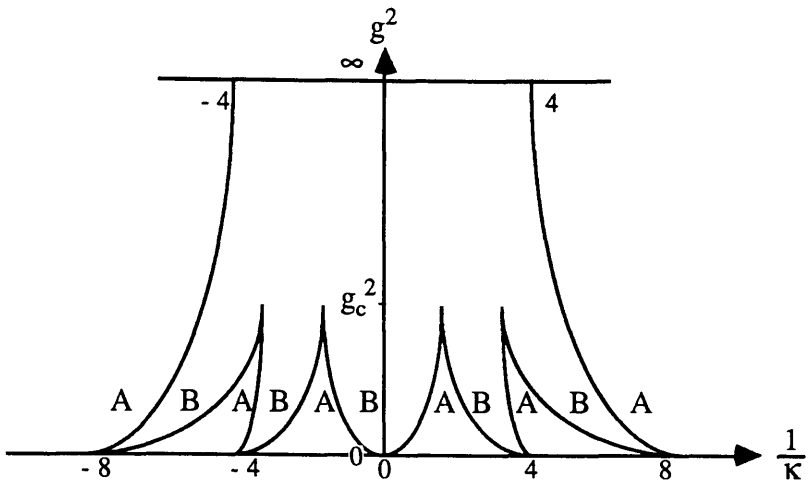

Fig. 3.3 The postulated phase diagram of lattice QCD in the presence of Wilson term. *A* is the normal phase for which $<\bar{\psi} i\gamma_5 \psi> = 0$ and *B* is the parity-violating phase which has $<\bar{\psi} i\gamma_5 \psi> \neq 0$.

II In the strong coupling limit there are only two critical values of $\kappa_c = \frac{1}{4}$ and $\kappa_c = -\frac{1}{4}$ where the pion mass vanishes. This is consistent with Eq. (3.27).

III In the intermediate-coupling regions and below a critical coupling g_c new critical lines emerge and five regions in momentum space become separated from one another.

IV Each critical line separates region *A* where $<\bar{\psi} i\gamma_5 \psi> = 0$ from region *B* where $<\bar{\psi} i\gamma_5 \psi> \neq 0$. On the critical line pion mass vanishes. Then $<\bar{\psi} i\gamma_5 \psi>$ is a good order parameter to detect this phase transition i.e. a transition from parity-conserving phase to parity-violating phase as κ crosses κ_c.

3.7 Monte Carlo Simulation

In the previous sections we reviewed general remarks regarding the existence of parity-violating phase transition in weak coupling region (§3.4) as well as strong coupling region (§3.5) as the massless pion could be observed in these regions. We also anticipated such a phase transition in intermediate-coupling region via a lattice QCD phase diagram (§3.6). In this section we aim to see if Monte Carlo results confirm such a phase transition. We will work in quenched approximation and if

this phase transition really exists it must also show up even in this approximation where the effect of quark loops are suppressed as it was revealed in both free case and strong coupling limit where effectively such an effect was ignored. To confirm the phase transition we should study the order parameter $<\pi(x)>$ and correlation function $<\pi(x)\ \pi(y)>$. In the following expressions the expectation values are implicitly summed over x in $<\pi(x)>$ and over origin, y as well as x in $<\pi(x)\pi(y)>$.

$$< \pi\,(x) > = < \bar{\psi}\, i\, \gamma_5 \psi >$$

$$= \frac{1}{Z} \int \mathcal{D}\bar{\psi}\, \mathcal{D}\psi\, \mathcal{D}U\, (\bar{\psi} i \gamma_5\, \psi)\, e^{-\bar{\psi} M \psi - S_g} \tag{3.31}$$

where the partition function Z is given by Eq. (1.83). Taking into account the general properties of Grassmann variables ψ and $\bar{\psi}$ we obtain:

$$< \pi\,(x) > = \frac{i}{Z} \int \mathcal{D}U\, \det M\,(U)\, \mathrm{Tr}\, (\gamma_5 M)^{-1}\, e^{-S_g} \tag{3.32}$$

and

$$Z = \int \mathcal{D}U\, \det M(U)\, e^{-S_g} \tag{3.33}$$

In quenched approximation, where $det\ M(U) = 1$, the pion field vacuum expectation value (3.32) is simplified as:

$$< \pi(x) > = i < \mathrm{Tr}\, (\gamma_5\, M)^{-1} >_G \tag{3.34}$$

where G means averaging over gauge field configurations. Similarly we get:

$$< \pi(x)\, \pi(y) > = < \mathrm{Tr}\, (M^{\dagger} M)^{-1} >_G \tag{3.35}$$

We are interested to study observables $<\pi(x)>$ and $<\pi(x)\ \pi(y)>$ by calculating the fermion matrix eigenvalue spectrum. In fact one of the clearest ways to study phase transitions involving fermions [49] is to calculate the eigenvalues of the fermion matrix. Let λ_i be the eigenvalues of $\gamma_5 M$. Then the above vacuum expectation values read:

$$< \pi(x) > = < i\sum_i \frac{1}{\lambda_i} >_G \tag{3.36}$$

$$< \pi(x)\, \pi(y) > = <\sum_i \frac{1}{\lambda_i^2} >_G \tag{3.37}$$

Working directly in terms of eigenvalues of M requires non-hermitian Lanczos algorithm to calculate eigenvalues of M as M is not hermitian. However, the major contributions to $<\pi(x)>$ and $<\pi(x)\pi(y)>$ are from the small modulus eigenvalues and specially from the zero modes of M. Moreover, as shown in Eq. (3.36), $<\pi(x)>$ is imaginary and can only develop a real part if there are zero modes in the infinite-volume limit. Also it is only at the presence of zero modes that the correlation function can diverge and signal the phase transition with a massless mode. On the other hand if M has a zero mode then so does $\gamma_5 M$ and $M^\dagger M$ and vice versa. Accordingly, without loss of generality, we study $\gamma_5 M$ spectrum and search for its zero modes. It is interesting to mention that exact zero modes do really exist even on a finite lattice for Wilson fermions [50, 51]. Our results, presented in §3.9, confirm this fact. However, in practice we never find exact zero modes so we define κ_z where $|\lambda_z| < 0.001$ provided that λ_z changes sign at some corresponding hopping parameter in the vicinity of κ_z. In passing one notes that hermicity and anticommutativity of γ-matrices make $\gamma_5 M$ hermitian so that hermitian lanczos algorithm developed in Chapter 2 can be applied for the corresponding eigenvalue calculations. Moreover the hermitian nature of $\gamma_5 M$ allows implementation of large lattices which are not possible to tackle in case of non-hermitian M.

To study Eqs. (3.36) and (3.37) more closely we see that as $\gamma_5 M$ is hermitian the r.h.s. of Eq. (3.36) is always pure imaginary whereas the l.h.s. is real as π-field is hermitian. As a result $<\pi(x)>$ vanishes even if the symmetry is broken spontaneously. To cope with this situation which is a finite-volume effect we can add a small explicit symmetry-breaking term, $iH\bar{\psi}\gamma_5\psi$, to the action and

study the limit in which $H \to 0$.[5] In this case Eq. (3.34) is modified as:

$$<\pi(x)> = \lim_{H\to 0} \lim_{vol\to\infty} i < Tr\,(\gamma_5 M_H)^{-1} >_G \tag{3.38}$$

where M_H is the modified fermion matrix,

$$M_H = M + iH\gamma_5 \tag{3.39}$$

Consequently Eq. (3.36) is converted to:

$$<\pi(x)> = \lim_{H\to 0} \lim_{vol\to 0} i < \sum_i \frac{1}{\lambda_i + iH} >_G \tag{3.40}$$

By a little algebraic manipulation Eq. (3.40) in infinite-volume limit reads:

$$<\pi(x)> = < \pi\rho(0) + i \int_{-\infty}^{\infty} \frac{\rho(\lambda)}{\lambda} d\lambda >_G \tag{3.41}$$

where $\rho(\lambda)$ is the density of eigenvalues around λ. The imaginary part in the r.h.s. of Eq. (3.41) is just r.h.s. of Eq. (3.36) which turned out to vanish. Therefore we have:

$$<\pi(x)> = \pi <\rho(0)>_G \tag{3.42}$$

Both Eq. (3.37) which might be written as:

$$<\pi(x)\,\pi(0)> = < \int_{-\infty}^{\infty} \frac{\rho(\lambda)}{\lambda^2} d\lambda >_G \tag{3.43}$$

and Eq. (3.42) show that the existence of zero modes alone do not confirm the phase transition unless $\rho(0) \neq 0$.[6]

3.8 Checks On The Eigenvalues

Some general properties of $\gamma_5 M$ can be used to set up checking conditions on its eigenvalues λ_i. The first check could be the calculation of the eigenvalues in the free case. In this case as we saw in Eq. (3.20) the eigenvalue squares are explicitly calculated as:

---

[5] This is analogous to the calculation of the chiral condensate $<\bar{\psi}\psi>$ at the limit in which $m \to 0$ [30].

[6] An example of a zero mode where $\rho(0)$ tends to vanish is given in Fig. 3.31.

$$\lambda^2 = (1-2\kappa r\sum_{\mu} \cos p_\mu)^2 + 4\kappa^2 \sum_{\mu} \sin^2 p_\mu \qquad (3.44)$$

With periodic boundary conditions on the fermion fields in all directions i.e.

$$\psi(x) = \psi(x+N_\mu a) \qquad \mu = 1, ..., 4 \qquad (3.45)$$

the momenta p_μ can only have the values:

$$p_\mu = \frac{2n\pi}{N_\mu a} \qquad n = 0, 1, 2, ... \qquad (3.46)$$

where N_μ is the number of sites in μ direction. The corresponding momenta with antiperiodic boundary conditions are:

$$p_\mu = \frac{(2n+1)\pi}{N_\mu a} \qquad n = 0, 1, 2, ... \qquad (3.47)$$

For example, a 4^4 lattice with periodic boundary conditions turns out to have 15 distinctive eigenvalues for $\gamma_5 M$ whose squares are as follows:

$$\{ (1 \pm 8\kappa r)^2, \quad (1\pm 4\kappa r)^2, \quad 1,$$
$$(1 \pm 6\kappa r)^2 + 4\kappa^2, \quad (1\pm 2\kappa r)^2 + 4\kappa^2,$$
$$(1 \pm 4\kappa r)^2 + 8\kappa^2, \quad 1+ 8\kappa^2,$$
$$(1 \pm 2\kappa r)^2 + 12\kappa^2,$$
$$1 + 16\kappa^2 \}. \qquad (3.48)$$

There are only 5 distinct eigenvalues with antiperiodic boundary conditions whose squares are:

$$\{ (1\pm 4\sqrt{2\kappa r})^2 + 8\kappa^2, \quad (1\pm 2\sqrt{2\kappa r})^2 + 8\kappa^2, \quad 1+ 8\kappa^2 \}. \qquad (3.49)$$

To check the program one can switch off the gauge fields and converts the theory to the free case and calculates the spectrum and compares the results with the analytic values of eigenvalue squares.

In the interacting case the sum of the eigenvalues and the sum of their squares can be checked against the corresponding analytic expressions. Using Eq. (1.112) and writing M as $-\kappa\tilde{M}+\mathbf{1}$, where

$$\tilde{M}_{nn'} = \sum_{\mu} \left[(r-\gamma_\mu)\, U_\mu(n)\, \delta_{n+\hat{\mu},n'} + (r+\gamma_\mu)\, U_\mu^{\dagger}(n-\hat{\mu})\, \delta_{n-\hat{\mu},n'} \right] \tag{3.50}$$

one notes that $\tilde{M}$ is manifestly traceless. Then as the diagonal elements of M are just unity and γ_5 is traceless it turns out that $\gamma_5 M$ is traceless. So as the first check the eigenvalues must satisfy the condition:

$$\Sigma \lambda_i = 0. \tag{3.51}$$

Another condition on eigenvalues λ_i is obtained by using the tracelessness property of $\tilde{M}$. We see that:

$$\mathrm{Tr}\left[(\gamma_5 M)^{\dagger}(\gamma_5 M) \right] = \mathrm{Tr}\,(M^{\dagger}M) = \kappa^2 \mathrm{Tr}\,(\tilde{M}^{\dagger}\tilde{M}) + \mathrm{Tr}\,\mathbb{1} \tag{3.52}$$

Making use of γ-matrices properties and the unitary nature of the gauge fields we obtain:

$$\mathrm{Tr}\,(\tilde{M}^{\dagger}\tilde{M}) = N_{spin} N_{color} N_{site}\, 8(1+r^2) \tag{3.53}$$

and since

$$\mathrm{Tr}\,\mathbb{1} = N_{spin}\, N_{color}\, N_{site} \tag{3.54}$$

then the eigenvalue squares satisfy the condition:

$$\sum_i \lambda_i^2 = N_{spin}\, N_{color}\, N_{site} \left[1 + 8\kappa^2 (1+r^2) \right] \tag{3.55}$$

The generality of the conditions (3.51) and (3.55) is in their gauge invariance and independence from the boundary conditions imposed on the fermion fields.

In practice we can compute the whole spectrum of $\gamma_5 M$ in a reasonable computational time for 4^4 lattices, for instance, and establish the correctness of the program by checking the sum and sum of the squares of the eigenvalues.

3.9 Monte Carlo Results

To investigate the $\gamma_5 M$ spectrum we have studied lattices of up to 8^4. Although the main concern is the existence of zero modes in the infinite-volume limit one notes

that working in bigger lattices becomes extremely time consuming even if only a few eigenvalues are to be calculated. In practice we only study the eigenvalues on a finite-size lattice and extrapolate the behaviour averaged over several gauge configurations to a continuous spectrum by considering the density of the eigenvalues. We have obtained the spectra at strong coupling limit as well as some weak coupling constants and in some cases the effect of boundary conditions has been observed too. We have worked in *SU(3)* gauge group throughout. In the following the Wilson parameter r is set equal to unity. Although different choices of r change the results quantitatively however, they do not modify our conclusions qualitatively as long as $r \neq 0$, otherwise the action converts to the naive action and doubling problem appears again.

3.9.1 Strong Coupling Limit

As the first attempt the eigenvalue distribution of $\gamma_5 M$ is obtained on a 4^4 lattice, with antiperiodic boundary conditions in all directions on fermion fields, using the Metropolis algorithm for a gauge field configuration generated from 20 sweeps starting from a hot start. The eigenvalue distribution shows that for small values of κ the eigenvalues are far from zero axis. This agrees with the expectation that as $\gamma_5 M \rightarrow \gamma_5$ when $\kappa \rightarrow 0$ all the eigenvalues of $\gamma_5 M$ converge only to +1 or -1. As κ increases the positive and the negative eigenvalues tend to approach zero axis in an almost symmetric manner. As one approaches κ_z where the first zero mode appears this approximate symmetry disappears. For $\kappa > \kappa_z$ the first positive and negative eigenvalues remain very close to zero and even vanish for some κ's. For this configuration we have found $\kappa_z = 0.266$ with the least modulus eigenvalue λ_z equal to -0.9911D-5. The described behaviour is plotted in Fig. 3.4 for the first few eigenvalues on either side of zero axis.

As we saw before in §3.7 what governs the observables such as $\langle Tr\,(\gamma_5 M)^{-1} \rangle_G$ or $\langle Tr\,(M^\dagger M)^{-1} \rangle_G$ is not only the existence of zero modes but also

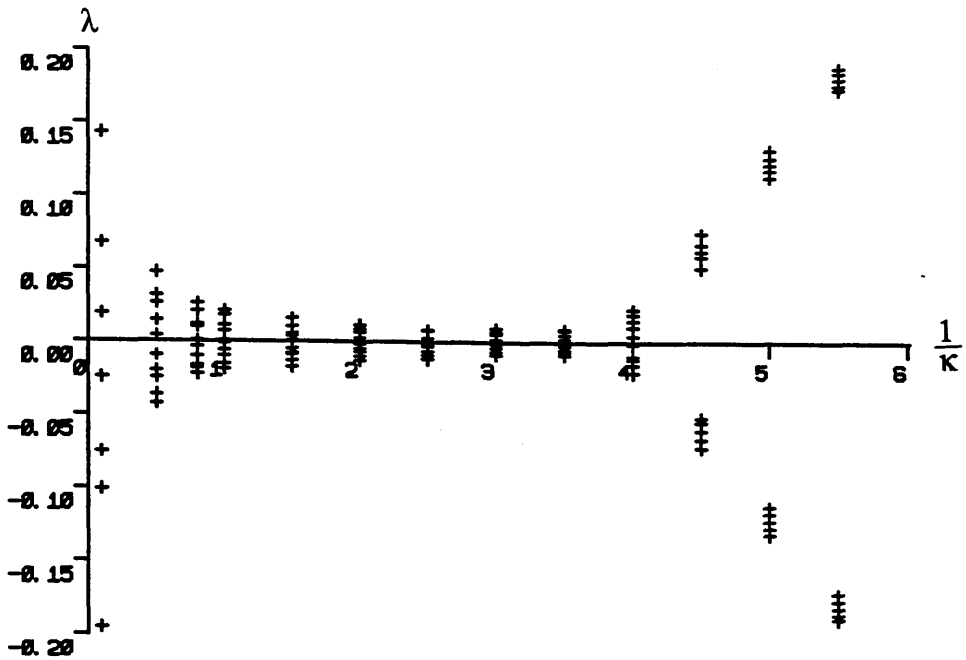

Fig. 3.4 $\gamma_5 M$ spectrum vs. $\frac{1}{\kappa}$ at $\beta = 0.0$ on a 4^4 lattice.

their density $\rho(0)$. If we number the eigenvalues with arbitrary origin, the density of eigenvalues $\rho(\lambda)$ i.e. the number of eigenvalues per unit eigenvalue separation is defined by:

$$\rho(\lambda) = \frac{dN(\lambda)}{d\lambda} \tag{3.56}$$

where $dN(\lambda)$ is the number of eigenvalues between λ and $\lambda+d\lambda$. Accordingly $\rho(0)$ is just the estimate of the the slope of the curve $N(\lambda)$ vs. λ at $\lambda = 0$. To study the behaviour of $\rho(0)$ as a function of κ we have generated five more configurations at every 60 iterations after the initial 261 sweeps starting from a hot start discarded for thermalization. There are very clear indications of vanishing $\rho(0)$ at the values of κ below a critical κ_z which changes from configuration to configuration. Crossing κ_z is accompanied by a sudden change in $\rho(0)$. The zero modes density remains actually non-zero for $\kappa \geq \kappa_z$, increasing first to a maximum value and then decreasing[7] and approaching zero as $\kappa \to \infty$ as shown in Fig. 3.5. One should

[7] Decreasing of $\rho(0)$ is presumably a finite-size effect. In the infinite-volume limit, however, we expect non-vanishing $\rho(0)$ at all values of κ above κ_c in the strong coupling limit.

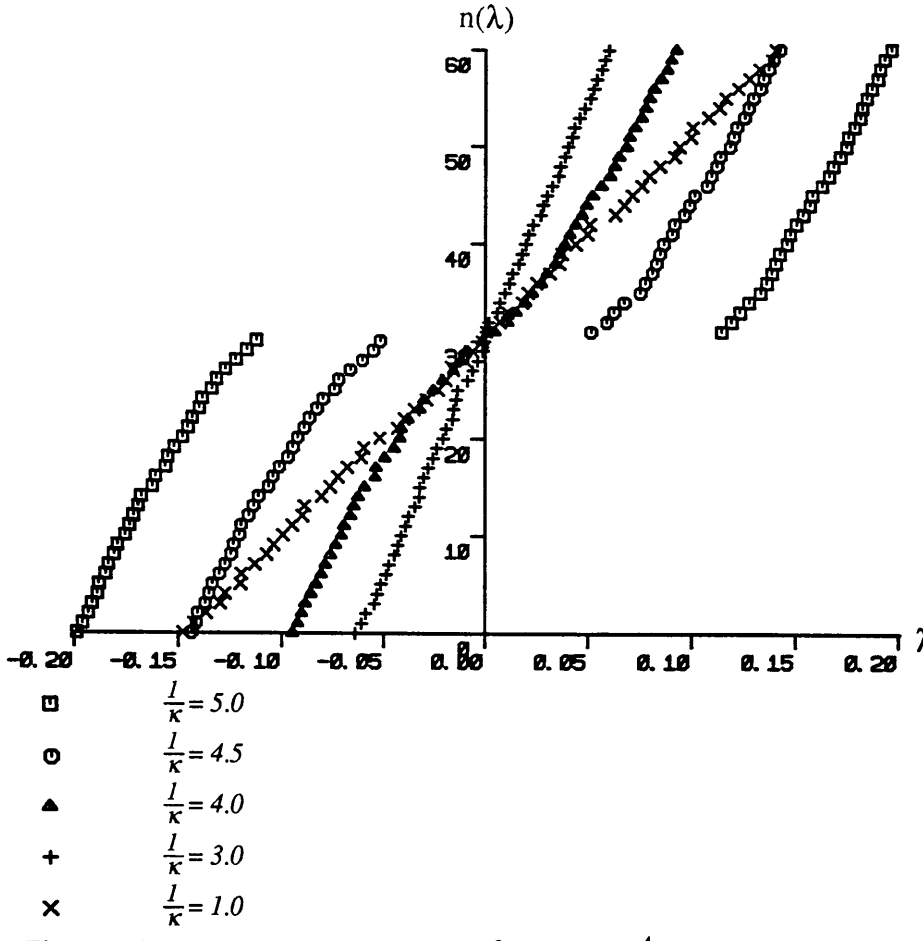

Fig. 3.5 Eigenvalue distribution of $\gamma_5 M$ at $\beta = 0.0$ on a 4^4 lattice for a number of κ.

note that κ_z is not necessarily the same as actual κ_c where average pion mass vanishes. In infinite-volume limit, however, κ_z calculated over the ensemble of all the gauge configurations would approach κ_c.

The κ_z for the above configurations and the corresponding least modulus eigenvalues are given in Table 3.1. In practice we notice that due to the discrete nature of eigenvalue distribution on a finite lattice, $\rho(0)$ begins to become different from zero slightly before the appearance of the first zero modes.

We also changed the boundary conditions to periodic and studied the corresponding spectra under the same conditions as for antiperiodic case. Although the κ_z's change slightly, the general behaviour is effectively the same as antiperiodic case.

We have extended our studies closer into continuum limit by working on 6^4

Table 3.1

κ_z for a number of 4^4 *SU(3)* gauge configurations at strong coupling limit.

κ_z	λ_z
0.266	- 0.9911D-5
0.270	- 0.2160D-3
0.260	- 0.1230D-3
0.260	- 0.4200D-3

and 8^4 lattices. For a 6^4 lattice and with a hot start we have generated two gauge configurations 100 iterations apart when the first 100 iterations discarded for thermalisation. The general behaviour obtained on a 6^4 lattice is the same as 4^4 lattice. The κ_z's in the two configurations are practically the same and approximately equal to 0.26 and the corresponding least modulus eigenvalues are 0.35D-4 and -0.126D-3 respectively. The approach toward κ_z is clearly indicated in Fig. 3.6 in which $N(\lambda)$ has been plotted against λ for a range of κ.

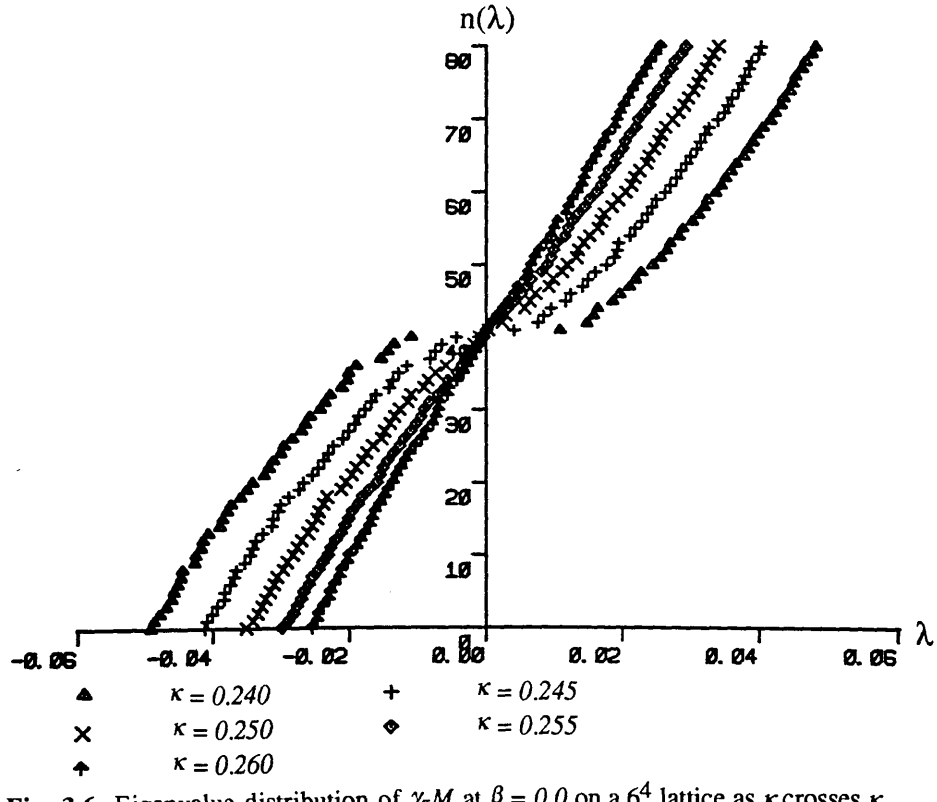

Fig. 3.6 Eigenvalue distribution of $\gamma_5 M$ at $\beta = 0.0$ on a 6^4 lattice as κ crosses κ_z.

Finally we have studied $\gamma_5 M$ spectrum on an 8^4 lattice by generating a configuration from 300 sweeps starting from a hot start. The results once again confirm the previous results of smaller lattices. For this 8^4 configuration κ_z is observed to be 0.252 with the smallest modulus eigenvalue 0.9764D-4.

For the same κ, there are apparently more eigenvalues in a given range of eigenvalues on larger lattices resulting in denser eigenvalue distribution compared with the smaller lattices. To extrapolate the results to infinite-volume limit one might normalize the eigenvalue distribution by the volume and study $\frac{n(\lambda)}{N_{site}}$ vs. λ as in Fig. 3.7. Interesting observation is that the κ_z seems to decrease as we approach infinite-volume limit on bigger lattices if we compare the κ_z's of the above 4^4, 6^4, 8^4 lattices. This is in agreement with the analytic prediction of $\kappa_z = 0.25$ in infinite-volume limit as stated in §3.5.

In closing this sub-section we conclude the existence of parity-violating

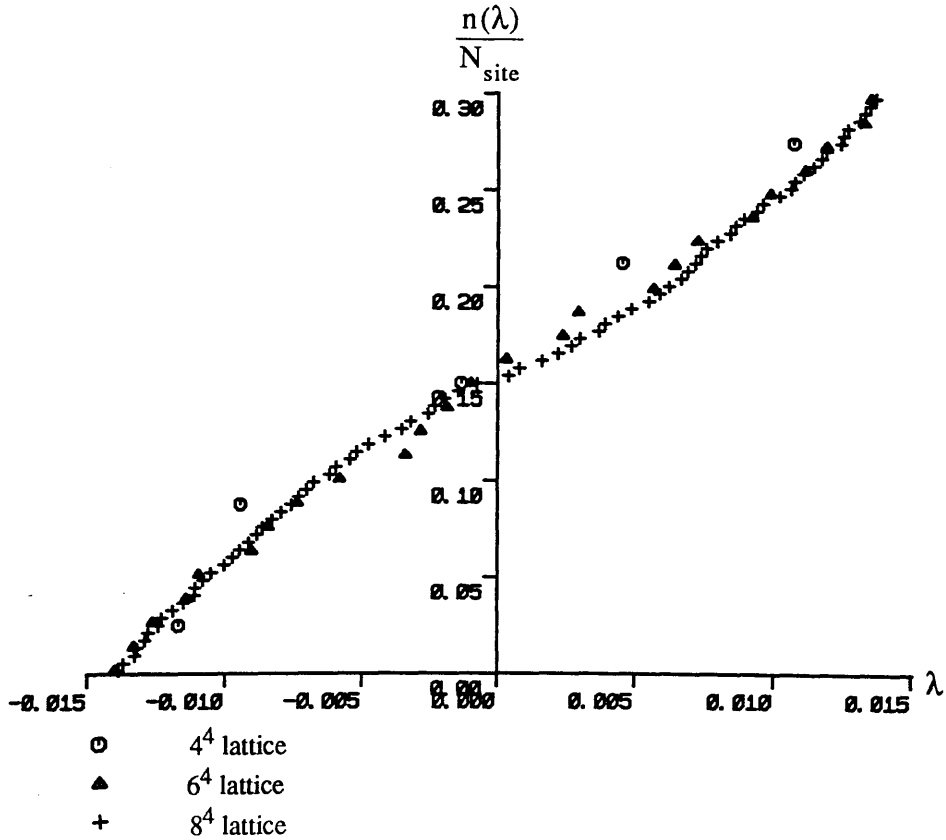

Fig. 3.7 Normalized eigenvalue distribution of $\gamma_5 M$ at $\beta = 0.0$ and $\kappa = 0.25$.

phase transition at strong coupling limit in quenched approximation as a result of which a massless pion, in infinite-volume limit, occurs at $\kappa_c = 0.25$ where pion propagator $(M^{\dagger}M)^{-1}$ is singular.

3.9.2 Weak Coupling

We classify our results of 4^4 and 8^4 lattices as follows:

4^4 Lattices

We have worked on a range of non-zero β's from $\beta = 5.0$ up to $\beta = 5.7$. As presented in Chapter 1, Wilson Line plots of the corresponding gauge configurations, show a clear deconfinement phase transition at $\beta = 5.5$ by breaking the Z_3 symmetry.[8]

At $\beta = 5.0$ two gauge configurations have been generated by 1000 and 4000 iterations from a hot start. The $\gamma_5 M$ spectra in this case show similar behaviour as $\beta = 0$ case. The κ_z's have apparently shifted toward lower values compared with the strong coupling limit κ_z's. They are 0.24 and 0.25 with the corresponding least modulus eigenvalues 0.775D-3 and 0.185D-3 for the two configurations respectively.

Similar behaviour is also observed at $\beta = 5.3$ for a gauge configuration obtained by 35000 sweeps from a hot start. The corresponding κ_z is still decreased further down to $\kappa_z = 0.1991$ with smallest modulus eigenvalue -0.1144D-6.

Decreasing of the κ_z as β increases from strong coupling limit to weaker coupling constants is in agreement with the phase diagram of Fig. 3.3 and confirms the existence of a massless mode in the confining phase at weak coupling constants.

The general behaviour of $\gamma_5 M$ spectrum changes as one crosses the deconfining phase transition temperature. To investigate $\gamma_5 M$ in the deconfining phase we have generated two configurations. One at $\beta = 5.5$ by 20000 sweeps from a hot start and the other at $\beta = 5.7$ by 55000 iterations from a hot start.

[8] See Fig. 1.3.

Careful studies of the spectra show that there are no zero modes for any values of κ as shown in Fig. 3.8 where the plot of first positive and negative eigenvalues against $\frac{1}{\kappa}$ at $\beta = 5.5$ never crosses zero axis. In other words $\rho(0) = 0$ for all κ. This is an indication that no massless pions exist in the deconfining phase. On the other hand, since massless pions are associated with chiral symmetry breaking, this observation in turn implicates the restoration of chiral symmetry at weak enough coupling constants in infinite-volume limit. Although the chiral symmetry is explicitly broken by Wilson term and one hopes to recover it only in the continuum limit, there are claims that even on lattices as small as $8^3 \times 4$ the chiral limit, in the presence of dynamical fermions, can be reached from the confined phase [52].

8^4 Lattices

Results more relevant to the continuum limit have been obtained by studying an 8^4 lattice on different gauge configurations from $\beta = 5.0$ up to $\beta = 5.8$ where we are still in the confining phase as indicated by the corresponding Wilson Line

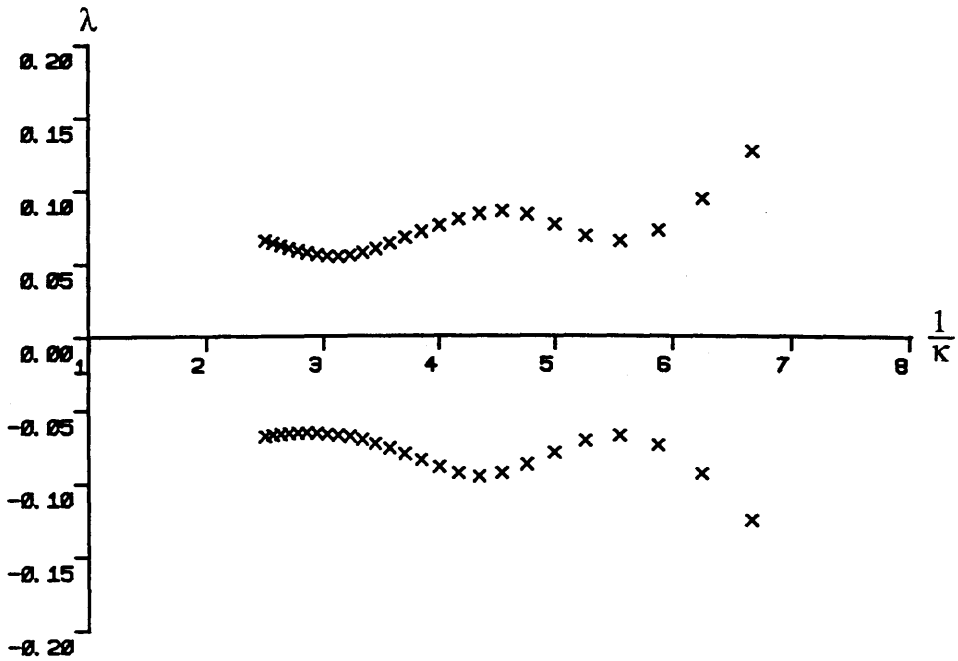

Fig. 3.8 The first positive and negative eigenvalues of $\gamma_5 M$ vs. $\frac{1}{\kappa}$ in the deconfining phase at $\beta = 5.5$ on a 4^4 lattice.

plot of Fig. 3.9. At $\beta = 5.0$ we have generated a gauge configuration by 6300 Metropolis sweeps from a hot start and have calculated the $\gamma_5 M$ spectrum over a range of κ. The behaviour is very similar to the strong coupling limit but with a lower κ_z equal to 0.22 with the least modulus eigenvalue -0.3621D-4. This means that $\rho(0)$ remains non-zero and the first positive and negative eigenvalues distribute very close around zero-axis for $\kappa \geq \kappa_z$ as shown in Fig. 3.10. One might notice that κ_z in this case is smaller than κ_z for a 4^4 configuration at the same β.

More analysis of $\gamma_5 M$ matrix has been performed at $\beta = 5.5$. Starting from a hot start we have generated two well separated gauge configurations obtained by 8300 and 13300 sweeps respectively. For each configuration we have calculated the almost exact zero mode as well as the first few eigenvalues on either side of the zero-eigenvalue-axis. The development of these eigenvalues are carefully observed by fine tuning of hopping parameter κ. In Figs. 3.11 and 3.12 we have plotted these eigenvalues for a range of κ for the first and the second configuration respectively. The existence of exact zero modes for Wilson fermions is remarkably obvious in these plots. The κ_z's are where the curves first cross the zero-

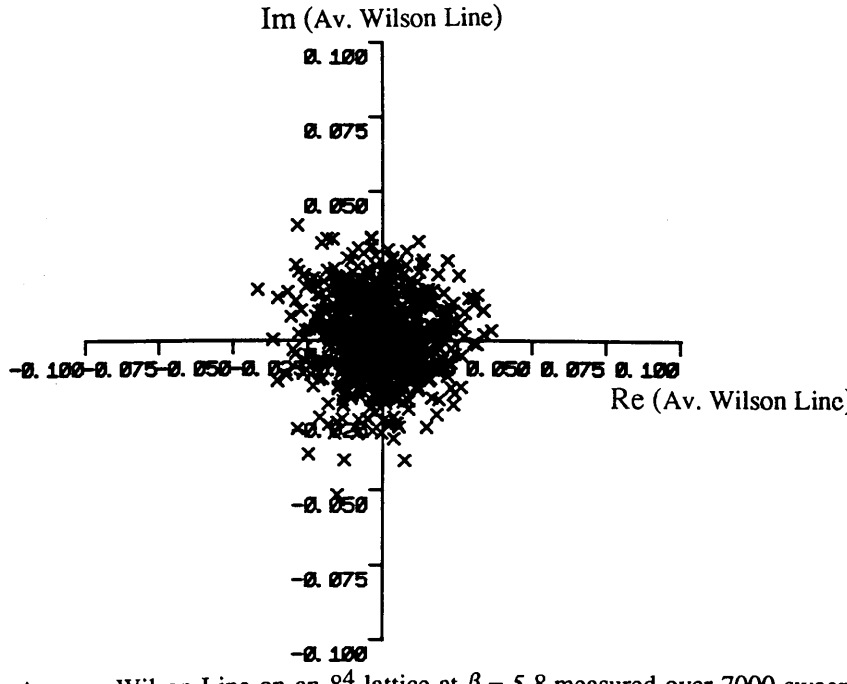

Fig. 3.9 Average Wilson Line on an 8^4 lattice at $\beta = 5.8$ measured over 7000 sweeps starting from a configuration at at $\beta = 5.0$ obtained by 6300 sweeps from a hot start.

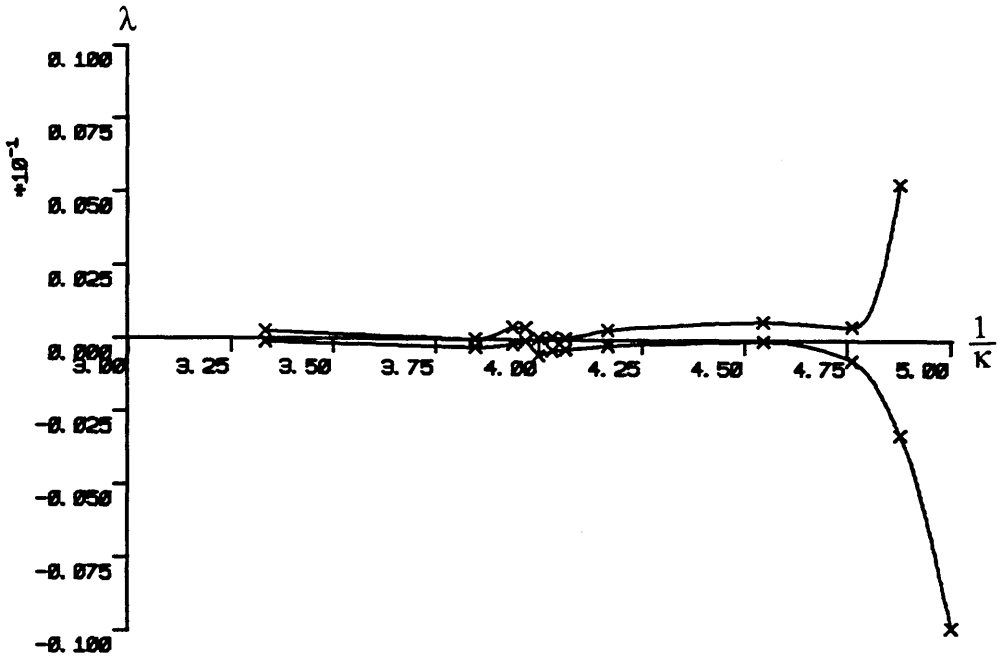

Fig. 3.10 $\gamma_5 M$ spectrum vs. $\frac{1}{\kappa}$ at $\beta = 5.0$ on an 8^4 lattice.

eigenvalue-axis from below. κ_z shifts from 0.197 in the first configuration to 0.1835 in the second configuration. This relatively large shift in κ_z on one hand indicates that the calculation of κ_c is subject to relatively large finite-size fluctuations and on the other hand for a wide range of κ above κ_c the fermion matrix has zero modes where averaged over all gauge configurations. This in turn is the sign of entering into the parity-violating phase by crossing κ_c.

It is interesting to see if the κ_z shifts, such as the observed one in the above two decorrelated configurations, follow a systematic pattern. This requires generating well correlated configurations i.e. those which differ from each other

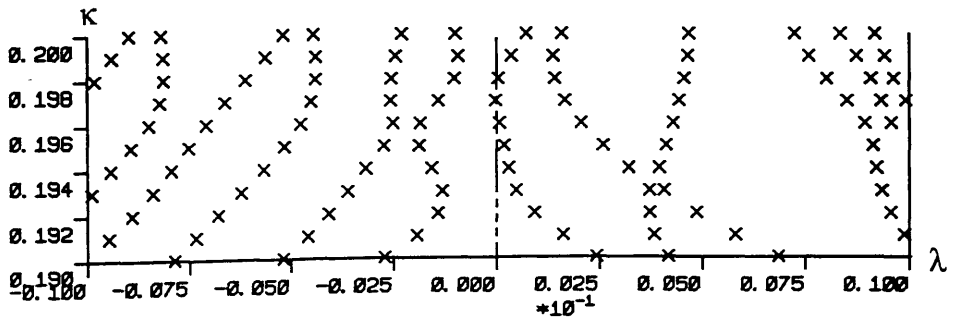

Fig. 3.11 $\gamma_5 M$ spectrum vs. κ in the first configuration at $\beta = 5.5$ on an 8^4 lattice with antiperiodic boundary conditions on fermion fields.

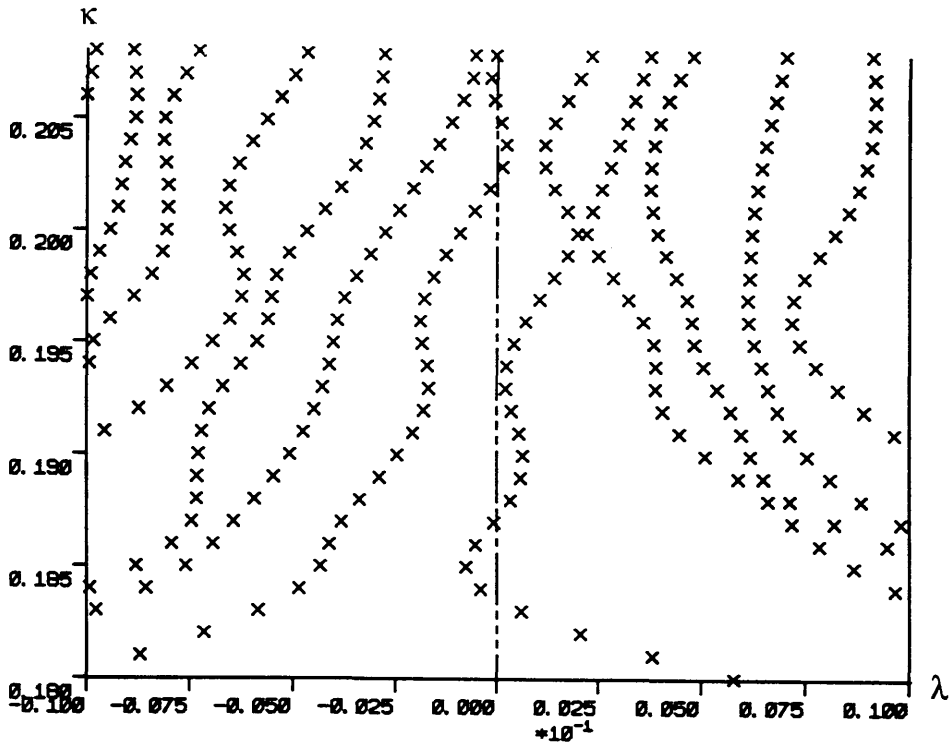

Fig. 3.12 $\gamma_5 M$ spectrum vs. κ in the second configuration at $\beta = 5.5$ on an 8^4 lattice with antiperiodic boundary conditions on fermion fields.

only by small changes. Accordingly we have generated three more configurations and studied the corresponding spectra. The third configuration is obtained from the above second configuration by changing ε-parameter[9] from 0.5 to 0.05 and performing 2 more Metropolis iterations. The fourth configuration is obtained from the second by only 2 more sweeps. And finally the fifth configuration is obtained from the second by performing 10 more sweeps. The corresponding spectra for these three correlated configurations are shown in Figs. 3.13 to 3.15.

The similarity of the spectra of the second and the third configurations which is demonstrated in Fig. 3.16 is consistent with the fact that the third configuration is quite correlated to the second one as it is generated from the second configuration by only a very small change.

[9] ε is the parameter introduced in footnote 13 of Chapter 1 to generate gauge fields (See §1.8). Except for the third configuration we have always set $\varepsilon = 0.5$.

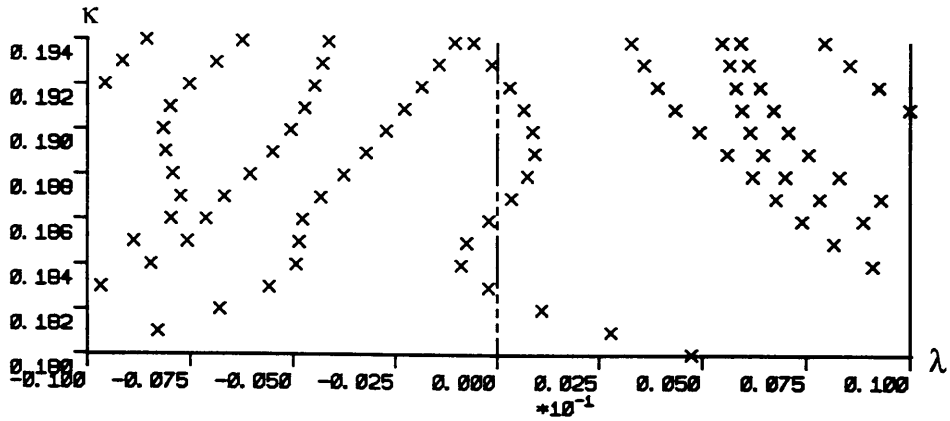

Fig. 3.13 $\gamma_5 M$ spectrum vs. κ in the third configuration at $\beta = 5.5$ on an 8^4 lattice with antiperiodic boundary conditions on fermion fields.

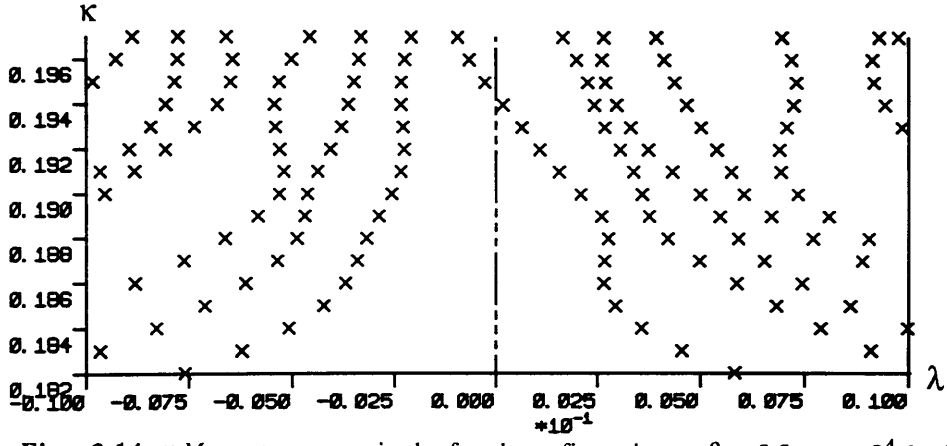

Fig. 3.14 $\gamma_5 M$ spectrum vs. κ in the fourth configuration at $\beta = 5.5$ on an 8^4 lattice with antiperiodic boundary conditions on fermion fields.

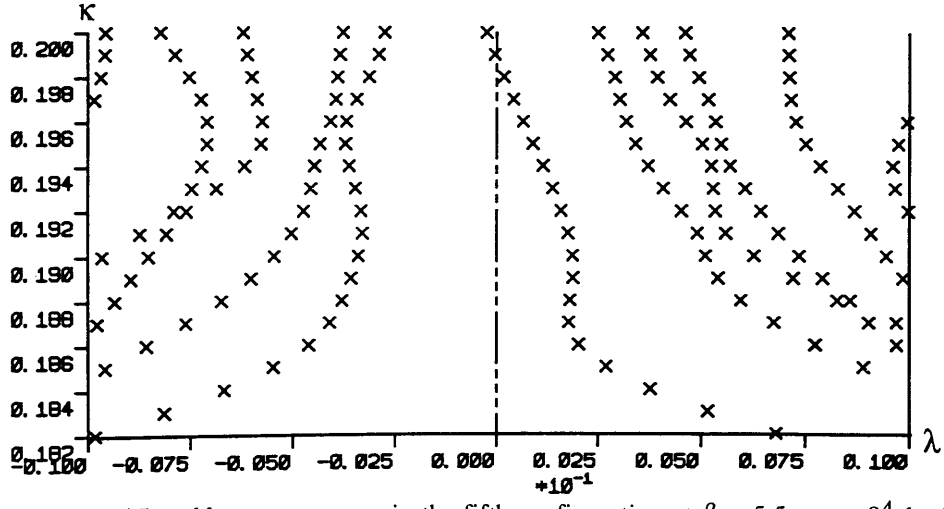

Fig. 3.15 $\gamma_5 M$ spectrum vs. κ in the fifth configuration at $\beta = 5.5$ on an 8^4 lattice with antiperiodic boundary conditions on fermion fields.

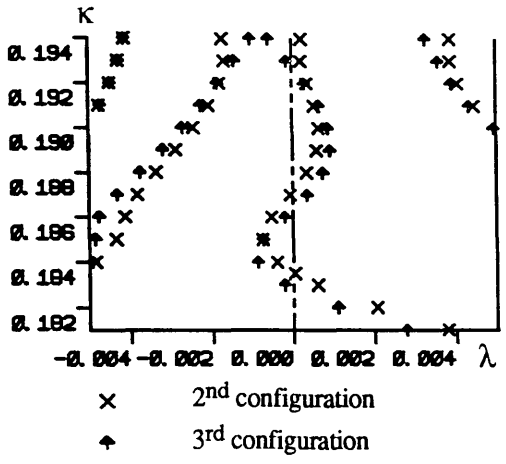

Fig. 3.16 $\gamma_5 M$ spectrum vs. κ in the second and third configurations at $\beta = 5.5$ on an 8^4 lattice with antiperiodic boundary conditions on fermion fields. κ_z changes from 0.1835 in the second configuration to 0.1828 in the third configuration.

The comparison of the spectra of the second and the fourth configurations in Fig. 3.17 shows that though the eigenvalues away from the zero-axis behave similarly in the two configurations, the closest eigenvalues to zero shift considerably and result a relatively large shift in κ_z. Accordingly one should bear in mind that the κ_c calculation is subject to relatively large errors. The above shift which is not substantial for the values of κ far below κ_z indicates that the pion mass is almost configuration independent for the lower values of κ and fluctuates from configuration to configuration as one approaches κ_c. This in turn is another reason for the large errors in the values of κ_c calculated from the extrapolation of pion mass data to the region of the hopping parameter where the pion mass vanishes [53]. Finally the lack of similarity in the above two spectra on one hand and the fact that the fourth configuration is different from the second one by only two sweeps on the other, confirm that at $\beta = 5.5$ the correlation lengths are short and actually less than two sweeps.

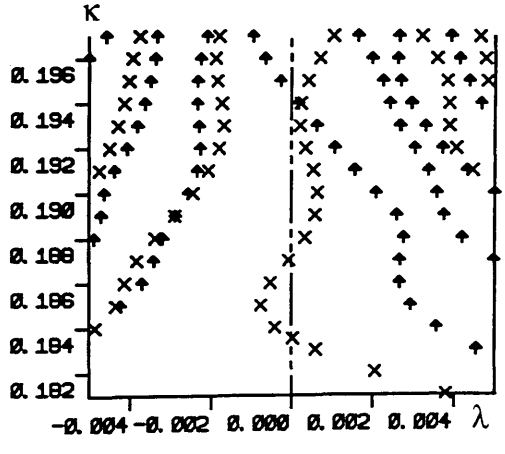

Fig. 3.17 $\gamma_5 M$ spectrum vs. κ in the second and fourth configurations at $\beta = 5.5$ on an 8^4 lattice with antiperiodic boundary conditions on fermion fields. κ_z changes from 0.1835 in the second configuration to 0.1945 in the fourth configuration.

The spectrum of the fifth configuration which has been compared with that of the second in Fig. 3.18 does not show any major qualitative difference from the eigenvalue spectrum of the fourth configuration. In fact as the fifth configuration is a long way apart from the second configuration, obviously there are no correlations in this case.

We have also changed the boundary conditions to periodic and repeated the same calculations. Although the general behaviour is seen to be qualitatively the same as previous case we note that the closest eigenvalues to zero undergo large fluctuations in some configurations. This phenomenon will in turn cause large shifts of κ_z's in the corresponding configurations. Such an example is given in Fig. 3.19 where the spectrum in the second configuration with periodic boundary conditions is compared with the corresponding spectrum with antiperiodic boundary conditions imposed on the fermion fields. This feature might be improved on larger lattices and/or by approaching continuum limit where the boundary effects are relatively suppressed. The spectra with periodic boundary conditions on fermion fields are shown in Figs. 3.20 to 3.24 for the five configurations.

In Figs. 3.25 to 3.27 we compare the spectra of the third, fourth and fifth configurations with that of the second configuration and observe qualitatively the same features as were observed in the corresponding antiperiodic cases i.e. still

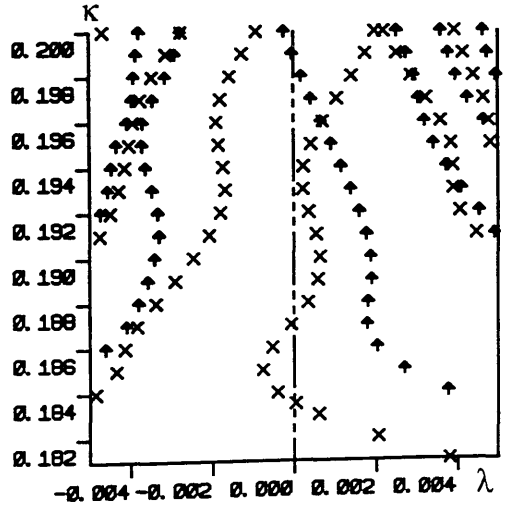

Fig. 3.18 $\gamma_5 M$ spectrum vs. κ in the second and fifth configurations at β = 5.5 on an 8^4 lattice with antiperiodic boundary conditions on fermion fields. κ_z changes from 0.1835 in the second configuration to 0.199 in the fifth configuration.

× 2nd configuration

♠ 5th configuration

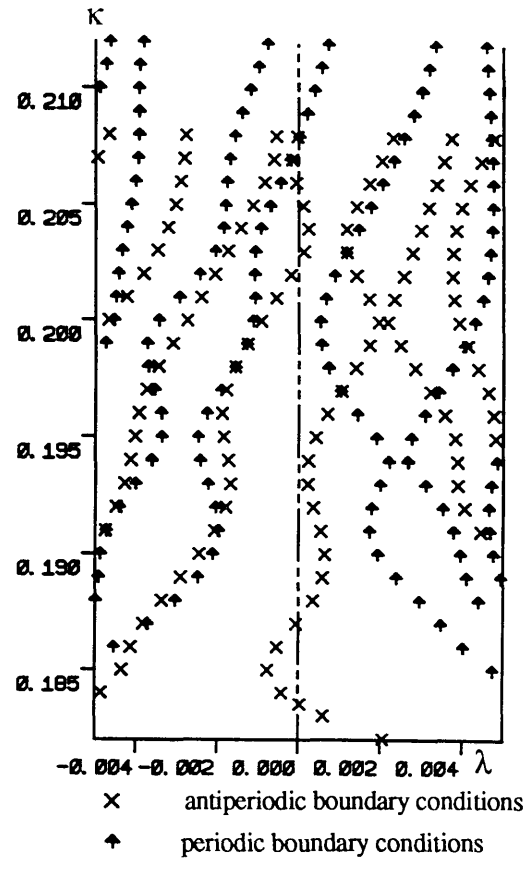

Fig. 3.19 $\gamma_5 M$ spectrum vs. κ in the second configuration at $\beta = 5.5$ on an 8^4 lattice. κ_z shifts from 0.1835 to 0.208 as boundary conditions are changed from antiperiodic to periodic.

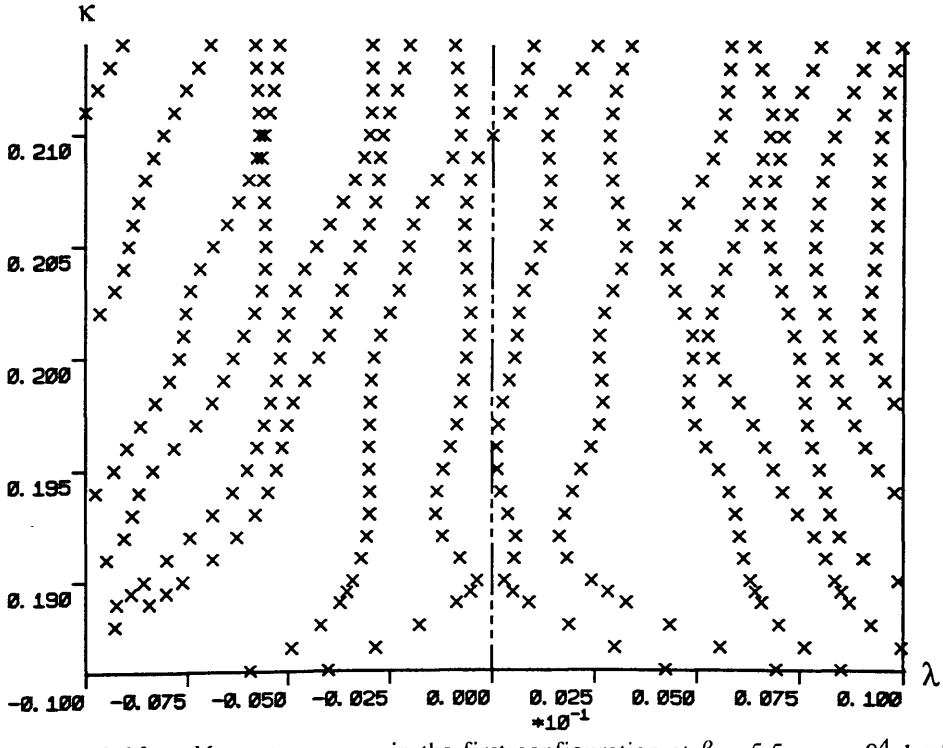

Fig. 3.20 $\gamma_5 M$ spectrum vs. κ in the first configuration at $\beta = 5.5$ on an 8^4 lattice with periodic boundary conditions on fermion fields.

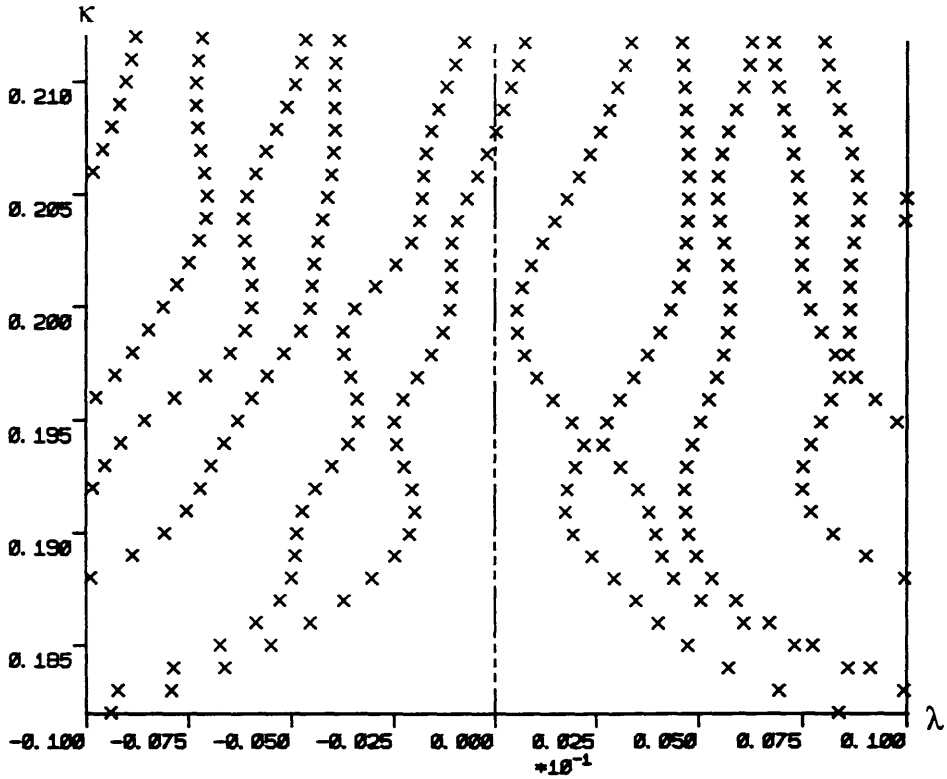

Fig. 3.21 $\gamma_5 M$ spectrum vs. κ in the second configuration at $\beta = 5.5$ on an 8^4 lattice with periodic boundary conditions on fermion fields.

there are some similarities between the spectra of the second and the third configurations while the corresponding spectra in the fourth and the fifth configurations behave almost differently from the second configuration spectrum. These results along with the corresponding results with the antiperiodic boundary conditions on the fermion fields indicate the lack of long distance correlations at $\beta = 5.5$. One really needs to look at β-values closer to the deconfining phase transition point e.g. $\beta = 5.8$ to observe better correlations. Alternatively one can work on larger lattices for better correlations. In this case the lattice spacing becomes smaller in terms of which the correlation lengths will become larger.

We have searched for some support for the phase diagram of §3.6 by probing more into weak coupling region. Up to $\beta = 5.65$ no noticeable change is observed in the behaviour of $\gamma_5 M$ spectrum compared with the stronger coupling cases i.e. $\rho(0) \neq 0$ for all $\kappa > \kappa_z$. At this β we generated a gauge configuration by 13300 sweeps from a hot start and found $\kappa_z = 0.19$ with smallest modulus

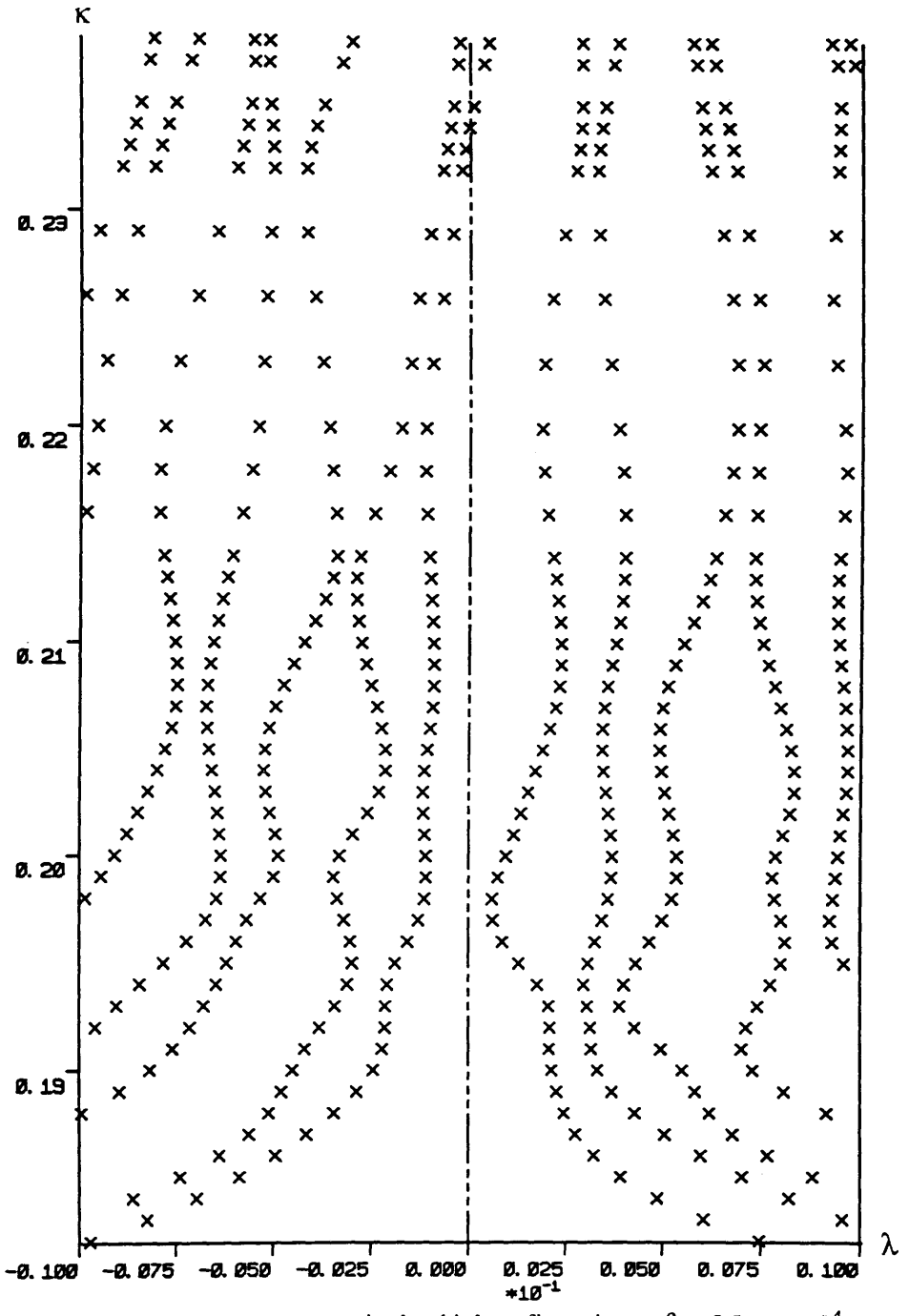

Fig. 3.22 $\gamma_5 M$ spectrum vs. κ in the third configuration at $\beta = 5.5$ on an 8^4 lattice with periodic boundary conditions on fermion fields.

eigenvalue -0.53821D-7.

New observations are made at $\beta = 5.8$. Working in three well separated configurations generated by 11300, 13300 and 16300 iterations respectively from a hot start we have searched for the κ_z's. Except for smaller values of κ_z, we see

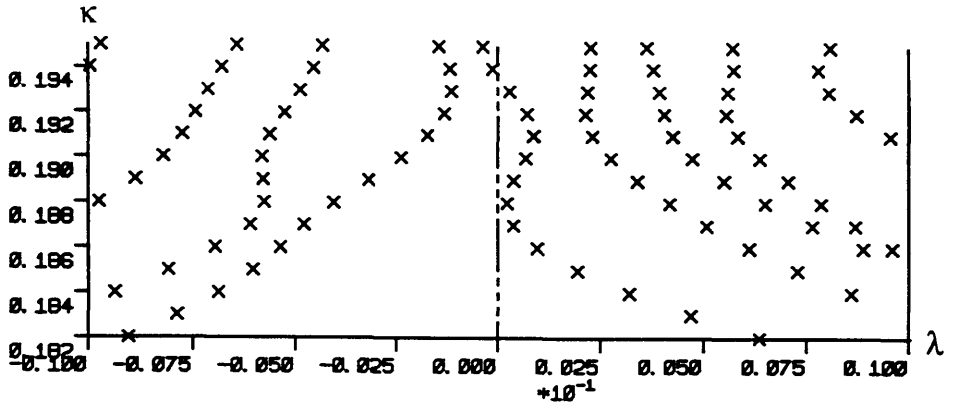

Fig. 3.23 $\gamma_5 M$ spectrum vs. κ in the fourth configuration at $\beta = 5.5$ on an 8^4 lattice with periodic boundary conditions on fermion fields.

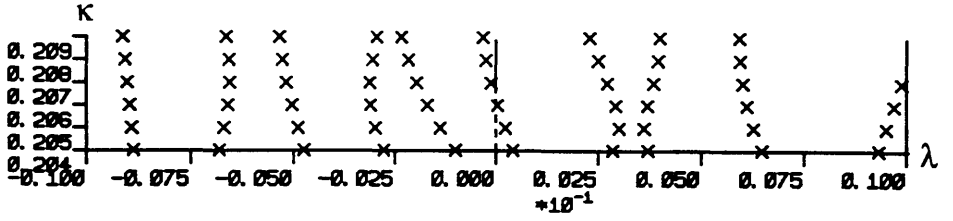

Fig. 3.24 $\gamma_5 M$ spectrum vs. κ in the fifth configuration at $\beta = 5.5$ on an 8^4 lattice with periodic boundary conditions on fermion fields.

more or less similar behaviour to the $\beta = 5.5$ cases as long as we are relatively close to κ_z. The major difference comes when we calculate $\gamma_5 M$ spectrum at higher values of κ. Previously at $\beta = 5.5$ in some configurations we could observe the existence of a second κ_z relatively close to the first κ_z and interpreted as a sign of filling the whole κ region above κ_c once the contributions from all configurations are superposed on each other. At $\beta = 5.8$ on the other hand, we observe the second κ_z appears almost far away from the first κ_z. This phenomenon which is observed in all three configurations implies that at infinite-volume limit we observe two separate regions of zero modes once averaged over all gauge fields. Fig. 3.28 shows how the first smallest modulus eigenvalues for three configurations approach zero axis to form the zero modes in two well separated regions. The third configuration shows rather different behaviour indicating either that the region of zero modes is larger than what is observed once more configurations are worked out or the infinite-volume behaviour is hampered by finite-size effects.

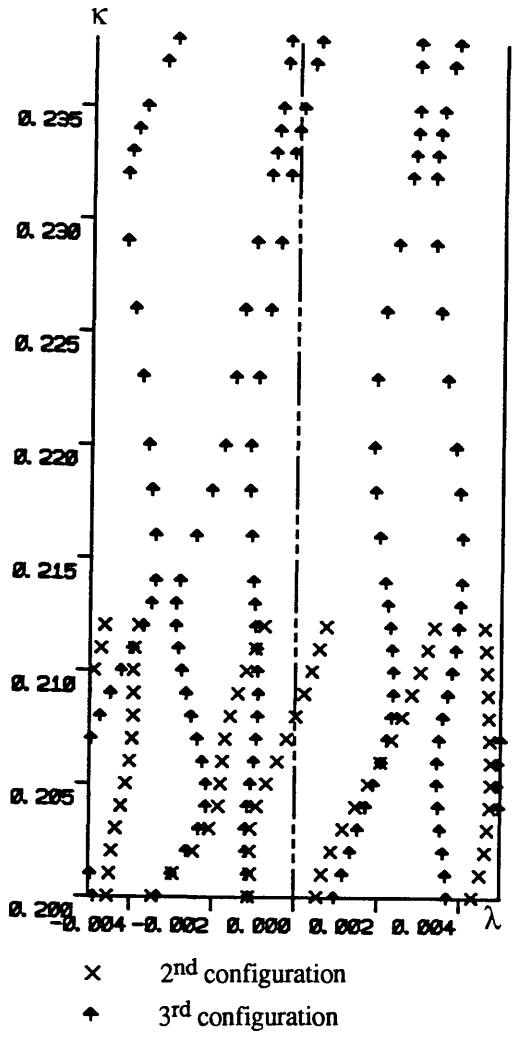

Fig. 3.25 $\gamma_5 M$ spectrum vs. κ in the second and the third configurations at $\beta = 5.5$ on an 8^4 lattice with periodic boundary conditions on fermion fields. κ_z changes from 0.208 in the second configuration to 0.234 in the third configuration.

We have also changed boundary conditions to periodic and worked out the spectra in the second and third configurations. At $\beta = 5.8$ the corresponding changes in the eigenvalue distributions are much less than similar modifications due to changing the boundary conditions at $\beta = 5.5$ and in particular the shifts of κ_z are about an order of magnitude less. This observation indicates that the boundary effects would gradually disappear as we approach the deconfining phase transition and eventually the continuum limit, bearing in mind that the actual continuum limit is approached by simultaneous increase in volume and β. In Figs. 3.29 and 3. 30 we have compared the spectra with different boundary conditions in the second and the third configurations at $\beta = 5.8$ respectively.

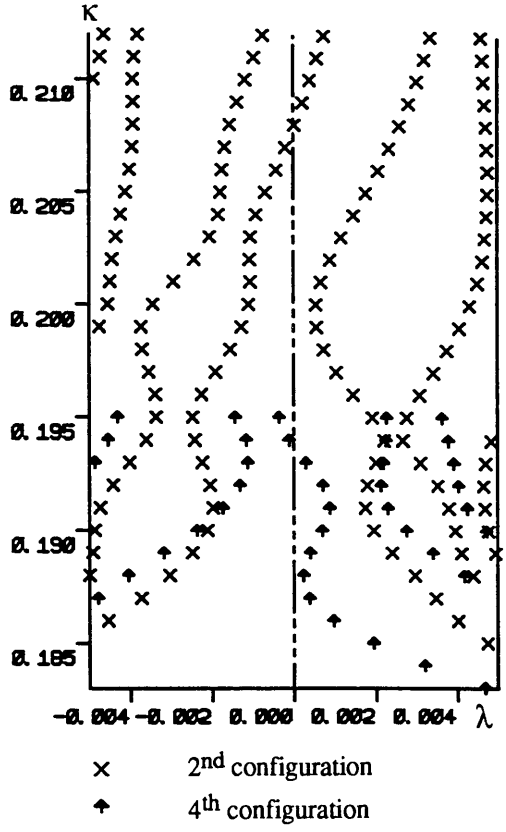

Fig. 3.26 $\gamma_5 M$ spectrum vs. κ in the second and the fourth configurations at β = *5.5* on an 8^4 lattice with periodic boundary conditions on fermion fields. κ_z changes from 0.1835 in the second configuration to 0.1937 in the fourth configuration.

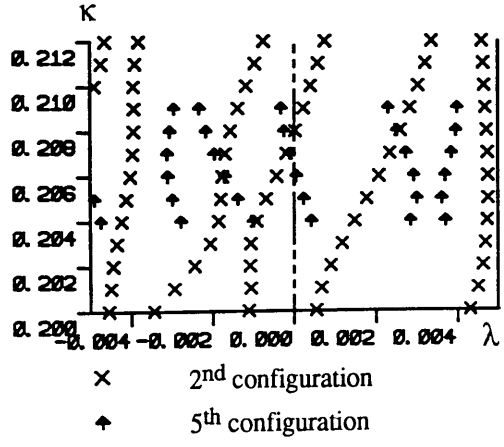

Fig. 3.27 $\gamma_5 M$ spectrum vs. κ in the second and the fifth configurations at β = *5.5* on an 8^4 lattice with periodic boundary conditions on fermion fields. κ_z changes from 0.1835 in the second configuration to 0.206 in the fifth configuration.

These observations at β = *5.8*, i.e. the existence of multiple phase transitions, are in full agreement with the speculations from the proposed phase diagram for single-flavour lattice QCD at weak coupling constants. Our results for 4^4 and 8^4 lattices are summarized in Tables 3.2 to 3.4.

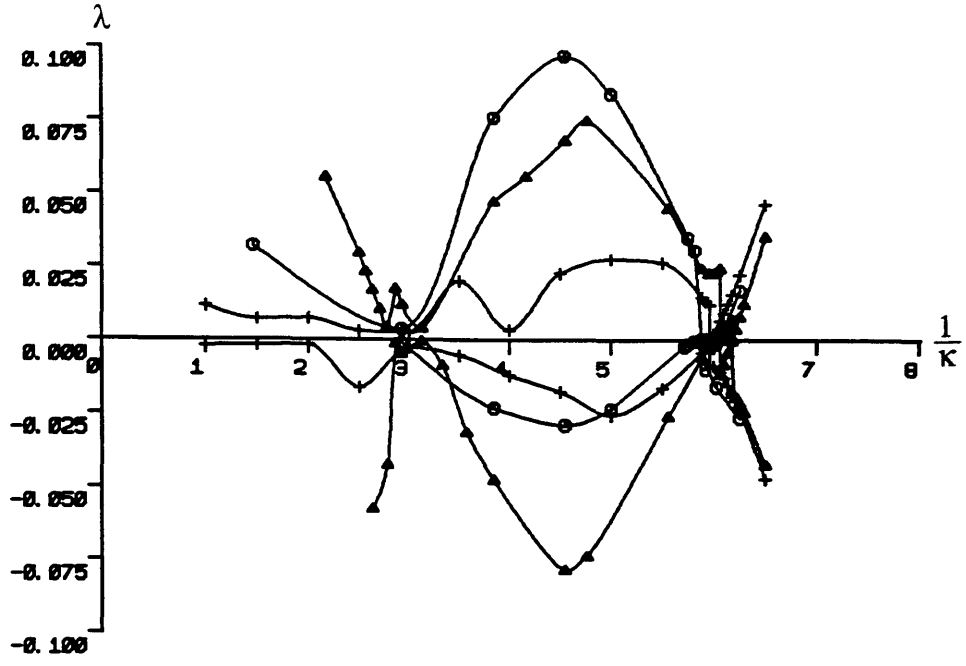

Fig. 3.28 The first positive and negative eigenvalues of $\gamma_5 M$ are plotted vs. $\frac{1}{\kappa}$ for three configurations at $\beta = 5.8$ on an 8^4 lattice.

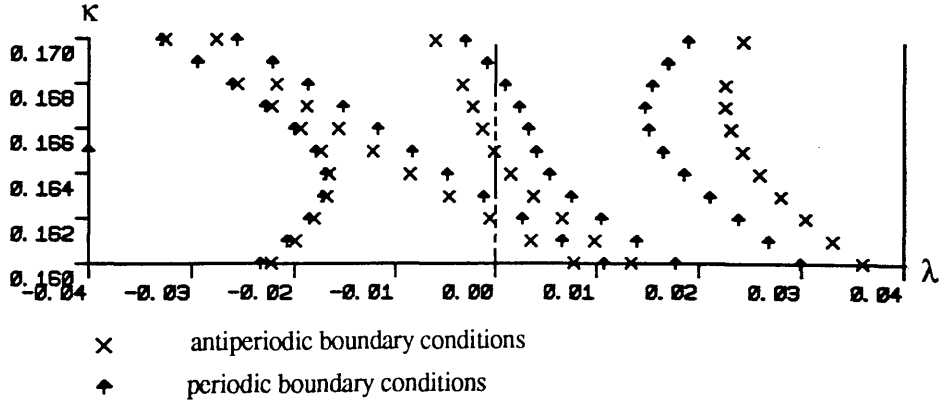

Fig. 3.29 $\gamma_5 M$ spectrum vs. κ in the second configuration at $\beta = 5.8$ on an 8^4 lattice. κ_z shifts from 0.1619 to 0.1627 as boundary conditions are changed from antiperiodic to periodic.

It is also interesting to note that under the same conditions the eigenvalue distribution tends to become thinner as β increases as shown in Fig. 3.31. This effect makes the eigenvalues and in particular the zero modes isolated and as a result makes the inversion programme easier to perform, as noticed before. This property

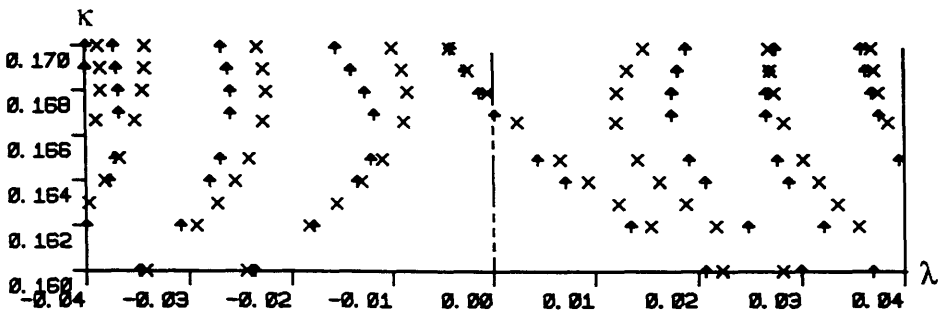

× antiperiodic boundary conditions

♦ periodic boundary conditions

Fig. 3.30 $\gamma_5 M$ spectrum vs. κ in the third configuration at $\beta = 5.8$ on an 8^4 lattice. κ_z shifts from 0.16775 to 0.1671 as boundary conditions are changed from antiperiodic to periodic.

Table 3.2

κ_z for a number of 4^4 *SU(3)* gauge configurations at weak coupling constants with antiperiodic boundary conditions on fermion fields.

β	configuration	κ_z	λ_z
5.0	1	0.2400	0.7750D-3
5.0	2	0.2500	0.1850D-3
5.3	1	0.1991	-0.1144D-4
5.5 *	1	-	-
5.7 *	1	-	-

* No κ_z exists.

which is more transparent in smaller lattices makes the $\rho(\lambda)$ behave as $\delta(\lambda)$ in a neighborhood around $\lambda = 0$ at $\kappa \geq \kappa_z$ in confining phase.

The above conclusions could be more transparent if we could work out the whole spectrum of M or $\tilde{M}$, defined by Eq. (3.50). In fact the regions of the zero modes of $\gamma_5 M$ or M in κ-space correspond to the regions of real eigenvalues of $\tilde{M}$[10]. Representing the whole eigenvalues in the complex plane and superposing the results of different gauge configurations reveal the exact regions of zero modes.

[10] See §4.3.

Table 3.3

κ_z for a number of 8^4 *SU(3)* gauge configurations at weak coupling constants with antiperiodic boundary conditions on fermion fields.

β	configuration	κ_z	λ_z
5.0	1	0.220	-0.3621D-4
5.5	1	0.197	-0.2220D-4
5.5	2	0.1835	0.3458D-4
5.5	3	0.1828	0.4337D-5
5.5	4	0.1945	-0.5021D-4
5.5	5	0.199	-0.4725D-4
5.65	1	0.190	-0.5382D-3
5.8	1	0.170	0.2209D-3
5.8	2	0.1619	-0.1820D-3
5.8	3	0.16775	0.2435D-6

Table 3.4

κ_z for a number of 8^4 *SU(3)* gauge configurations at weak coupling constants with periodic boundary conditions on fermion fields.

β	configuration	κ_z	λ_z
5.5	1	0.210	-0.4935D-6
5.5	2	0.208	0.2064D-4
5.5	3	0.234	-0.2053D-4
5.5	4	0.1937	-0.1011D-4
5.5	5	0.206	-0.4585D-4
5.8	2	0.1627	-0.4834D-4
5.8	3	0.1671	0.1509D-4

Such information at different values of β construct the corresponding phase structure. Though, due to storage limitations, such a work on 8^4 lattices is really far from one's ability, however a parallel study has been performed on a 4^4 lattice. The corresponding results for each individual *SU(3)* configurations, presented in [54], actually support our conclusions. One should note that despite the small size of this lattice it is still very time consuming to work out the whole spectrum for a

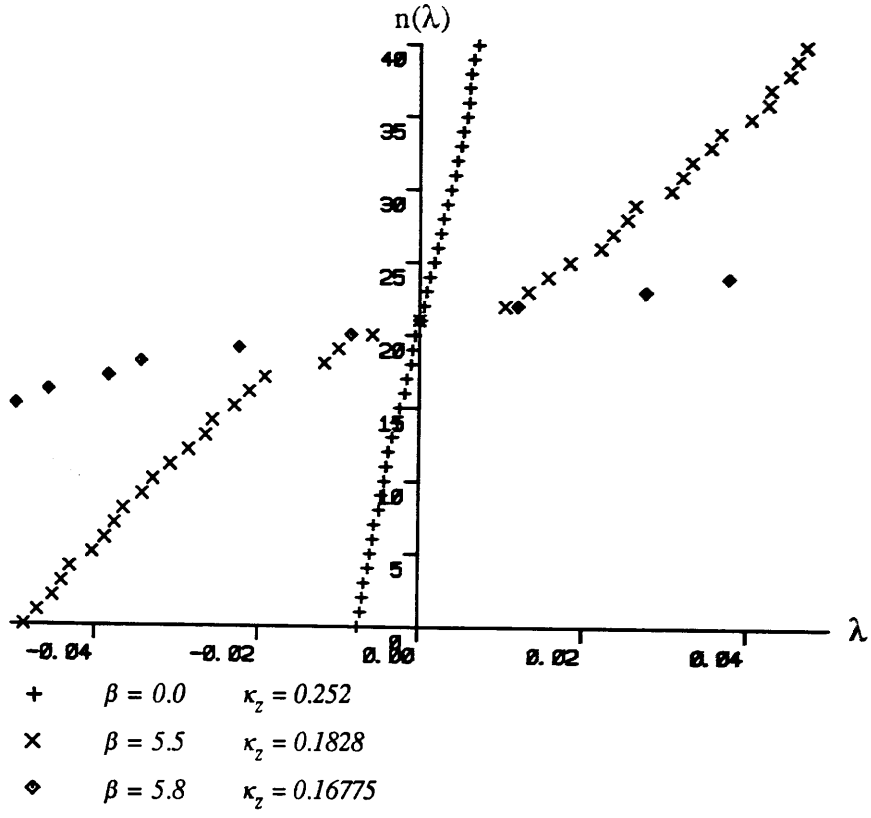

Fig. 3.31 $\gamma_5 M$ eigenvalue distributions for three gauge configurations with different β's at the corresponding κ_z's on an 8^4 lattice with antiperiodic boundary conditions on fermion fields.

considerable number of gauge configurations. Alternatively one might calculate the eigenvalues on a *SU(2)* gauge configuration which presumably take much less time in favour of a large number of gauge configurations. The histogram plots showing the frequency of the real eigenvalues obtained over a large number of *SU(2)* gauge configurations [55] indicate clear confirmation of our results and accordingly support the proposed phase structure.

Chapter 4

Meson Propagators

In the preceding chapter we showed how Monte Carlo simulations confirmed the phase structure of Aoki. This explains why the pion becomes massless at a critical hopping parameter κ_c. Our investigations there were based on the eigenvalue spectrum studies. Alternatively, we might observe how pion mass vanishes as $\kappa \rightarrow \kappa_c$ by direct calculation of its mass. This is normally done by studying the large distance behaviour of the pion propagator. In this chapter we adopt this approach while applying block Lanczos algorithm to calculate the relevant propagators.

4.1 Correlation Functions And Masses

QCD energy levels and in particular particle masses can be obtained from the large distance behaviour of connected correlation functions $C(\underline{x},t)$ of appropriate operators $\Phi(\underline{x},t)$ i.e. operators with the quantum numbers of the desired particle state,

$$\begin{aligned} C(\underline{x},t) &= < 0 \mid \Phi^{\dagger}(\underline{x},t)\, \Phi(0,0) \mid 0 >_c \\ &= < 0 \mid \Phi^{\dagger}(\underline{x},t)\, \Phi(0,0) \mid 0 > \\ &\quad - < 0 \mid \Phi^{\dagger}(\underline{x},t) \mid 0 > < 0 \mid \Phi(0,0) \mid 0 > \end{aligned} \tag{4.1}$$

The operator $\Phi(\underline{x},t)$ is evolved from its initial value at $t = 0$ through,

$$\Phi(\underline{x},t) = e^{iHt}\, \Phi(\underline{x},0)\, e^{-iHt} \tag{4.2}$$

where H is the Hamiltonian. Using the operator (4.2) and inserting a complete set of energy eigenstates $|n>$ into correlation function (4.1) we get:

$$C(\underline{x},t) = \sum_{n} < 0 \mid e^{iHt} \Phi^{\dagger}(\underline{x},0)\, e^{-iHt} \mid n > < n \mid \Phi(0,0) \mid 0 > - < 0 \mid e^{iHt} \Phi^{\dagger}(\underline{x},0)\, e^{-iHt} \mid 0 > < 0 \mid \Phi(0,0) \mid 0 > \qquad (4.3)$$

Let E_n be the energy level corresponding to state $|n>$. Then we have,

$$C(\underline{x},t) = \sum_{n \neq 0} e^{-it(E_n - E_0)} \left| < n \mid \Phi(\underline{x},0) \mid 0 > \right|^2 \qquad (4.4)$$

We continue to Euclidean space from Minkowski space by adopting $t \rightarrow -it$ in Eq. (4.4). As $t \rightarrow \infty$ the excited states contributions die out and Eq. (4.4) behaves asymptotically as:

$$C(\underline{x},t) \underset{t \to \infty}{\rightarrow} e^{-t(E_1 - E_0)} \left| < 1 \mid \Phi(\underline{x},0) \mid 0 > \right|^2 \qquad (4.5)$$

Actually the correlation function must also include the contribution from propagation round the lattice in the opposite direction. If the lattice extension in the temporal direction is L_T then the times t and L_T-t have the same time separation from the time origin at $t = 0$ for the two propagations in the opposite directions. The correlation function, then, becomes:

$$C(\underline{x},t) \underset{t \to \infty}{\rightarrow} \left[e^{-t(E_1 - E_0)} + e^{-(L_T - t)(E_1 - E_0)} \right] \times \left| < 1 \mid \Phi(\underline{x},0) \mid 0 > \right|^2 \qquad (4.6)$$

We usually sum over $\underline{x}$ to project on zero momentum states.[1] This results in:

$$\tilde{C}(t) = \sum_{\underline{x}} C(\underline{x},t) \underset{t \to \infty}{\rightarrow} A \cosh\left[m_{\Phi} \left(\frac{L_T}{2} - t \right) \right] \qquad (4.7)$$

where A is a constant and m_{Φ} is the mass gap E_1-E_0. The reason for using $\underline{p} = 0$ operators is that it makes the extraction of the mass very direct. The price to pay is that on an $L_S^3 L_T$ lattice one will get only L_T independent *measurements* of correlation function $\tilde{C}(t)$ per generated gauge field configuration.

[1] This is equivalent to Fourier transforming Eq. (4.6) to momentum space and letting $\underline{p} = 0$.

4.2 Particle Propagators

The correlation functions can be thought of expressions representing a particle being created at the origin, travelling to x and being annihilated at x i.e. they are just the Feynman propagators for the corresponding particles. In the case of hadrons which are fermion composite fields, the corresponding propagators can be worked out in terms of fermion propagators M^{-1} or $(\gamma_5 M)^{-1}$. For instance let us consider pseudoscalar meson (π) and non-singlet scalar meson (a_0) propagators. The pseudoscalar meson (pion) is written in terms of its components as:

$$\pi(x) = \bar{\psi}^{f'}_{\alpha a}(x)(i\gamma_5)_{\alpha\beta}\psi^{f}_{\beta a}(x) \tag{4.8}$$

where in Eq. (4.8) and the subsequent equations α, β, ... refer to spin indices, a, b, ... to colour indices and f and f' to flavour indices. The pion propagator (i.e. the pion correlation function) is then:

$$C(x) = \langle 0 \mid \pi(x)\,\pi(0) \mid 0 \rangle$$

$$= \langle \bar{\psi}^{f}_{\alpha a}(x)\,(\gamma_0\gamma_5^{\dagger}\gamma_0)_{\alpha\beta}\,\psi^{f'}_{\beta a}(x)\,\bar{\psi}^{f'}_{\gamma b}(0)\,(\gamma_5)_{\gamma\delta}\,\psi^{f}_{\delta b}(0) \rangle \tag{4.9}$$[2]

Using the relation:

$$\langle \bar{\psi}_i B \psi_j \rangle = \langle (BM^{-1})_{ji} \rangle_G \tag{4.10}$$

which is valid in quenched approximation for any fermion independent matrix B, Eq. (4.9) would read:

$$C(x) = \langle (\gamma_5)_{\alpha\beta}\,(M^{-1})^{f}_{0\delta b,x\alpha a}\,(\gamma_5)_{\gamma\delta}\,(M^{-1})^{f'}_{x\beta a,0\gamma b} \rangle_G$$

$$= \mathrm{Tr}_{spin,color} \langle \gamma_5\,(M^{-1})^{f}_{0,x}\,\gamma_5\,(M^{-1})^{f'}_{x,0} \rangle_G \tag{4.11}$$

In Eq. (4.11) we have ignored the contribution from the disconnected piece,

$$C(x)_{DC} = \langle \left[\mathrm{Tr}_{spin} \sum_{color} \pi(x) \right] \left[\mathrm{Tr}_{spin} \sum_{color} \pi(0) \right] \rangle$$

---

[2] The unimportant minus sign arising from the term $\gamma_0\gamma_5^{\dagger}\gamma_0 = -\gamma_5$ is eliminated when we change the integrand from $\psi^{f'}(x)\,\bar{\psi}^{f'}(0)$ to $\bar{\psi}^{f'}(0)\,\psi^{f'}(x)$. If we choose $\bar{\psi}\,\gamma_0\,\gamma_5\,\psi$ for pion rather than $\bar{\psi}\,\gamma_5\,\psi$ the first minus sign disappears but the second one changes the sign of $C(t)$.

$$= < \Big[\mathrm{Tr}_{spin} \sum_{color} (M^{-1})_{x,x} \gamma_5 \Big] \Big[\mathrm{Tr}_{spin} \sum_{color} (M^{-1})_{0,0} \gamma_5 \Big] >_G \quad (4.12)$$

because, due to the properties of Grassmann variables i.e. Eqs. (1.37) and (1.39), it vanishes when $f \neq f'$[3] as for π^+ and π^-.

If f and f' are degenerate in mass then $\kappa_f = \kappa_{f'}$ and as a result $(M^{-1})^f = (M^{-1})^{f'} = M^{-1}$. Moreover since $M^\dagger = \gamma_5 M \gamma_5$ for Wilson fermion matrix M, Eq. (4.11) reduces to:

$$C(x) = \sum_{spin,color} < (M^{-1})^*_{x,0} (M^{-1})_{x,0} >_G$$

$$= \sum_{spin,color} < | (M^{-1})_{x,0} |^2 >_G \quad (4.13)$$

As before we sum over spatial coordinates $\underline{x}$ to project on zero momentum states,

$$\tilde{C}(t) = < \sum_{\underline{x}} \sum_{spin,color} | (M^{-1})_{\underline{x},t\ 0,0} |^2 >_G \quad (4.14)$$

We will find it more convenient if we write $\tilde{C}(t)$ in terms of $(\gamma_5 M)^{-1}$. The hermicity of $\gamma_5 M$ can be used to write Eq. (4.11) as:

$$\tilde{C}(t) = < \sum_{\underline{x}} \sum_{spin,color} | [(\gamma_5 M)^{-1}]_{\underline{x},t\ 0,0} |^2 >_G \quad (4.15)$$

In principal the expressions (4.14) and (4.15) should be summed over all origins as well. However in practice this is really impossible and one is content only with averaging over just a few origins or only one.

Similarly we derive the propagator for the non-singlet scalar meson identified by the local operator $\overline{\psi}^{f'}_{\alpha a}(x)\ \psi^{f}_{\alpha a}(x)$ as:

$$\tilde{C}(x) = < \sum_{\underline{x}} \mathrm{Tr}_{spin,color} [\ (M^{-1})_{0,0\ \underline{x},t}\ (M^{-1})_{\underline{x},t\ 0,0}\ ] >_G \quad (4.16)$$

Eq. (4.16) is expressed in terms of $(\gamma_5 M)^{-1}$ as:

---

[3] If $f = f'$ e.g. in η meson the relevant propagator is modified by $-n_f C(x)_{DC}$ where n_f is the number of flavours and $C(x)_{DC}$ is the corresponding disconnected piece.

$$\tilde{C}(t) = < \sum_{\underline{x}} \sum_{spin,color} \left\{ \left[(\gamma_5 M)^{-1} \gamma_5 \right]_{\underline{x},t\ 0,0} \left[\gamma_5 (\gamma_5 M)^{-1} \right]^{*}_{\underline{x},t\ 0,0} \right\} >_G \quad (4.17)$$

Likewise the other hadron propagators can be obtained only in terms of fermion propagator or $(\gamma_5 M)^{-1}$ in quenched approximation.

4.3 Zero Modes And Hadron Propagators

We can analyze the hadron propagators, at least qualitatively, as κ approaches κ_c. Following Itoh *et al.* [56] this is done if we represent fermion matrix elements M_{xy} by its eigenfunctions. To carry out this procedure we need first to prove the following relations. In the following we denote by $\phi_i(n)$ the eigenfunction of M corresponding to eigenvalue λ_i i.e.

$$M\phi_i = \lambda_i \phi_i \quad (4.18)$$

I Writing M as $-\kappa\tilde{M}+\mathbf{1}$ where $\tilde{M}$ is κ-independent and denoting the eigenfunctions of $\tilde{M}$ which are, of course, κ-independent by ζ_i with the κ independent eigenvalues ρ_i then:

$$M\zeta_i = (-\kappa\tilde{M}+\mathbf{1})\ \zeta_i = \zeta_i - \kappa\rho_i\zeta_i = (-\kappa\rho_i+1)\ \zeta_i \quad (4.19)$$

The comparison of Eq. (4.18) with Eq. (4.19) shows that the eigenfunctions of M are κ-independent and its eigenvalues are related to those of $\tilde{M}$ by,

$$\lambda_i = -\kappa\rho_i+1 \quad (4.20)$$

From Eq. (4.20) we see that any real ρ_i fixes a κ_z equal to $\frac{1}{\rho_i}$ since it is at these values of κ that M has a zero eigenvalue. Accordingly we write the real eigenvalues of M as:

$$\lambda = 1 - \frac{\kappa}{\kappa_z} \quad (4.21)$$

II Multiplying both sides of Eq. (4.18) by γ_5 and making use of hermicity of $\gamma_5 M$, we therefore have:

$$\phi_i^\dagger \gamma_5 M = \lambda_i^* \phi_i^\dagger \gamma_5 \tag{4.22}$$

The secular equation for Eq. (4.22) reads:

$$\det (M - \lambda_i^* \mathbb{1}) = 0 \tag{4.23}$$

Eq. (4.23) shows that for any eigenvalue λ_i of M, λ_i^* is an eigenvalue too. We denote the corresponding eigenfunction by $\tilde{\phi}_i$:

$$M\tilde{\phi}_i = \lambda_i^* \tilde{\phi}_i \tag{4.24}$$

III Multiplying both sides of Eq. (4.22) by ϕ_j on the right we obtain:

$$\phi_i^\dagger \gamma_5 \lambda_j \phi_j = \lambda_i^* \phi_i^\dagger \gamma_5 \phi_j \tag{4.25}$$

from which we conclude:

$$\phi_i^\dagger \gamma_5 \phi_j = 0 \quad \text{for } \lambda_i^* \neq \lambda_j \tag{4.26}$$

The orthogonality relations of Eq. (4.26) can be applied to any pair of eigenfunctions, in particular we have:

$$\phi_i^\dagger \gamma_5 \phi_j = \tilde{\phi}_i^\dagger \gamma_5 \tilde{\phi}_j = 0 \quad \text{for } \lambda_i^* \neq \lambda_j \tag{4.27}$$

$$\phi_i^\dagger \gamma_5 \tilde{\phi}_j = \tilde{\phi}_i^\dagger \gamma_5 \phi_j = 0 \quad \text{for } ^4 \lambda_i \neq \lambda_j \tag{4.28}$$

IV Without loss of generality we transform the eigenfunctions ϕ_i and $\tilde{\phi}_i$ as follows:

$$\phi_i \to P_i = \frac{\phi_i}{(\tilde{\phi}_i^\dagger \gamma_5 \phi_i)^{\frac{1}{2}}} \tag{4.29}$$

$$\tilde{\phi}_i \to \tilde{P}_i = \frac{\tilde{\phi}_i}{(\tilde{\phi}_i^\dagger \gamma_5 \phi_i)^{\frac{1}{2}}} \tag{4.30}$$

Then we get:

$$\tilde{P}_i^\dagger \gamma_5 P_i = 1 \tag{4.31}$$

Combining Eqs. (4.28)-(4.31) we obtain:

---

[4] Assuming non-degeneracy this is equivalent to $i \neq j$.

$$\tilde{P}_i^{\dagger}\gamma_5 P_j = \delta_{ij} \tag{4.32}$$

Let us define the matrices P, $\tilde{P}$ and $\tilde{P}^{\dagger}$ as:

$$P = [P_1, P_2, P_3, \ldots] \tag{4.33}$$

$$\tilde{P} = [\tilde{P}_1, \tilde{P}_2, \tilde{P}_3, \ldots] \tag{4.34}$$

$$\tilde{P}^{\dagger} = \begin{bmatrix} \tilde{P}_1^{\dagger} \\ \tilde{P}_2^{\dagger} \\ \tilde{P}_3^{\dagger} \\ \vdots \end{bmatrix} \tag{4.35}$$

The set of Eqs. (4.31) and (4.32) is equivalent to bi-unitary relation:

$$\tilde{P}^{\dagger}\gamma_5 P = (\gamma_5\tilde{P})^{\dagger} P = \mathbf{1} \tag{4.36}$$

From Eq. (4.29) we see that,

$$MP_j = \lambda_j P_j \tag{4.37}$$

and therefore from Eq. (4.32) we have:

$$\tilde{P}_i^{\dagger}\gamma_5 M P_j = \delta_{ij}\lambda_j \tag{4.38}^5$$

If we define the matrix Λ as:

$$\Lambda_{ij} = \begin{cases} 0 & \text{for } i \neq j \\ \lambda_j & \text{for } i = j \end{cases} \tag{4.39}$$

then we write Eq. (4.38) as:

$$\tilde{P}^{\dagger}\gamma_5 MP = (\gamma_5\tilde{P})^{\dagger} MP = \Lambda \tag{4.40}$$

So M is diagonalizable under the bi-unitary transformation defined by matrices $\gamma_5\tilde{P}$ and P. Using the bi-unitary relation (4.36) one finds M and M^{-1} as:

$$M = P\Lambda\,(\gamma_5\tilde{P})^{\dagger} \tag{4.41}$$

---

[5] No summations over j assumed.

$$M^{-1} = \left[(\gamma_5 \tilde{P})^{\dagger}\right]^{-1} \Lambda^{-1} P^{-1} = P \Lambda^{-1} (\gamma_5 \tilde{P})^{\dagger} \tag{4.42}$$

or equivalently the latter reads:

$$(M^{-1})_{xy} = P_i(x)(\Lambda^{-1})_{ij}\left[\gamma_5 \tilde{P}(y)\right]^{\dagger}_{j} = P_i(x)\frac{1}{\lambda_i}\left[\gamma_5 \tilde{P}(y)\gamma_5\right]^{\dagger}_{i}$$

$$= \sum_i \frac{1}{\lambda_i} \frac{\phi_i(x)\,\tilde{\phi}_i^{\dagger}(y)\gamma_5}{(\tilde{\phi}_i^{\dagger}\gamma_5\phi_i)} \tag{4.43}$$

As shown in Eq. (4.43) the major contributions to M^{-1} and accordingly to hadron propagators are due to the small eigenvalues. When we are close to a zero mode the propagator is mainly dominated by the corresponding state, otherwise a lot of eigenfunctions will contribute. This implies that those gauge configurations with no zero modes or those with zero modes of opposite chirality do not contribute to the hadron propagators[6] once the propagators are averaged over all gauge configurations. If $\lambda = (1 - \frac{\kappa}{\kappa_z})$ is an eigenvalue corresponding to a zero (or almost zero) mode, then the most divergent terms contributing to the meson propagators are proportional to λ^{-2}. In cases where such terms cancel out, the divergent terms $(\lambda\,\lambda_i)^{-1}$, where $\lambda_i \neq \lambda$, will contribute most.

4.4 π And a_0 Meson Propagators

We represent hadron propagators in terms of eigenfunctions of M by using Eq. (4.43) in propagators. In case of pion Eq. (4.11) or its Fourier transformed version, Eq. (4.14) would then become:

---

[6] This is because the factor

$$\tilde{\phi}_i^{\dagger}(y)\,\gamma_5 = \left[\gamma_5 \tilde{\phi}_i(y)\right]^{\dagger}$$

in Eq. (4.43) changes sign for chirally opposite modes.

$$\tilde{C}_\pi(t) = < \sum_{i,j} \frac{1}{\lambda_i \lambda_j} \sum_{\underline{x}} \frac{\tilde{\phi}_i^\dagger \phi_j(0)\, \tilde{\phi}_j^\dagger \phi_i(\underline{x},t)}{(\tilde{\phi}_i^\dagger \gamma_5 \phi_i)\,(\tilde{\phi}_j^\dagger \gamma_5 \phi_j)} >_G \qquad (4.44)$$

Similarly for the non-singlet scalar meson correlation function we use Eq. (4.43) in Eq. (4.16) to get:

$$\tilde{C}_S(t) = < \sum_{i,j} \frac{1}{\lambda_i \lambda_j} \sum_{\underline{x}} \frac{\tilde{\phi}_i^\dagger \gamma_5 \phi_j(0)\, \tilde{\phi}_j^\dagger \gamma_5 \phi_i(\underline{x},t)}{(\tilde{\phi}_i^\dagger \gamma_5 \phi_i)\,(\tilde{\phi}_j^\dagger \gamma_5 \phi_j)} >_G \qquad (4.45)$$

We are interested to see how zero modes contribute to the propagators. Let us assume that $\phi(x)$ is a zero mode. Then from Eq. (4.21) the corresponding vanishing eigenvalue λ approaches $(1-\frac{\kappa}{\kappa_z})^{-1}$ as $\kappa \to \kappa_z$. Moreover since λ is real we have $\tilde{\phi} = \phi$. We then approximate fermion propagator (4.43) as $\kappa \to \kappa_z$:

$$(M^{-1})_{xy} \approx \frac{1}{1-\frac{\kappa}{\kappa_z}} \frac{\phi(x)\phi^\dagger(y)\gamma_5}{(\phi^\dagger \gamma_5 \phi)} \qquad (4.46)$$

and the meson correlation functions (4.44) and (4.45) as:

$$\tilde{C}_\pi(t) \approx < \frac{1}{(1-\frac{\kappa}{\kappa_z})^2} \sum_{\underline{x}} \frac{\left[\phi^\dagger \phi(0)\right]\left[\phi^\dagger \phi(\underline{x},t)\right]}{(\phi^\dagger \gamma_5 \phi)^2} >_G \qquad (4.47)$$

Similarly for the non-singlet scalar meson correlation function we use Eq. (4.44) in Eq. (4.16) to obtain:

$$\tilde{C}_S(t) \approx < \frac{1}{(1-\frac{\kappa}{\kappa_z})^2} \sum_{\underline{x}} \frac{\left[\phi^\dagger \gamma_5 \phi(0)\right]\left[\phi^\dagger \gamma_5 \phi(\underline{x},t)\right]}{(\phi^\dagger \gamma_5 \phi)^2} >_G \qquad (4.48)^7$$

---

[7] The implicit application of the following abbreviations should be realized:

$$\phi^\dagger \phi(0) = \sum_{spin,color} \phi^\dagger(0)\,\phi(0)$$

$$\phi^\dagger \gamma_5 \phi(0) = \sum_{color} Tr_{spin}\, \phi^\dagger(0) \gamma_5 \phi(0)$$

and similar expressions at point x. Also

$$\phi^\dagger \gamma_5 \phi = \sum_x \sum_{color} Tr_{spin}\, \phi^\dagger(x) \gamma_5 \phi(x)$$

etc.

In the hopping parameter region close to κ_z, the comparison of Eq. (4.47) with (4.48) shows that:

I The pseudoscalar correlation function is greater than the non-singlet scalar correlation function. This can be seen if we write ϕ in terms of ζ_1 and ζ_2 the eigenfunctions of γ_5 with eigenvalues +1 and -1 respectively,

$$\phi(x) = c_1(x)\zeta_1 + c_2(x)\zeta_2 \tag{4.49}$$

where $c_1(x)$ and $c_2(x)$ are spin independent. Then:

$$\phi^\dagger\phi(x) = |c_1(x)|^2 + |c_2(x)|^2 \tag{4.50}$$

and

$$\phi^\dagger\gamma_5\phi(x) = |c_1(x)|^2 - |c_2(x)|^2 \tag{4.51}$$

so we have,

$$\phi^\dagger\phi(x) \geq \phi^\dagger\gamma_5\phi(x) \tag{4.52}$$

As a result each term in Eq. (4.47) is greater than the corresponding term in Eq. (4.48). This results in:

$$\tilde{C}_\pi(t) \geq \tilde{C}_s(t) \tag{4.53}$$

II Both non-singlet scalar and pseudoscalar meson propagators are of the same order as we approach continuum limit. This is the consequence of a numerical check [57] that the ratio of $\phi^\dagger\phi(x)$ and $\phi^\dagger\gamma_5\phi(x)$ is of order (plus or minus) unity for any eigenfunction with real eigenvalue.

III As κ approaches κ_z both $\tilde{C}_\pi(t)$ and $\tilde{C}_s(t)$ become large proportional to $(1-\frac{\kappa}{\kappa_z})^{-2}$ and diverge at $\kappa = \kappa_z$. In other words both non-singlet scalar and pseudoscalar mesons become massless at $\kappa = \kappa_z$. We emphasize that these conclusions are valid only in the region $\kappa \approx \kappa_z$ where only one eigenstate i.e. the zero mode contributes to the propagators. Actually any comparison of non-singlet scalar and pseudoscalar meson propagators should be in a region where more states

contribute. This means that we have to work in regions relatively far away from κ_z in which case one must really consider relations (4.44) and (4.45) instead of Eqs. (4.47) and (4.48), though complicated mixture of states now makes it extremely difficult to predict the propagators behaviours in such regions.

4.5 Numerical Analysis Of The Propagators

We already know that the lattice formulation appears to be the most promising method to compute the hadron mass spectrum within the framework of QCD. The prediction of such a spectrum is indeed one of the crucial tests for establishing QCD as the correct theory of strong interactions. Unfortunately any realistic calculation of hadron masses is faced with a number of difficulties. First of all due to the nature of theories with infinite number of degrees of freedom any approximation of fields requires the Monte Carlo simulations on large lattices not only to represent continuum limit but also to eliminate the finite-size effects. Obviously the presence of the dynamical fermions does not let one tackle the full theory on large lattices. If we accept quenched approximation then the main limitation in the lattice size comes from the inversion of large fermion matrix. Moreover to obtain reasonable results a good statistics is needed. This requires the calculations on a considerable number of gauge configurations as well as origin points. Bearing these considerations in mind we have worked out only pion and non-singlet scalar meson propagators in just a few limited cases in quenched approximation on an $8^3\times16$ lattice in only one gauge field configuration. The aim is, on one hand, to demonstrate the efficiency of block Lanczos algorithm in such calculations, and at the same time gain some qualitative insight into the hadron propagators and specially understand how propagators behave when we are close to the zero modes.

Since we always use hermitian Lanczos algorithm we work with hermitian $\gamma_5 M$ and accordingly we work with Eqs. (4.15) and (4.17) to calculate pion and non-singlet scalar correlation functions.

We need to invert $\gamma_5 M$. If the origin is located at site n, then we actually need only the n^{th} column of $(\gamma_5 M)^{-1}$. This is obtained by choosing a δ-function located at site n for the initial Lanczos vector as mentioned in §2.4. Taking into account the number of spins and colours one has to do $N_{spin} N_{color}$ inversions at the same site but at different spins and colours. Block Lanczos algorithm with block size of $N_{spin} N_{color}$ is the most efficient way to calculate all $N_{spin} N_{color}$ required columns of $(\gamma_5 M)^{-1}$ at once. In practice due to storage limitations we should be content with smaller blocks in favour of larger lattices.

The correlation functions behave like hyperbolic cosine functions only at large distances where the excited states have died out. To observe such a behaviour one really must be able to calculate correlation functions at large values of t. This requires working on more extended lattices, at least in temporal direction. Though generating gauge configurations on large lattices is extremely time consuming however for qualitative research purposes we might pretend to work with a large gauge configuration just by multiplication of smaller gauge configurations for a number of times. Here we consider the case of duplication of a gauge configuration. Triplicating and making four or more copies of the configuration follow similarly.

Let U be a gauge configuration generated on an $L_S^3 L_T$ lattice with periodic boundary conditions on the gauge fields. If we duplicate the lattice along the temporal extension to construct an $L_S^3 \times 2L_T$ lattice and copy U on the duplicated part then we have a gauge configuration on an $L_S^3 \times 2L_T$ lattice where still periodic boundary conditions on the gauge fields are maintained [58]. Due to periodicity of gauge fields the corresponding fermion matrix $\boldsymbol{m}$ can be represented as:

$$\boldsymbol{m} = \begin{pmatrix} \mathrm{M} & 0 \\ 0 & \mathrm{M} \end{pmatrix} \tag{4.54}$$

We can construct the corresponding periodic eigenfunctions of $\boldsymbol{m}$ from the

eigenfunctions of M once periodic boundary conditions are imposed on the fermion fields for larger lattice. Let ϕ_p and ϕ_a be eigenfunctions of M where periodic and antiperiodic boundary conditions are imposed on the fermion fields along temporal direction respectively while spatial boundary conditions remain periodic. Also let λ_p and λ_a be the corresponding eigenvalues. Then we have:

$$\phi_p(x+2L_T) = \phi_p(x+L_T) = \phi_p(x) \tag{4.55}$$

$$\phi_a(x+2L_T) = -\phi_a(x+L_T) = \phi_a(x) \tag{4.56}$$

therefore both $\phi_p$and ϕ_a are periodic with the period of $2L_T$. Moreover if we write the eigenfunctions in the range of $0 \le x \le 2L_T$ as:

$$\Phi_1 = \begin{pmatrix} \phi_p \\ \phi_p \end{pmatrix} \tag{4.57}$$

$$\Phi_2 = \begin{pmatrix} \phi_a \\ -\phi_a \end{pmatrix} \tag{4.58}$$

where $\phi_p$and ϕ_a are just the eigenfunctions in the range $0 \le x \le L_T$ then we have:

$$\boldsymbol{m}\Phi_1 = \begin{pmatrix} M & 0 \\ 0 & M \end{pmatrix}\begin{pmatrix} \phi_p \\ \phi_p \end{pmatrix} = \begin{pmatrix} M\phi_p \\ M\phi_p \end{pmatrix}$$

$$= \lambda_p \begin{pmatrix} \phi_p \\ \phi_p \end{pmatrix} = \lambda_p \Phi_1 \tag{4.59}$$

and,

$$\boldsymbol{m}\Phi_2 = \begin{pmatrix} M & 0 \\ 0 & M \end{pmatrix}\begin{pmatrix} \phi_a \\ -\phi_a \end{pmatrix} = \begin{pmatrix} M\phi_a \\ -M\phi_a \end{pmatrix}$$

$$= \lambda_a \begin{pmatrix} \phi_a \\ -\phi_a \end{pmatrix} = \lambda_a \Phi_2 \tag{4.60}$$

So the spectrum of $\boldsymbol{m}$ with periodic boundary conditions on fermion fields is just composed of the spectra of M with periodic and antiperiodic boundary conditions on fermion fields. The same statement holds if M is replaced with $\gamma_5 M$.

Starting with the third configuration generated at $\beta = 5.8$ on an 8^4 lattice in §3.9.2 we have generated an $8^3 \times 16$ gauge configuration by the above procedure

while periodic boundary conditions are imposed on all directions. Its double valued nature of eigenvalue distribution vs. κ shown in Fig. 4.1 clearly indicates that the $8^3\times16$ $\gamma_5 M$ matrix spectrum is the superposition of 8^4 $\gamma_5 M$ matrix spectra. Comparing Fig. 4.1 with eigenvalue spectra of $\gamma_5 M$ at $\beta = 5.8$ on an 8^4 lattice with periodic boundary conditions on fermion fields (Fig. 3.30) indicates that the first $\kappa_z = 0.1671$ ($\lambda_z = 0.1509D\text{-}4$) is the κ_z of 8^4 lattice with periodic boundary conditions on time direction at $\beta = 5.8$. The branch of eigenvalues corresponding to antiperiodic boundary conditions on time direction crosses zero at $\kappa = 0.1676$ ($\lambda_z = 0.1867D\text{-}4$).

The observables must really be calculated in physical region where $\kappa < \kappa_z$. Due to the sign change of *det M* in crossing κ_z the probability distribution becomes meaningless in non-physical region in full theory. However in quenched approximation where *det M* is suppressed there is nothing to prevent us from entering into non-physical region. As we saw before the fermion matrix eigenfunctions are κ-independent and as a result the κ-dependence of correlation functions in quenched approximation is only through the eigenvalues[8] and in particular the major contributions to the magnitude of the correlation functions come from small modulus eigenvalues regardless of the region of calculation. Accordingly we have studied pion and non-singlet scalar meson correlation functions for 5 values of κ in different regions in κ-space for this $8^3\times16$ lattice.

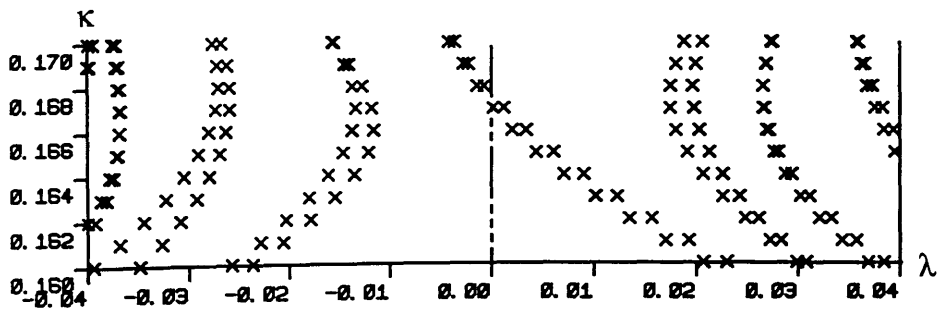

Fig. 4.1 Spectrum of $\gamma_5 M$ for an $8^3\times16$ lattice at $\beta = 5.8$ with periodic boundary conditions on fermion fields on all directions.

[8] E.g. see Eq. (4.44).

The storage limitation does not allow to implement inversions on block sizes greater than 4 for an $8^3 \times 16$ lattice.

4.5.1 π Meson

We have calculated pion (π) correlation function at 4 κ values of 0.165, 0.167, 0.1672, and 0.169. For each of these κ's we have found that there are only 2 eigenvalues with modulus less than 0.01, one, λ_p, corresponding to the periodic and the other, λ_a, to the antiperiodic boundary conditions imposed on the fermion fields on temporal directions as given in Table 4.1. The order of least modulus eigenvalues and similarity of small eigenvalue distributions at $\kappa = 0.165$ and $\kappa = 0.169$ and also closeness of such distributions at $\kappa = 0.167$ and $\kappa = 0.1672$ agree with the observed behaviour of correlation functions shown in Fig. 4.2 as discussed before.

It is also interesting to see how the choice of origin affects the correlation function. As seen in Eq. (4.44) the origin dependence of correlation function comes from the terms $\tilde{\phi}_i \phi_j(0)$. The variation of such terms as we change the origin from one point to another on the lattice can cause major changes in the correlation functions. In particular if antiperiodic boundary conditions are imposed on the fermion fields then this antiperiodicity along with the continuity of the eigenfunctions make every eigenfunction vanish at the boundaries. Excited states vanish also at the nodes different from the boundaries. As a result if the origin is

Table 4.1

Least modulus eigenvalues of $\gamma_5 M$ for an $8^3 \times 16$ lattice at $\beta = 5.8$.

κ	λ_p	λ_a	$\frlambda_a\lambda_p$
0.1650	0.4371D-2	0.6074D-2	1.39
0.1670	0.1823D-3	0.1186D-2	6.50
0.1672	-0.1491D-3	0.7816D-3	5.24
0.1690	-0.2790D-2	-0.2244D-2	0.80

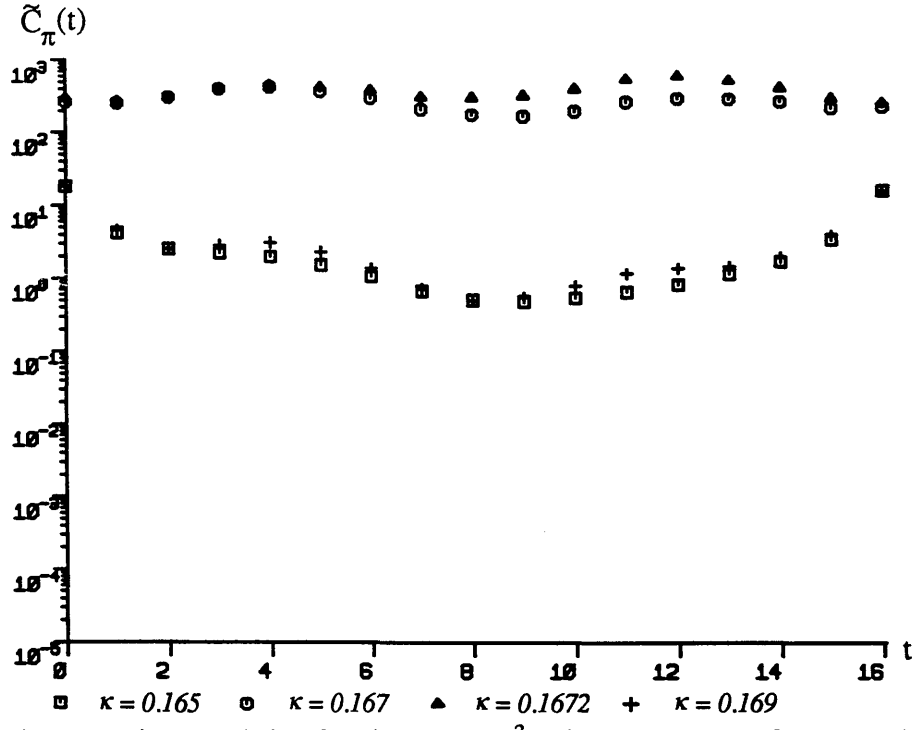

Fig. 4.2 Pion correlation function for an $8^3 \times 16$ lattice at $\beta = 5.8$. The origin is located at $t = 0$ (site $n = 1$).

located on or near a node then the contribution to $\tilde{C}_\pi(t)$ from the corresponding eigenfunction will be suppressed unless the corresponding least modulus eigenvalue is extremely small. To see these qualitative modifications of the propagators as the origin shifted we calculated $\tilde{C}_\pi(t)$ at $\kappa = 0.165$ and $\kappa = 0.167$ for several origins. Except the first origin which is located at the corner of the lattice at site $n = 1$ $(t = 0)$ the rest are located at the time slice centers for $t = 1, 2, ..., 7$. The results are shown in Figs. 4.3 and 4.4 for $\kappa = 0.165$ and $\kappa = 0.167$ respectively.

Although the results at $\kappa = 0.165$ show a systematic shift as we shift the origin, the corresponding results at $\kappa = 0.167$ are very different. Regardless of slight changes in the magnitudes of the propagators it seems that they are independent of the choice of the origin at this value of κ which is relatively close to κ_z. We conclude that as $\kappa \to \kappa_z$ the choice of origin becomes immaterial because only one eigenfunction is involved.

It is interesting to note that one might obtain the square of the zero mode

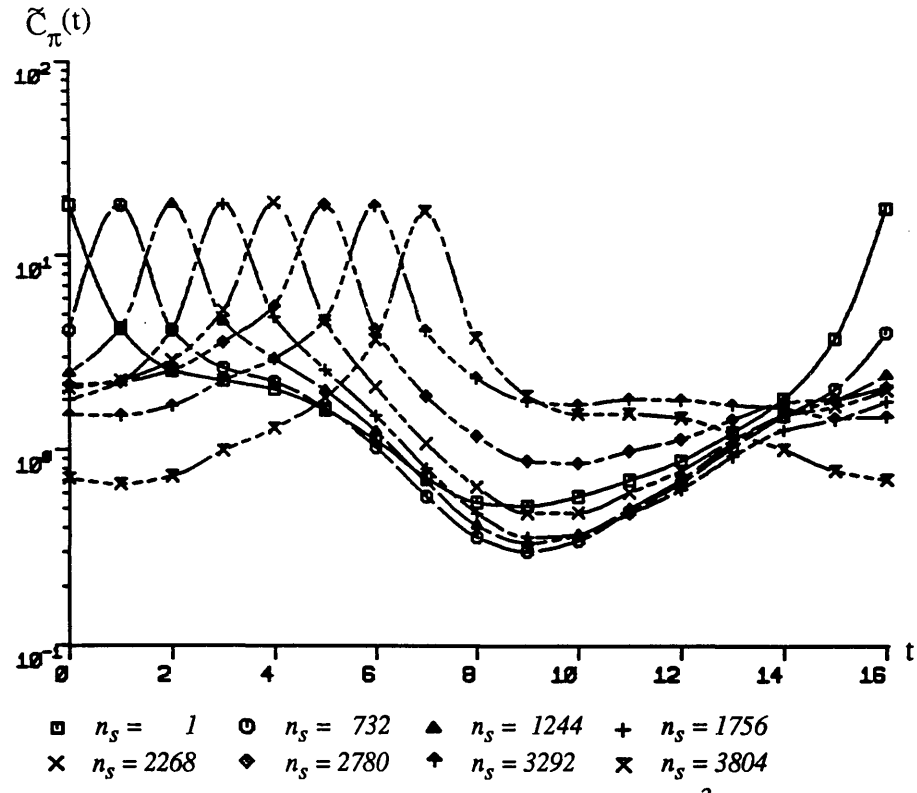

Fig. 4.3 Pion correlation function from different origins in an $8^3 \times 16$ lattice at $\beta = 5.8$ and $\kappa = 0.165$.

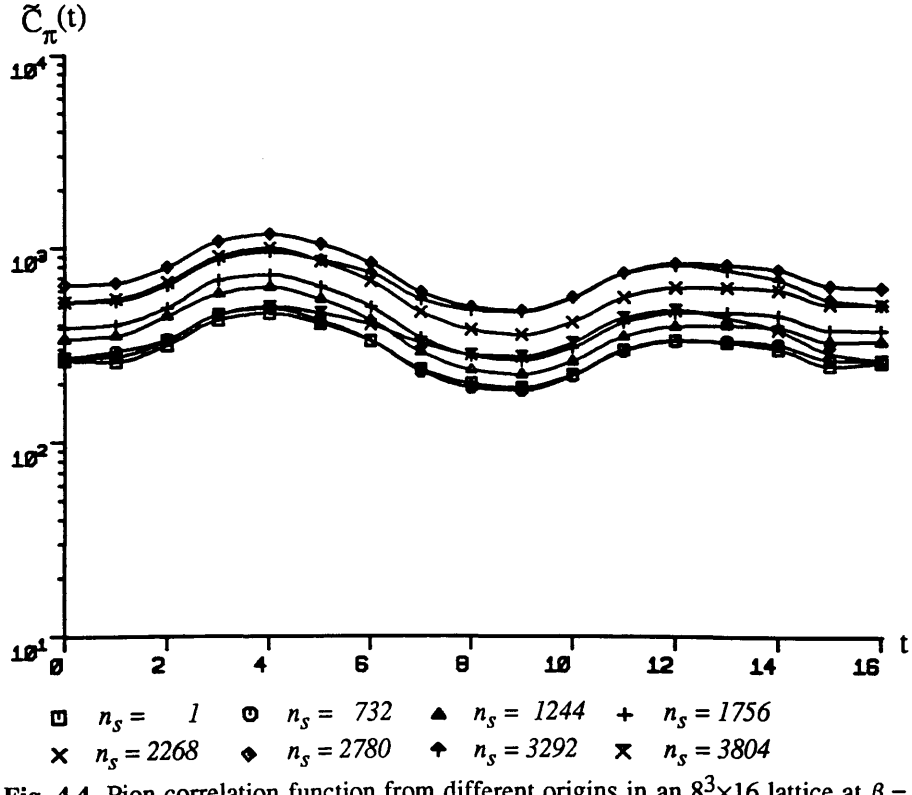

Fig. 4.4 Pion correlation function from different origins in an $8^3 \times 16$ lattice at $\beta = 5.8$ and $\kappa = 0.167$.

eigenfunction i.e. $\sum_{\underline{x}} \phi^{\dagger}\phi\ (\underline{x},t)$ as a function of time from $\tilde{C}_{\pi}(t)$. In fact as shown in Eq. (4.47) $\tilde{C}_{\pi}(t)$ becomes proportional to the zero mode square as $\kappa \rightarrow \kappa_z$. Let us consider $\tilde{C}_{\pi}(t)$ at $\kappa = 0.1677$ which is very close to the second $\kappa_z = 0.1676$ with $\lambda_z = 0.1867D\text{-}4$. As this eigenvalue belongs to the branch of eigenvalues of $\gamma_5 M$ with antiperiodic boundary conditions on fermion fields in time direction, the corresponding zero mode $\phi(t)$ would be antiperiodic in each 8^4 lattice. But anyway, $\phi^{\dagger}\phi(t)$ remains periodic in the same time interval. As a result $\phi^{\dagger}\phi(t)$ and consequently the correlation functions must have a maximum around $t = 4$ and two minima (nodes) at the boundaries of first 8^4 lattice i.e. at $t = 0$ and $t = 8$. Similar pattern is expected in the second 8^4 lattice. Fig. 4.5 shows agreement with these considerations.[9] Due to the mixing of the modes as well as origin dependence of the propagators such a pattern can not be recognized at values of κ far from κ_z.

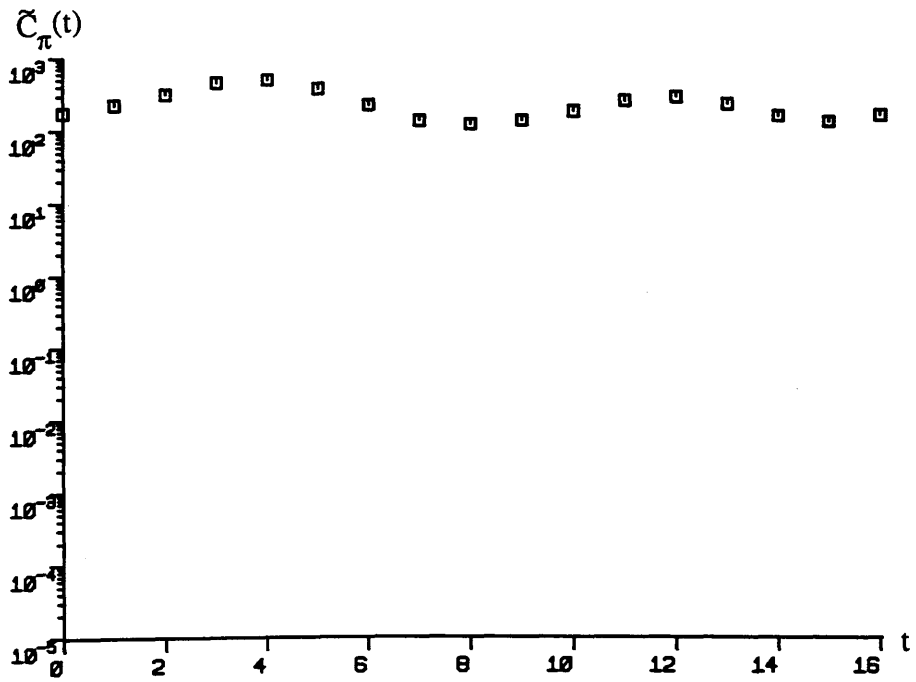

Fig. 4.5 Pion correlation function where origin is located at site 2000 in an $8^3 \times 16$ lattice at $\beta = 5.8$ and $\kappa = 0.1677$.

[9] In Fig. 4.5 the origin is in fact on $t = 3$. However, as mentioned in the previous paragraph, due to the closeness of $\kappa = 0.1677$ to the second $\kappa_z = 0.1676$ we expect no shifts in the behaviour of the propagator.

Finally we have calculated $\tilde{C}_\pi(t)$ at $\kappa = 0.165$ and $\kappa = 0.167$ by averaging over the above 8 origin points. We have also symmetrized the correlation function by replacing its value at time separation t with its average value over equi-distance time slices from the origin. We have considered the signals propagated from different origins as statistically independent and calculated the errors. The results show that the process of summing over the origins removes the unsystematic variations observed on each correlation function.

At $\kappa = 0.165$ the smooth large distance ($6 \leq t \leq 10$) behaviour of $\tilde{C}_\pi(t)$ shows non-vanishing slope as a sign of a massive pion while $\tilde{C}_\pi(t)$ is much larger at $\kappa = 0.167$ and becomes independent of t as shown in Fig. 4.6. The flat behaviour of the propagator at large distances is a necessary but not sufficient condition for the pion to become massless. Actually we must work in a region where entering into the parity-violating phase is accompanied by entering into a dense region of zero modes. The spectrum of $8^3 \times 16$ lattice at $\beta = 5.8$ in Fig. 4.1

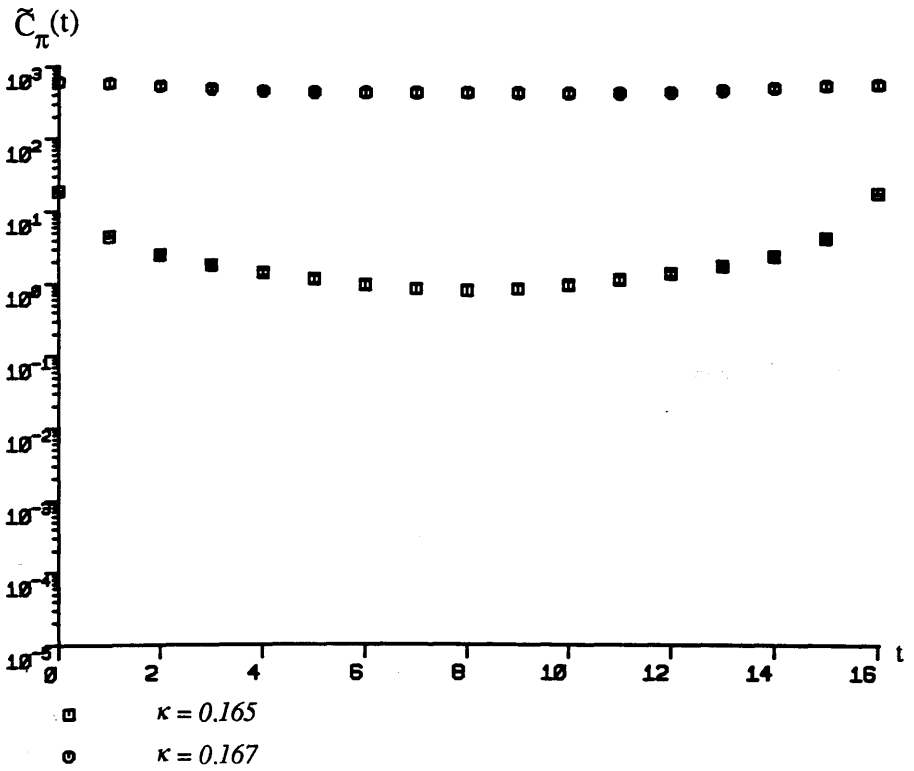

Fig. 4.6 Pion correlation functions averaged over 8 different origins in an $8^3 \times 16$ lattice at $\beta = 5.8$.

shows that the eigenvalues are isolated[10] and as mentioned at the end of §3.9.2 and indicated in Fig. 3.31 such an eigenvalue distribution is represented by a δ-function. In other words $\rho(0)$ vanishes everywhere except at κ_z. In this situation only one mode contributes to the propagators if we are close enough to a zero mode and as mentioned in section III of §4.4 both non-singlet scalar and pseudoscalar mesons become massless which is of course a wrong result! Our results in the following sub-section show that this is actually what happens when we work in such a wrong region. To cope with this situation we should either work at lower values of β which of course would take us far from the continuum limit, or increase the lattice size.

4.5.2 a_0 Meson

We have made use of Eq. (4.17) to calculate non-singlet scalar meson (a_0) correlation functions. We need to multiply $(\gamma_5 M)^{-1}$ by γ_5 once on the left and once on the right. Let only one column of $[(\gamma_5 M)^{-1}]_{\underline{x},t\ 0,0}$ be already calculated for a fixed spin and colour at a certain origin site. Though there is no need of other spin components of $(\gamma_5 M)^{-1}$ to perform $[\gamma_5(\gamma_5 M)^{-1}]_{\underline{x},t\ 0,0}$ multiplication, it is impossible to carry out the latter operation if $(\gamma_5 M)^{-1}$ is not known for the spins at the origin since now all the origin spins are involved in the multiplication. This requirement makes it impossible to compute non-singlet scalar meson propagators by non blocked algorithms without storing propagators. In fact we have to have 4 columns of the inverse at a time and accordingly work in a block of size 4 to be able to do spin multiplications simultaneously. The situation here is different from pion correlation function (4.15) where we could calculate the correlation function for each spin of the origin separately and add the result together at the end. In other words no restrictions could be imposed on the size of blocks to calculate pion propagators while in non-singlet scalar meson propagator calculations the block size

[10] The next least modulus eigenvalue at $\kappa = 0.167$ is about 65 times greater than the smallest one! This ratio is about 2.7 at $\kappa = 0.165$.

must be at least 4 and if there is no storage limitation the bigger possible block sizes can then only be 8, 12, etc.

We have calculated non-singlet scalar meson correlation function under the same conditions the pion calculations were done. The results obtained at 4 κ values of 0.165, 0.167, 0.1672 and 0.169 are plotted in Fig. 4.7. The correlation function at $\kappa = 0.167$ and $\kappa = 0.1672$ which are close to first κ_z is flatten and its magnitudes at large distances ($6 \leq t \leq 10$) become considerably larger than these magnitudes at $\kappa = 0.165$ and $\kappa = 0.169$ which are far from κ_z. Compared with the corresponding results for pion i.e. Fig. 4.2 the non-singlet scalar correlation functions are less smooth and even negative at some time separations so that we can not show them on the logarithmic plot in Fig. 4.7. Comparing Eq. (4.14) with Eq. (4.16) indicates that all the terms in pion correlation function are positive whereas, due to non-hermicity of M, there is no such definiteness in non-singlet scalar correlation function terms. This can explain the unpleasant non-smooth feature of

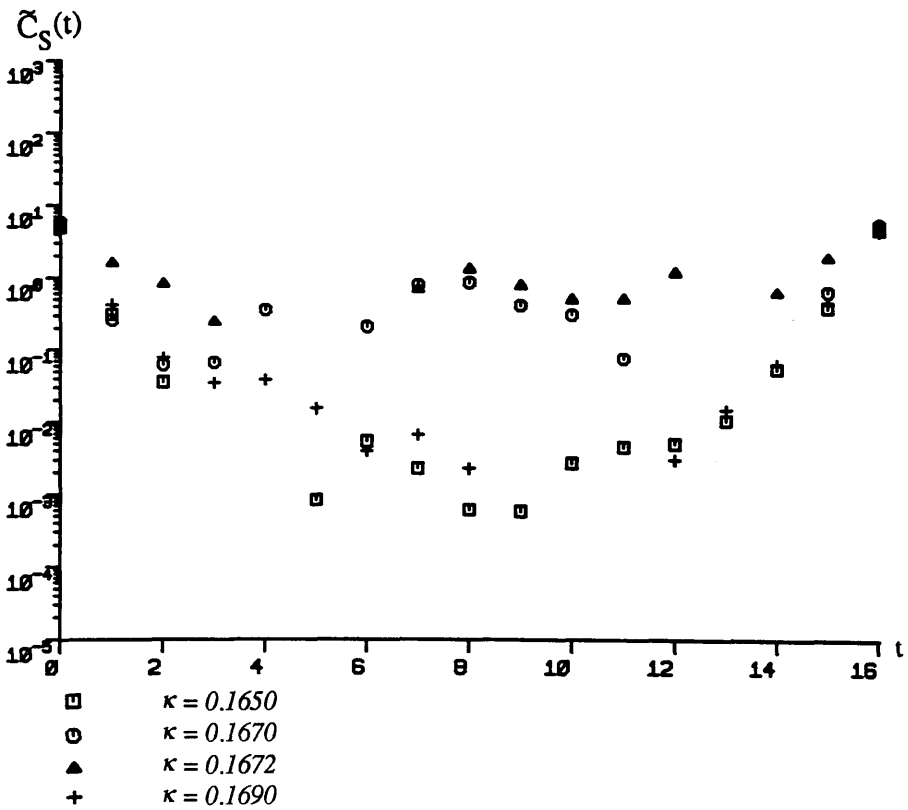

Fig. 4.7 Non-singlet scalar meson correlation functions for an $8^3 \times 16$ lattice at $\beta = 5.8$.

non-singlet scalar correlation functions.

It has been argued that large fluctuations and instabilities in hadron propagators in quenched approximation should generally be eased by the effects of dynamical fermions [59]. However, these fluctuations have been still observed in pion mass calculations with two degenerate flavours of staggered dynamical fermions, though they have been believed to be caused by the doubling of the lattice [60].

We expected in §4.4 that at κ's very close to κ_z both $\tilde{C}_\pi(t)$ and $\tilde{C}_S(t)$ behave similarly while $\tilde{C}_S(t)$ still remains smaller than $\tilde{C}_\pi(t)$. Fig. 4.8 compares $\tilde{C}_S(t)$ with $\tilde{C}_\pi(t)$ at $\kappa = 0.1672$ and confirms this expectation as the non-singlet scalar meson propagator is pretty flat.

We have also calculated $\tilde{C}_S(t)$ averaged over the previous 8 origins at $\kappa = 0.165$ and $\kappa = 0.167$. As before we have calculated the errors as if the signals from different origins were statistically independent. The corresponding results are

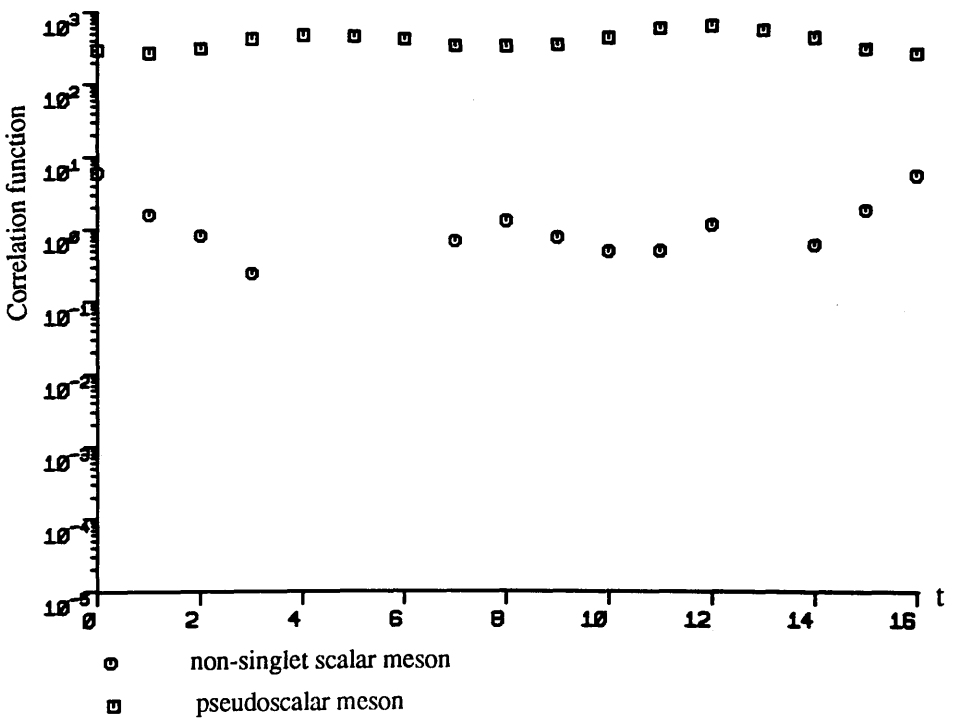

Fig. 4.8 Non-singlet scalar and pseudoscalar meson correlation functions for an $8^3 \times 16$ lattice at $\beta = 5.8$ and $\kappa = 0.1672$.

plotted in Fig. 4.9 in which the missing points are indicative of negative signals as well as infinitely large errors. Again we see that $\tilde{C}_S(t)$ behaves more smoothly once averaged over a number of origin points. As expected as $\kappa \rightarrow \kappa_z$ the correlation function grows and diverges at κ_z. Large errors at large distances ($6 \leq t \leq 10$) can more be associated with non-hermitian nature of M as explained above and may partially be attributed to the fact that exponentially decaying functions become very small at large distances and as a result these extremely small signals get lost in the noise. Such errors become larger for heavier particles as their correlation functions e^{-mt} [or $\cosh m(\frac{L_T}{2} - t)$] die out more rapidly than for the lighter particles with longer correlation lengths.

It is interesting to compare average values of $\tilde{C}_S(t)$ with $\tilde{C}_\pi(t)$. Accordingly we have put plots of $\tilde{C}_S(t)$ and $\tilde{C}_\pi(t)$ at $\kappa = 0.165$ together in Fig. 4.10. Corresponding results at $\kappa = 0.167$ are shown in Fig. 4.11. $\tilde{C}_S(t)$ decreases more rapidly at $\kappa = 0.165$ than it does at $\kappa = 0.167$ and always remains smaller

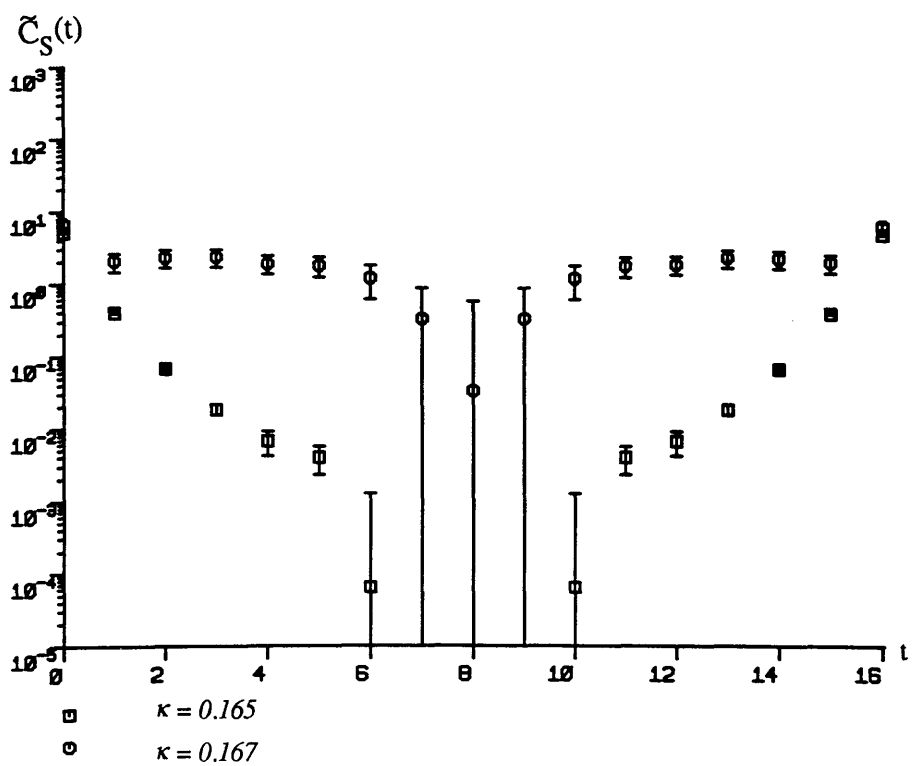

Fig. 4.9 Non-singlet scalar meson correlation functions averaged over 8 different origins on an $8^3 \times 16$ lattice at $\beta = 5.8$.

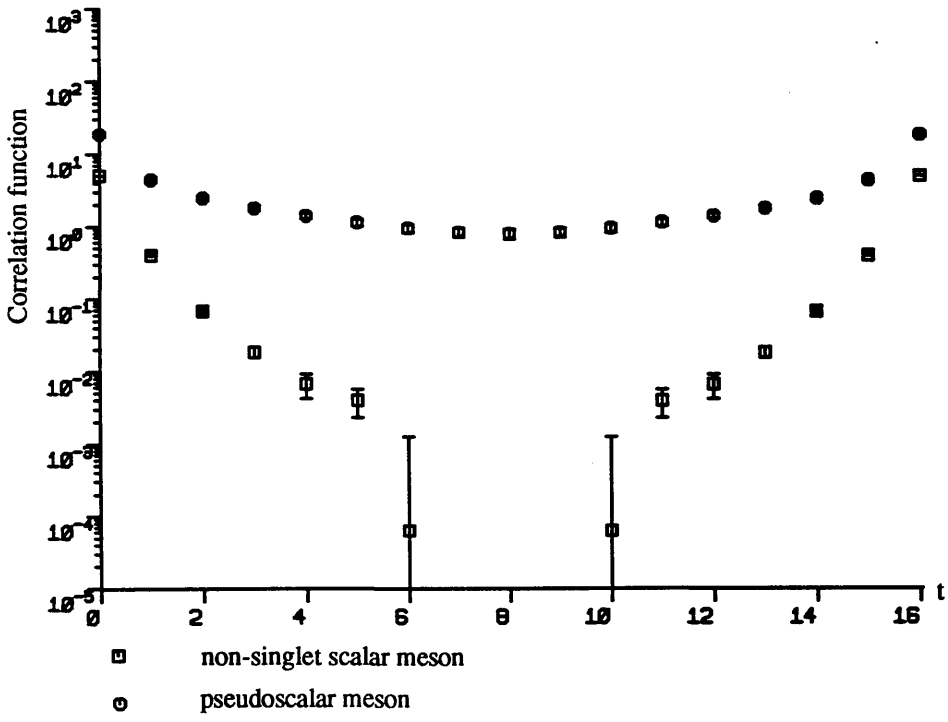

Fig. 4.10 Non-singlet scalar and pseudoscalar correlation functions averaged over 8 different origins in an $8^3 \times 16$ lattice at $\beta = 5.8$ and $\kappa = 0.165$.

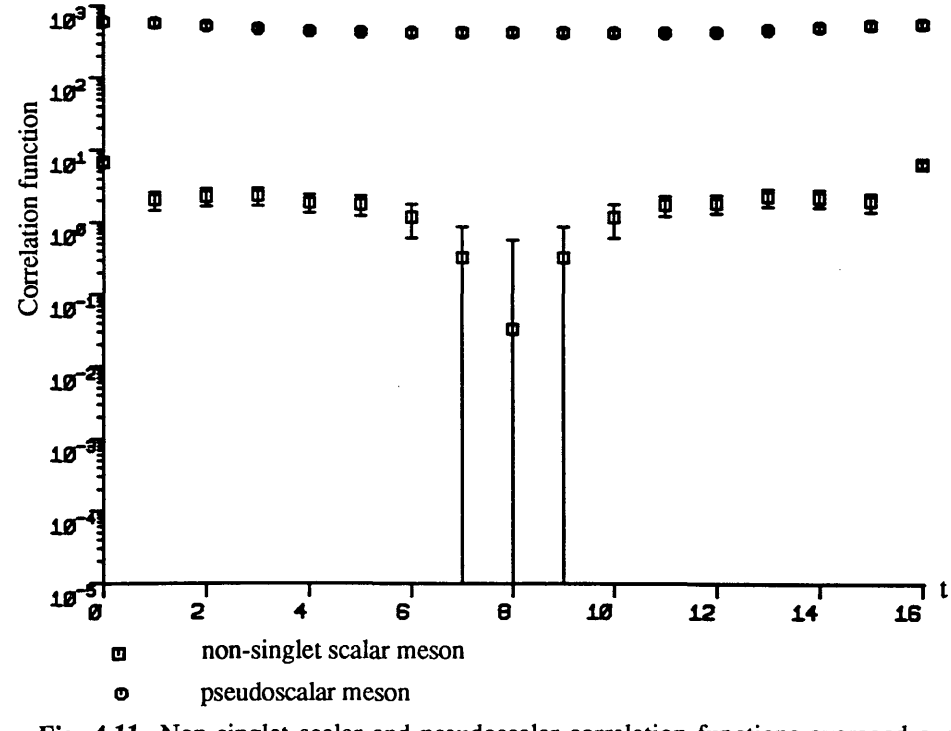

Fig. 4.11 Non-singlet scalar and pseudoscalar correlation functions averaged over 8 different origins in an $8^3 \times 16$ lattice at $\beta = 5.8$ and $\kappa = 0.167$.

than $\tilde{C}_\pi(t)$. At $\kappa = 0.167$ both $\tilde{C}_S(t)$ and $\tilde{C}_\pi(t)$ have become large compared with their values at $\kappa = 0.165$. Unfortunately due to the large errors in $\tilde{C}_S(t)$ at large distances ($6 \leq t \leq 10$) we can not make a clear and definite statement about the large t behaviour of non-singlet scalar meson correlation function and its mass while it is relatively easy to analyze pion correlation function over large distances. This allows us to also estimate the pion mass rather accurately as $\kappa \rightarrow \kappa_z$.

In brief, the conclusion we draw from our work on meson propagators once again confirms that block Lanczos algorithm is an efficient method to implement hadron mass calculations. By this method we could see that κ_z defined by a critical value of hopping parameter where fermion matrix has a zero mode, is indeed the place where pion mass vanishes. However, we also observed that the non-singlet scalar meson becomes massless at the same place where the pion mass vanishes! This irrational conclusion, which is the result of working in a region where only one state i.e. the zero mode contributes to the propagators, shows that this region is in fact a wrong one to calculate hadron propagators. To obtain reliable results one should really work in a region where more states contribute i.e. relatively away from zero modes. Moreover large lattices, in particular for computing the hadron masses are needed to reduce finite-size effects. In addition higher statistical accuracy is required not only in terms of source points but also in number of gauge configurations. One might even think of a realistic calculation of the hadron masses by the inclusion of fermion loops into the calculations. Again block Lanczos method is well suited for updating dynamical fermions. To summarize if enough computer time is given, a quantitative calculation of the hadron spectrum at least in quenched approximation is quite feasible.

Chapter 5

Conclusion

Having investigated the Lanczos and conjugate gradient algorithms on 4^4 and 8^4 lattices convergence rate of inversion is observed to be governed by $/\lambda/_{min}$ and its density and slows down as we approach κ_z. Our results strongly confirm the equivalence of the conjugate gradient to Lanczos algorithm despite the fact that $\gamma_5 M$ is not positive definite. Due to non-definiteness of $H = \gamma_5 M$ both norm of residue and norm of solution vector behave as if they are superpositions of two independent residues or solution vectors. This behavior improves when we modify the algorithms to their $H^\dagger H$ versions. However, inspite of the stability of $H^\dagger H$ conjugate gradient algorithm compared with the fluctuating behaviour of the original algorithm, it is slower specially as κ_z is approached.

One might achieve a relatively considerable improvement factor in convergence rate by blocking the algorithms. The blocking approach does not alter the above general characteristics, for instance the block conjugate gradient algorithm is still faster than the corresponding block version of $H^\dagger H$ conjugate gradient algorithm.

Our results at strong coupling limit, in particular indicate that the blocking procedure has a better performance once applied to H conjugate gradient rather than to $H^\dagger H$ conjugate gradient algorithm. Though the single versions of Lanczos and conjugate gradient algorithms are essentially identical, however their blocked forms behave differently as we increase the block size. The block Lanczos algorithm proved much better and faster than the block conjugate gradient algorithm

specially as $\kappa \rightarrow \kappa_z$.

At weaker coupling constants $H^{\dagger}H$ conjugate gradient algorithm works well when $|\lambda|_{min}$ is not too small. Unfortunately it fails as one approaches κ_z in large blocks. Under the same conditions block Lanczos algorithm works very well in all cases.

Although the algorithms slow down to converge as one decreases β and/or approaches κ_z (in the confining phase), however they tend to behave more independently of details of fermion matrix such as hopping parameter or gauge configuration as one increases the block size.

Based on our results we really conclude that the block Lanczos algorithm is more efficient than the original single algorithm and more stable than both versions of conjugate gradient algorithm and in particular faster than $H^{\dagger}H$ conjugate gradient algorithm especially near κ_z. As a result, the block Lanczos algorithm is recommended for updating dynamical fermions and studying hadron propagators and critical phenomena.

The application of the Lanczos algorithm to investigate the $\gamma_5 M$ spectrum on 4^4, 6^4 and 8^4 lattices reveals very clear indications of vanishing of zero modes density $\rho(0)$ at the values of κ below a certain κ_z which changes from configuration to configuration in the confining phase. $\rho(0)$ picks up a non-vanishing value by crossing κ_z. At strong coupling limit the zero modes density remains actually non-zero for $\kappa \geq \kappa_z$. This observation implies the existence of parity-violating phase transition (at strong coupling limit in the quenched approximation) accompanied by a massless pion occurring at critical hopping parameter κ_c where fermion propagator M^{-1} is singular.

Decreasing of the κ_z as β increases from strong coupling limit to weaker coupling constants is in agreement with the ideas of Aoki's phase diagram and confirms the existence of massless modes in the confining phase at weak coupling constants. Slight changes in gauge configurations can cause relatively large shifts in

κ_z. This is an indication that fermion propagator diverges for a wide range of κ above κ_c once averaged over all gauge configurations. This is the sign of entering into the parity-violating phase by crossing κ_c.

Although the fermion spectrum at not so weak coupling constants behaves similarly to the strong coupling limit, one encounters a different scenario at weak enough coupling constants. Now a second κ_z appears almost far away from the first κ_z. This phenomenon implies that at infinite-volume limit we observe separate regions of zero modes once averaged over all gauge fields, a phenomenon predicted by the proposed lattice QCD phase diagram.

The eigenvalue distribution tends to become thinner as β increases. This effect makes the eigenvalues and in particular the zero modes isolated. This property which is more transparent in smaller lattices makes $\rho(0)$ behave like a δ-function in a neighborhood around $\lambda = 0$ at $\kappa \geq \kappa_z$ in the confining phase. Accordingly work in such a region where only one mode (zero mode) overcomes and contributes leads to unrealistic conclusions!

The general behaviour of $\gamma_5 M$ spectrum changes as one crosses the deconfining phase transition temperature. No zero modes are found in the deconfining phase for any values of κ. This in turn shows that no massless pions exist in the deconfining phase. On the other hand, since massless pions are associated with chiral symmetry breaking, this observation also implicates the restoration of chiral symmetry at weak enough coupling constants.

The conclusions obtained from fermion matrix eigenvalue studies are further supported by the results of meson propagator calculations. Applying the block Lanczos algorithm to work out the pion and non-singlet scalar meson propagators in the quenched approximation on $8^3 \times 16$ lattices, the non-vanishing slope of pion correlation function at large distances confirms non-vanishing pion mass at the values of κ far from κ_z while it flattens as κ approaches κ_z. This result is an indication that κ_c defined by a critical value of hopping parameter where fermion matrix has a zero mode at infinite-volume limit, is indeed the place where pion mass

vanishes. This conclusion which is the result of superposing the contributions from a number of source origins would be altered if we consider only individual propagators. In this case the periodic nature of propagators are clearly observed at the values of κ very close to κ_z in which case only one isolated zero mode contributes to the propagators.[1] The number of modes contributing to the correlation functions at κ's far from κ_z is relatively large which makes the behaviour of individual propagators unpredictable in such regions of hopping parameter.

Compared with the corresponding results for individual pion propagators the non-singlet scalar correlation functions behave very badly. However, the average non-singlet scalar correlation functions over a number of origins behave slightly better though they are still subject to large errors at large distances. This does not let us make a clear and definite statement about the large time behaviour of the non-singlet scalar propagator and its mass while it is relatively easy to analyse pion correlation function over large distances. Anyway the non-singlet scalar propagators grow as $\kappa \rightarrow \kappa_z$ and diverge at κ_z! This unexpected behavior which really does not distinguish so much between non-singlet scalar and pseudoscalar propagators i.e. results in massless non-singlet scalar meson as well, is the result of working very close to a zero mode where the contributions from the other states are effectively suppressed, and is also partially stemmed from ignoring the dynamical fermions.

As far as the Wilson fermion spectrum is concerned there are still open problems for future investigations. In the quenched approximation one can still work at higher values of β for better correlations as our eigenvalue results at $\beta = 5.5$ on 8^4 lattices showed short range correlation lengths. The inclusion of dynamical fermions will naturally alter the results quantitatively. However, does it modify those results qualitatively? For instance will the results of Monte Carlo

[1] We have calculated the propagators in a relatively large vale of β where the eigenvalues have been isolated and their distribution has been fairly thin.

simulations of the full theory still agree with the proposed lattice QCD phase structure? In 2-flavour lattice QCD with dynamical fermions we have to see if π^+ and π^- behave differently from π^0 in parity-violating phase. Do $<\bar{u}\gamma_5 u>$ and $<\bar{d}\gamma_5 d>$ really pick up opposite vacuum expectation values? One really needs a reliable result of such an investigation in order to explain the π-η mass difference.

The conclusions we obtained from studying the meson propagators point out that a realistic hadron spectroscopy requires more extended lattices than we have used, not only to extract the masses from the propagators at large distances where the excited states have died out but to reduce the finite-size effects as well. Also required is higher statistical accuracy in terms of origin points and the number of gauge configurations. More appealing hadron calculations would, of course, include fermion loops into the calculations in which case block Lanczos algorithm is well suited for updating dynamical fermions. In short if enough computer time is given the block Lanczos algorithm can efficiently provide one with a quantitative calculation of the hadron spectrum (at least in the quenched approximation).

Appendix

1 Dirac Matrices

Dirac matrices combine the spinor and antispinor to four-vectors. They are standard and in Minkowski space satisfy the relation [61]:

$$\{\gamma_\mu,\gamma_\nu\} = 2g_{\mu\nu} \tag{A.1}$$

and the hermicity conditions:

$$\gamma_\mu{}^\dagger = \gamma_0\gamma_\mu\gamma_0 \tag{A.2}$$

where $g_{\mu\nu}$ is the metric tensor with components

$$g_{\mu\nu} = \begin{cases} +1 & \text{if } \mu = \nu = 0 \\ -1 & \text{if } \mu = \nu \neq 0 \\ 0 & \text{if } \mu \neq \nu \end{cases} \tag{A.3}$$

A fifth anticommuting γ-matrix is defined by:

$$\gamma_5 = i\,\gamma_0\gamma_1\gamma_2\gamma_3 \tag{A.4}$$

γ_5 has the properties:

$$\{\gamma_\mu,\gamma_5\} = 0 \tag{A.5}$$

$$\gamma_5{}^\dagger = \gamma_5 \tag{A.6}$$

$$(\gamma_5)^2 = 1 \tag{A.7}$$

2 Gell-Mann matrices

Gell-Mann matrices are the generators of *SU(3)* group. They are denoted by t^a for the colour and and by τ^a (or λ^a) for the flavour variables. They are traceless and hermitian and their most commonly used properties are as follows [62]:

$$t^a t^b = \frac{2}{3}\delta^{ab} + (d^{abc} + if^{abc})t^c \tag{A.8}$$

$$\mathrm{Tr}\, t^a t^b = 2\delta^{ab} \tag{A.9}$$

3 Euclidean Space Relations

Transition to the Euclidean space-time from Minkowski space-time is made by the following relations:

$$t \rightarrow -it = -ix_4 \tag{A.10}$$

$$A_0 \rightarrow iA_0 = iA_4 \tag{A.11}$$

$$A_i \rightarrow -A_i \qquad i = 1, 2, 3 \tag{A.12}$$

The Euclidean definition of gauge fields A_μ is done so that the covariant derivative remains in the same form in both spaces. Also we have:

$$\gamma_i \rightarrow i\gamma_i \qquad i = 1, 2, 3 \tag{A.13}$$

which modify the relations among the γ-matrices as:

$$\{\gamma_\mu, \gamma_\nu\} = 2\delta_{\mu\nu} \tag{A.14}$$

$$\gamma_\mu{}^\dagger = \gamma_\mu \tag{A.15}$$

$$\gamma_5 = \gamma_1\gamma_2\gamma_3\gamma_4 \tag{A.16}$$

γ_5 has the same properties as in the Minkowski space. These transitions along with the Euclidean versions of fermion fields,

$$\psi \rightarrow \psi \tag{A.17}$$

$$\overline{\psi} \rightarrow -i\overline{\psi} \tag{A.18}$$

will result in the following transition of fermionic action to Euclidean space:

$$\int dt\, d^3x\, \overline{\psi}(i\not{D} - m)\psi \rightarrow \int d^4x\, \overline{\psi}\,(\not{D} + m)\psi \tag{A.19}$$

while the gluonic part of the Lagrangian density has the same form in both spaces i.e. $-\frac{1}{4} F_{\mu\nu} F^{\mu\nu}$. This implies $S \rightarrow iS$ or,

$$\int -dt\; d^3x \frac{1}{4} F_{\mu\nu}F^{\mu\nu} \rightarrow \int + d^4x \frac{1}{4} F_{\mu\nu}F^{\mu\nu} \tag{A.20}$$

References

[1] K.G. Wilson, Phys. Rev. D10 (1974) 2445

[2] T. Banks, S. Raby, L. Susskind, J. Kogut, D.R.T. Jones, P.N. Scharbach and D.K. Sinclair, Phys. Rev. D15 (1977) 1111

[3] J. Shigemitsu, Phys. Rev. D18 (1978) 1709

[4] R.P. Feynman and A.R. Hibbs, *Quantum mechanics and path integrals* (McGraw-Hill, New York, 1965)

[5] R.H. Ryder, *Quantum field theory* (Cambridge University Press, Cambridge, 1985) pp. 157-289

[6] T.P. Cheng and L.F. Li, *Gauge theory of elementary particle physics* (Clarendon Press, Oxford, 1984) pp. 23-29

[7] M. Creutz, *Quarks, gluons and lattices* (Cambridge University Press, Cambridge, 1986) pp. 39-49

[8] D. Gross and F. Wilczek, Phys. Rev. Lett. 30 (1973) 1343

[9] S. Coleman and D.J. Gross, Phys. Rev. Lett. 31 (1973) 851

[10] H. Politzer, Phys. Rev. Lett. 30 (1973) 1346

[11] T.P. Cheng and L.F. Li, *Gauge theory of elementary particle physics* (Clarendon Press, Oxford, 1984) p. 335

[12] A.D. Kennedy, The theory of hybrid stochastic algorithms, Fermilab preprint Fermilab-Conf-89/237T (1989)

[13] N.A. Metropolis, M.N. Rosenbluth, A.H. Rosenbluth, E. Teller and J. Teller, J. Chem. Phys. 21 (1953) 1087

[14] L.H. Karsten and J. Smit, Nucl. Phys. B183 (1981) 103

[15] T.P. Cheng and L.F. Li, *Gauge theory of elementary particle physics* (Clarendon Press, Oxford, 1984) p. 488

[16] H.B. Nielsen and M. Ninomiya, Nucl. Phys. B185 (1981) 20

[17] J.B. Kogut and L. Susskind, Phys. Rev. D11 (1975) 395

[18] K.C. Bowler and C. Rebbi, in *Statistical and particle physics-Common problems and techniques*, eds. K.C. Bowler and A.J. McKane, Proc. The 26th Scottish Universities Summer School in Physics, Edinburgh, 1983

(SUSSP, Edinburgh, 1984) p. 469

[19] K. Wilson, in *New phenomena in subnuclear physics*, ed. A. Zichichi, Proc. Int. Sch. Subnucl. Phys., Erice, 1975 (Plenum, New York, 1977) p. 13

[20] C. Lanczos, J. Res. Nat. Bur. Stand. 45 (1950) 255

[21] C. Lanczos, J. Res. Nat. Bur. Stand. 45 (1952) 409

[22] G.H. Golub and C. F. Van Loan, *Matrix computations* (North Oxford, Academic, Oxford, 1983) pp. 362-377

[23] D. Henty, R. Setoodeh and C.T.H. Davies, Nucl. Phys. B337 (1990) 487

[24] J.H. Wilkinson, *The algebraic eigenvalue problem* (Clarendon Press, Oxford, 1965) pp. 290-299

[25] J.H. Wilkinson, *The algebraic eigenvalue problem*, (Clarendon Press, Oxford, 1965) pp. 300-302

[26] B.N. Parlett and D.S. Scott, Math. Comp. 33 (1979) 217

[27] D.S. Scott, in *Sparse matrices and their uses*, ed. I. S. Duff, (Academic Press, New York, 1981) p. 139

[28] G.R. Katz et al., Phys. Rev. D37 (1988) 1589

[29] I.M. Barbour et al., J. Comp. Phys. 68 (1987) 227

[30] I.M. Barbour, N. Behilil, P.E. Gibbs, G. Schierholz and M. Teper, in *The recursion method and its applications-Lecture notes in physics* (Springer Verlag, Berlin, 1985)

[31] W.H. Press, B.P. Flannery, S.A. Teukolsky and W.T. Vetterling, *Numerical recipes-The art of scientific computing* (Cambridge University Press, Cambridge, 1986) pp. 301-307

[32] P. Rossi, C.T.H. Davies and G.P. Lepage, Nucl. Phys. B297 (1988) 287

[33] J. Cullum and R.A. Willoughby, Lin. Algebra Appl. 90 (1980) 63-90

[34] D. O'Leary, Lin. Algebra Appl. 29 (1980) 63

[35] A.S. Householder, *The theory of matrices in numerical analysis*, (Blaisdell, New York, 1964) pp. 139-141

[36] A. Gasser, and H. Leutwyler, Nucl. Phys. B94 (19751) 269

[37] G. 't Hooft, Phys. Rev. Lett. 37 (1976) 8;
G. 't Hooft, Phys. Rev. D141 (1976) 3432

[38] N. Kawamato, Nucl. Phys. B190 [F53] (1981) 617

[39] S. Aoki, Ph.D. thesis, University of Tokyo (1987)

[40] S. Aoki, Ph.D. thesis, University of Tokyo (1987) pp. 9-10

[41] S. Aoki, Ph.D. thesis, University of Tokyo (1987) pp. 28-37

[42] N. Kawamato and J. Smit, Nucl. Phys. B192 (1981) 100

[43] S. Aoki, Ph.D. thesis, University of Tokyo (1987) p. 25

[44] D.J. Gross and A. Neveu, Phys. Rev. D10 (1974) 3235

[45] T. Eguchi and R. Nakayama, Phys. Lett. B126 (1983) 89

[46] S. Aoki, Phys. Rev. D30 (1984) 2653

[47] S. Aoki, Phys. Rev. Lett. 57 (1986) 3136

[48] S. Aoki, Phys. Lett. B190 (1987) 140

[49] I.M. Barbour et al., Phys. Lett. B127 (1983) 433

[50] J. Smit and J.C. Vink, Nucl. Phys. B286 (1987) 485

[51] J. Smit and J.C. Vink, Nucl. Phys. B307 (1988) 549

[52] K.M. Bitar, A.D. Kennedy and P. Rossi, The chiral limit and phase structure of QCD with Wilson fermions, The Florida State University preprint FSU-SCRI-89-101 (1989)

[53] Y. Iwasaki, in *Lattice gauge theory '86*, eds. H. Satz, I. Harrity and J. Potvin (Plenum Press, New York, 1987)

[54] R. Setoodeh, C.T.H. Davies and I.M. Barbour, Phys. Lett. B213 (1988) 195

[55] C.T.H. Davies, I.M. Barbour and R. Setoodeh, Wilson fermions in lattice QCD, Glasgow University preprint GUTPA/90/6-2 (1990), in prepration.

[56] S. Itoh, Y. Iwasaki and T. Yoshie', Phys. Rev. D36 (1987) 527

[57] S. Itoh, Y. Iwasaki and T. Yoshie', Phys. Lett. B184 (1987) 375

[58] P.E. Gibbs, Ph.D. thesis, University of Glasgow (1985)

[59] K.H. Mütter et al, in *Lattice gauge theory '86*, eds. H. Satz, I. Harrity, and J. Potvin (Plenum Press, New York, 1987)

[60] K.M. Bitar et al., QCD with dynamical staggered quarks, Indiana University preprint IUHET-188

[61] F. Mandl and G. Shaw, *Quantum field theory* (John Wiley & Sons, Chichester, 1984) pp. 327-331

[62] E.V. Shuryak, *The QCD vacuum, hadrons and the superdense matter* (World scientific, Singapore, 1988) p. 351